

# DISSERTATION

## **The Potential of Modernized GNSS Signal Linear Combinations for Real-Time Positioning on Small and Medium Baselines**

ausgeführt zum Zwecke der Erlangung des akademischen Grade eines

**Doktors der technischen Wissenschaften**

unter der Leitung von

Ao. Prof. Dr. techn. Dipl.Ing. Robert Weber  
Department für Geodäsie und Geoinformation

eingereicht an der Technischen Universität Wien  
Fakultät für Mathematik und Geoinformation  
von

**Dhota Pradipta M.T.**

1129682

Ikan Sepat 1/16, 65125, Malang, East Java, Indonesia

Wien, April 2016

---

eigenhändige unterschrift



TECHNISCHE  
UNIVERSITÄT  
WIEN  
Vienna University of Technology

## **Doctoral Thesis**

### **The Potential of Modernized GNSS Signal Linear Combinations for Real-Time Positioning on Small and Medium Baselines**

to achieve the university degree  
**Doktor der technischen Wissenschaften**

Supervisor:

Ao. Prof. Dr. techn. Dipl.Ing. Robert Weber  
Department für Geodäsie und Geoinformation

submitted to:

Technische Universität Wien  
Fakultät für Mathematik und Geoinformation

**Dhota Pradipta M.T.**

1129682

Ikan Sepat 1/16, 65125, Malang, East Java, Indonesia

Vienna, April 2016

---

Signature



# Acknowledgements

*All praises and thanks to the grace of almighty **God (Allah)**, the Beneficent, the Merciful, and the Supreme source of all the knowledge, to Him I do serve and to Him I ask for help, Who gave me the strength and drive to achieve this task and made me reach this present pedestal of knowledge.*

*I would like to express my sincere gratitude towards my thesis advisor **Ao. Prof. Dr. techn. Robert Weber** for giving support and guidance during my studies. Also, for all his efforts in helping me to perform this work in the best way I could, with his technical advices and for providing a good work environment. It has been a pleasure being your student over the last years. I am very grateful for his keen interest, behavior and constant advice.*

*To the member of my thesis advisory committee, **Prof. Hasanuddin Z. Abidin Ph.D.**, I offer my sincere appreciation for his technical advises, opportunities, and cooperation during my defense.*

*I would like to thank for all the support I have received during the last years, particularly present Engineering Geodesy Research Group members **Prof. Dr. Ing. Hans Neuner, Claudia Eder** for her assistance during my studies, **Tanja Vicovac, Stefan Niedermayer, Claudius Schmitt** for their advices. Acknowledgement is extended to the present Advanced Geodesy Research Group members, particularly **Fabian Hinterberger, Jadre Maras, Gregor Möller, Elke Maria Umrig, and Michael Schindelegger.***

*I would like to thank and acknowledge **Prof. Dr. techn. Andreas Wieser** for giving the opportunity of coming to TU-Wien and for his support, advice, and assistance over the course of my work, particularly during his guidance in my early year.*

*My personal thanks are extended to **my parents** for providing me excellent upbringing, education, and guidance, which helped me reaching at this point in my life. Heartfelt thanks go to **my brother and sisters**, for their unconditional support and understanding that always encouraged me to follow the path I have chosen.*

*I thank also all my **Indonesian friends in Vienna and Austria** for all of our good experiences, journeys and cheerful times together. My thanks also go to numerous of peoples whom I may not name all, for their grateful and joyful support, encouragement and helpfulness.*

*Last but not least, I would like to thank the **OeAD Asea-Uninet scholarship** for providing me with funding for financial assistance during my three years of graduate study.*

# List of Abbreviations

AMU	Arbitrary Manufacture Unit
ARNS	Aeronautical Radio Navigation Service
AltBOC	Alternative Binary Offset Carrier
BOC	Binary Offset Carrier
BPSK	Binary Phase-Shift Keying
CBOC	Composite Binary Offset Carrier
CODE	Center of Orbit Determination in Europe
CORS	Continuous Operating Reference Stations
CDMA	Code Division Multiple Access
C/N <sub>0</sub>	Ratio of average signal power to noise power spectral density
CL	Civil Long
CM	Civil Moderate
DS-SS	Direct Sequence-Spread Spectrum
DGNSS	Differential GNSS
ECEF	Earth Centered Earth Fixed
EGNOS	European Geostationary Navigation Overlay Service
ESA	European Space Agency
FAGS	Federation of Astronomical and Geophysical Data Analysis Services
FDMA	Frequency Division Multiple Access
FEC	Forward Error Correction
FKP	Flächen Korrektur Parameter
GLONASS	GLObal'naya NAvigatsionnaya Sputnikovaya Sistema
GNSS	Global Satellite Navigation System
GPS	Global Positioning System
GPST	GPS Time
GST	Galileo System Time
GTRF	Galileo Terrestrial Reference Frame
IERS	International Earth Rotation and Reference Systems Service
IGS	International GNSS Service
ITRF	International Terrestrial Reference Frame
ITRS	International Terrestrial Reference System
LAMBDA	Least-squares AMBiguity Decorrelation Adjustment
MBOC	Multiplexed Binary Offset Carrier
MSAS	Multi-functional Satellite Augmentation System
NMEA	Nation Maritime Electronics Association
NWP	Numerical Weather Prediction
PCV	Phase Center Variation
PRN	Pseudo-Random Noise
PRS	Public Regular Service

PSD	Power Spectral Density
QPSK	Quadrature Phase-Shift Keying
RAIM	Receiver Autonomous Integrity Monitoring
RFI	Radio Frequency Identification
RTK	Real-Time Kinematic
RTCM	Radio Technical Commission for Maritime Services
SBAS	Satellite-Based Augmentation System
SNR	Signal to Noise Ratio
SoL	Safety of Life
TAI	International Atomic Time
TDM	Time-Division Multiplexed
TMBOC	Time Multiplexed Binary Offset Carrier
UTC	Coordinated Universal Time
VRS	Virtual Reference System
WAAS	Wide Area Augmentation System

# List of Symbols

$c$	speed of light
$d_{ion}$	ionosphere signal delay
$d_r$	inaccuracy in satellite position
$d_t, d_T$	satellite and receiver clock drift
$d_{trop}$	tropospheric delay
$e$	partial pressure of water vapor
$g$	gravity acceleration
$f$	frequency
$h$	orthometric height
$D_P$	line of signal of multipath
$IF$	ionosphere free linear combination
$k_1, k_2, k_3$	refractivity constant
$M_d, M_w$	molar mass for dry air and water vapor
$n$	refractivity index
$N_d, N_w$	dry and wet refractivity
$N_L$	ambiguity at carrier phase L
$N_{WL}$	wide lane phase ambiguity
$P$	atmospheric pressure
$P_A^i$	pseudorange observation
$q$	specific humidity
$r/R$	geometric range
$R_d, R_w$	gas constants for dry air and water vapor
$WL$	wide-lane linear combination
$MW$	melbourne-wubbena linear combination
$MP$	code multipath
$mp$	carrier phase multipath
$T$	temperature
$X_{sv}, Y_{sv}, Z_{sv}$	position of satellite
$X_r, Y_r, Z_r$	position of receiver
$\sigma_{\Phi_{i,j,k}}$	observation noise
$\lambda$	wavelength
$\varepsilon$	multipath and receiver noise
$\Phi_A^i$	carrier phase observation
$\sigma_L$	standard deviation of signal
$\Delta$	single difference
$\Delta\nabla$	double difference

# List of Contents

Acknowledgements.....	iv
List of Abbreviations .....	v
List of Symbols .....	vii
List of Contents .....	viii
List of Figures .....	xi
List of Tables .....	xv
Abstract.....	1
Zusammenfassung .....	2
1. Introduction .....	3
1.1 Research Goals.....	3
1.2 Motivation.....	4
1.3 Previous Relevant Works .....	5
1.4 The Scope of Research .....	7
1.5 Thesis Organization.....	8
2. GNSS Overview .....	9
2.1 The GPS System.....	9
2.1.1 L2C GPS .....	12
2.1.2 L5 GPS.....	13
2.1.3 L1C GPS .....	14
2.2 The Galileo System.....	15
2.2.1 E1 Galileo .....	15
2.2.2 E5 Galileo .....	16
2.3 Interoperability .....	17
2.3.1 Reference Frames .....	17
2.3.2 Navigation Message.....	18
2.3.3 Time Systems .....	19
2.4 Absolute Positioning .....	20
2.5 Differential Positioning .....	20
2.5.1 Carrier phase observations and error sources.....	20
2.5.2 Double Carrier Linear Combinations.....	21
2.6 GNSS Error Sources .....	23
2.6.1 Ephemeris Errors.....	23



2.6.2	Satellite Clock Errors .....	24
2.6.3	Troposphere.....	24
2.6.4	Ionosphere .....	28
2.6.5	Multipath .....	30
2.6.6	Antenna Phase Center Variation.....	31
2.6.7	Phase Wind-up.....	32
2.6.8	Receiver Errors.....	33
3.	Real-Time Positioning and RTKLIB software .....	34
3.1	Real-Time Positioning .....	34
3.1.1	Integer Ambiguity Resolution for Real-Time GNSS Positioning.....	35
3.1.2	Network Real Time Kinematic (Network - RTK) .....	36
3.1.3	Message Decoding .....	39
3.2	RTKLIB software .....	41
3.2.1	RTKLIB Algorithm .....	42
3.2.2	Integer Ambiguity Resolution .....	44
3.3	Data Sources .....	45
4.	Signal to Noise Ratio and Code Multipath.....	48
4.1	SNR( $C/N_0$ ) on GNSS Observations.....	48
4.2	Multipath Line of Sight.....	50
4.3	Code and Phase Multipath on GNSS Observations.....	53
4.4	Signal to Noise Ratio and Code Multipath Data Processing .....	54
4.4.1	SNR and Code Multipath on GNSS signals .....	55
4.4.2	Conclusions on SNR and Code Multipath .....	62
5.	GNSS Carrier-Phase Linear Combinations.....	65
5.1	Triple Carrier Linear Combinations .....	65
5.1.1	Noise and Multipath Observation.....	66
5.1.2	Wide-lane Combination .....	67
5.1.3	Melbourne-Wübbena Combination.....	68
5.1.4	Ionosphere linear combination.....	69
5.2	Calculation Tests of Linear Combinations.....	71
5.2.1	The effect of baseline length on ambiguity resolution.....	73
5.2.2	The effect of observation time on ambiguity resolution .....	81
5.2.3	Modernized GNSS signal linear combinations .....	85
6.	Real Data and Simulation Test .....	93
6.1	GNSS Reference Station Network .....	93
6.2	Test Stations.....	94

6.3	Simulated Data.....	95
6.4	Investigated Characteristics.....	96
6.5	Results.....	97
6.5.1	Real Data Results.....	99
6.5.2	Simulated Data Results.....	107
7.	Conclusions and Recommendations.....	115
7.1	Summary.....	115
7.2	Conclusions and Recommendations.....	117
	References.....	119
	Appendix A.....	127
	Appendix B.....	129

# List of Figures

Figure 2-1. Binary phase shift keying modulation of code and data signals (Spilker, 1996).....	11
Figure 2-2. GPS signals present and future (Walter et al., 2008).....	11
Figure 2-3. Power spectral of Galileo (Wallner et al., 2005).....	16
Figure 2-4. Power Spectral and Signal Density of Galileo (European GNSS-Galileo open service, 2010) .....	17
Figure 2-5. Double Difference Observations.....	22
Figure 2-6. Illustration of ambiguity resolution methods (compiled from several sources) .....	23
Figure 2-7. Multipath Environments (Hannah, 2001) .....	31
Figure 2-8. Geometric Effects on Phase (Wu et al. 1993).....	33
Figure 3-1. RTK System utilizing GPS signals .....	36
Figure 3-2. Network RTK Data Processing Steps (Wanninger, 2008).....	37
Figure 3-3. RCTM Message .....	40
Figure 4-1. Forward scatter geometry (Hannah, 2001) .....	51
Figure 4-2. Back scatter geometry from above (Hannah, 2001).....	51
Figure 4-3. SNR and Multipath at CHPG station (Trimble NetR9, TRM59800) w.r.t. elevation of GPS PRN25 .....	56
Figure 4-4. SNR and Code Multipath/Noise Residuals of L1 GPS signals of various IGS stations w.r.t. elevation of GPS PRN25 .....	56
Figure 4-5. SNR and Code Multipath/Noise Residuals of L5 GPS signals of various IGS stations w.r.t. elevation of GPS PRN25 .....	57
Figure 4-6. SNR and Code Multipath/Noise at CHPG (Trimble NetR9, TRM59800) w.r.t. elevation of Galileo E11 .....	58
Figure 4-7. SNR and Code Multipath/Noise Residuals of Galileo signals of various IGS stations w.r.t. elevation of E11 .....	59
Figure 4-8. SNR and Code Multipath/Noise at NNOR (Sept Polar X4, Sepchoke_MC) w.r.t. elevation of Galileo E11 .....	59

Figure 4-9. SNR and Code Multipath/Noise Residuals of L1 GPS signal of various IGS stations w.r.t. elevation of PRN24 .....	60
Figure 4-10. SNR and Code Multipath/Noise Residuals of GPS L2 signal of various IGS stations w.r.t. elevation of PRN24 .....	60
Figure 4-11. SNR and Code Multipath/Noise Residuals of GPS L5 signal of various IGS stations w.r.t. elevation of PRN24 .....	61
Figure 4-12. SNR and Code Multipath/Noise Residuals of E1 Galileo of various IGS stations w.r.t. elevation of E19 .....	61
Figure 4-13. SNR and Code Multipath/Noise Residuals of E5 Galileo of various IGS stations w.r.t. elevation of E19 .....	62
Figure 4-14. Code Range Residuals (m) of GNSS signals, DOY 081, 2014 .....	63
Figure 4-15. SNR of GNSS Signals, DOY 081, 2014 .....	64
Figure 5-1. Ambiguity resolution success-rate.....	74
Figure 5-2. The effect of baseline length on coordinate standard deviation .....	75
Figure 5-3. L1 GPS and L1/L5 GPS position biases w.r.t. L1/L2 GPS solution (reference); TLMF-TLSE baseline (8.7 km) .....	75
Figure 5-4. L1 GPS and L1/L5 GPS position biases w.r.t. L1/L2 GPS solution (reference); AXPV-MARS baseline (23.7 km) .....	76
Figure 5-5. L1 GPS and L1/L5 GPS position biases w.r.t. L1/L2 GPS solution (reference); VILL-CEBR baseline (35.3 km).....	77
Figure 5-6. L1 GPS and L1/L5 GPS position biases w.r.t. L1/L2 GPS solution (reference); GANP-KRA1 baseline (>100 km).....	78
Figure 5-7. GPS solutions calculated from L1/L2 GPS and L1/L2/L5 GPS on VILL-CEBR baseline at DOY 240, 2014 (35.3 km).....	79
Figure 5-8. The satellites visibility at TUWI station in DOY 343, 2014 .....	84
Figure 5-9. The standard deviation of coordinate solutions IF-LC w.r.t. L1/L2 IF-LC GPS at 5-15 <sup>0</sup> satellite elevation mask on VILL-CEBR baseline (35 km) .....	90
Figure 5-10. The standard deviation of coordinate solutions IF-LC w.r.t. L1/L2 IF-LC GPS at 15-30 <sup>0</sup> satellite elevation mask on VILL-CEBR baseline (35 km) .....	91
Figure 5-11. The standard deviation of coordinate solutions IF-LC w.r.t. L1/L2 IF-LC GPS at 30-60 <sup>0</sup> satellite elevation on VILL-CEBR baseline (35 km) .....	91

Figure 5-12. E1/E5 Galileo kinematic solutions w.r.t. L1/L2 GPS.....	92
Figure 6-1. Austria Station Networks.....	93
Figure 6-2. Excerpt of RINEX header for station Kirchdorf (EAG) .....	94
Figure 6-3. Excerpt of RINEX header from NavX-Simulator (TIME station) .....	95
Figure 6-4. Excerpt of the solution file (TIME-WIND) .....	99
Figure 6-5. Satellite visibility at KIRC station, DOY 193, 2014 (green plot – L1/L2 GPS; blue plot - L1/L2/L5 GPS; red plot – E1/E5 Galileo).....	100
Figure 6-6. SNR and Code Multipath residual values of E1 and E5 Galileo at 4 stations (E11, E12, E19 Galileo).....	101
Figure 6-7. SNR and Code Multipath residuals for Galileo E11 at KIRC station, DOY 193, 2014.....	101
Figure 6-8. SNR and Code Multipath residuals for Galileo E12 at KIRC station, DOY 193, 2014.....	101
Figure 6-9. SNR and Code Multipath residuals for Galileo E19 at KIRC station, DOY 193, 2014.....	102
Figure 6-10. SNR and Code Multipath/noise residuals of GNSS (all satellites, GPS and Galileo) at KIRC station, DOY 193, 2014.....	102
Figure 6-11. Pseudorange and Carrier Phase Residuals of E1/E5 Galileo w.r.t L1/L2 GPS (WIND – KIRC baseline, 29.1 km) at DOY 193, 2014 .....	103
Figure 6-12. Time series position results w.r.t L1/L2 GPS LC at WIND-KIRC (29.1 km), DOY 193, 2014 .....	104
Figure 6-13. Pseudorange and Carrier Phase Residuals using Galileo satellites (KIRC – UNTE baseline, 50.5 km) at DOY 193, 2014 .....	105
Figure 6-14. Time series position using E1/E5 Galileo wr.t. L1/L2 GPS (KIRC – UNTE baseline, 50.5 km) at DOY 193, 2014 .....	106
Figure 6-15. Galileo solution w.r.t. L1/L2 GPS at KIRC (29.1 km, DOY 193, 2014).....	107
Figure 6-16. 3 hours satellite visibility at KIRC station. (Yellow plot – L1 GPS, red plot – E1/E5 Galileo), DOY 001, 2014 .....	107
Figure 6-17. Static and kinematic position w.r.t. reference position at UNTE (24.9 km), DOY 001, 2014.....	109
Figure 6-18. Static and kinematic position w.r.t. reference position at KIRC (40.8 km), DOY 001, 2014.....	111

Figure 6-19. Static and kinematic position w.r.t. reference position at WIND (66.5 km), DOY 001, 2014.....	112
Figure 6-20. Height difference, standard deviation, and ambiguity success-rate at TIME-UNTE baseline (24.9 km), DOY 001, 2014 .....	113
Figure 6-21. Height difference, standard deviation, and ambiguity success-rate at TIME-KIRC baseline (40.8 km) DOY 001, 2014.....	113
Figure 6-22. Height difference, standard deviation, and ambiguity success-rate at TIME-WIND baseline (66.5 km), DOY 001, 2014 .....	114

# List of Tables

Table 2-1. GPS Time and GST (Moudrak et al., 2004) .....	19
Table 2-2. Frequently used refractivity constants (Langley, 1996).....	26
Table 3-1. Interpolation methods of network RTK (Dai et al., 2004).....	39
Table 3-2. Data Sources (IGS, 2009).....	45
Table 3-3. IGS Products – GPS and GLONASS Satellite Ephemerides. (IGS, 2009).....	46
Table 3-4. IGS Products – GNSS Earth Rotation and Atmospheric Parameters (IGS, 2009) .....	47
Table 4-1. Geometry Delays and Phases (Hannah, 2001).....	52
Table 4-2. Site Information, DOY 081, 2014 .....	55
Table 4-3. Code Range Residuals (m) of GNSS signals, DOY 081, 2014 .....	63
Table 4-4. SNR of GNSS signals, DOY 081, 2014 .....	64
Table 5-1. Optimal Wide Lane Combinations (Urquhart, 2009) .....	68
Table 5-2. Optimal Combination for GPS (Urquhart, 2009).....	70
Table 5-3. Scenario for Post-processing Calculations .....	71
Table 5-4. List of Test Stations .....	72
Table 5-5. Ambiguity Resolution using L1 GPS at DOY 240, 2014. ....	73
Table 5-6. Ambiguity Resolution using L1 and L2 GPS at DOY 240, 2014.....	73
Table 5-7. The cut-off Angle effect on Ambiguity Resolution at DOY 240, 2014.....	74
Table 5-8. Coordinate differences and standard deviation w.r.t. L1/L2 GPS solution; TLMF-TLSE baseline (8.7 km) .....	76
Table 5-9. Coordinate differences and standard deviation w.r.t. L1/L2 GPS solution; AXPV-MARS baseline (23.7 km) .....	77
Table 5-10. Coordinate differences and standard deviation w.r.t. L1/L2 GPS solution; VILL - CEBR baseline (35.3 km) .....	77
Table 5-11. Coordinate differences and standard deviation w.r.t. L1/L2 GPS solution; GANP-KRA1 baseline (>100 km) .....	78

Table 5-12. Ambiguity resolution on various baselines (DOY 240, 2014).....	80
Table 5-13. Ambiguity resolution w.r.t observation time (VILL – CEBR baseline); DOY 300, 2014, 1 second sampling rate.....	81
Table 5-14. Ambiguity resolution w.r.t. observation time (TUWI-LEOP baseline); DOY 343, 2014, 1 second sampling rate.....	82
Table 5-15. Ambiguity resolution w.r.t. observation time (1 second sampling rate GNSS data) at DOY 300 and DOY 240, 2014 (morning).....	83
Table 5-16. Ambiguity resolution w.r.t. observation time (1 second sampling rate GNSS data) at DOY 300 and DOY 240, 2014 (afternoon) .....	84
Table 5-17. The Effect of satellite geometry on position (L1/L2 GPS, 1 hour observation) .....	85
Table 5-18. DOP Value at DOY 343, 2014 (TUWI-LEOP) .....	85
Table 5-19. GNSS signals .....	86
Table 5-20. Results of GNSS Signals Linear Combinations .....	89
Table 5-21. The Influence of Linear of combinations on Position (VILL-CEBR, 35 km, DOY 300, 2014).....	89
Table 6-1. List of selected stations of Austria Network .....	94
Table 6-2. Ionosphere-free Linear Combinations based on two signals.....	98
Table 6-3. Positioning results at KIRC (29.1 km), DOY 193, 2014. ....	103
Table 6-4. The influence of length of observation time at KIRC (29.1 km) w.r.t. reference position at DOY 193, 2014.....	105
Table 6-5. The influence of length of observation time at KIRC (50.5 km) w.r.t. reference position at DOY 193, 2014.....	106
Table 6-6. The influence of length of observation time at UNTE (24.9 km) w.r.t. reference position at DOY 001, 2014.....	109
Table 6-7. The influence of length of observation time at KIRC (40.8 km) w.r.t. reference position at DOY 001, 2014.....	110
Table 6-8. The influence of length of observation time at WIND (66.5 km) w.r.t. reference position at DOY 001, 2014.....	111



# Abstract

GNSS positioning has become popular in the past decade as an efficient method of precise and real-time positioning. It is relatively low cost and ease-of-use. Up to now, several parameters were defined to characterize the performance of real-time positioning: availability, precision, accuracy. This research evaluates the performance of signal linear combinations for real-time positioning, both for static as well as the kinematic positioning.

This thesis starts with the investigation of linear combinations (LC) rising from the carrier frequencies of the GPS and Galileo system. Some Linear Combination shows potential benefits in carrier phase integer ambiguity resolution, particularly utilizing the E5 Galileo signal phase carrier. For each system, a set of combinations was studied, analyzed, and then selected during the development of a GPS/Galileo positioning method utilizing the Least-squares Ambiguity Decorrelation Adjustment (LAMBDA).

Special signal selection can affect the estimated position and its standard deviation. To further analyze, the results obtained from data processing are compared with respect to baselines and signals. The ambiguity fixing rate is correlated with the baseline length and the method as well as the signals that were used. The analysis of the measurement noise level was first conducted to set a baseline for the real-time GNSS positioning application.

According to the test results with real and simulated data, the combined GPS/Galileo approach always performs the best, albeit dominated by GPS. Moreover, a combined Galileo linear combination shows the best insusceptibility in the presence of any errors using simulated and real data. Further efforts were spent for the last step. Tests, analysis and comparison of the algorithms were made in simulated scenarios of the two systems under error conditions of typical multipath, troposphere, and ionosphere. Baselines of a length between 1 km to 70 km using real and simulated data were evaluated, followed by final conclusions and suggestions for future work.

As the conclusion, Galileo signals have potencies to provide best performances for static and kinematic positioning, particularly when utilizing the E5 Galileo signal. Since the performance was tested using only a limited amount of real and simulated data, further investigations how to fulfill technical and user requirements are recommended.

# Zusammenfassung

Real-time Positionierung hat sich in den letzten zehn Jahren als eine effiziente Methode zur präzisen Echtzeit-Positionierung entwickelt. Es zeichnet sich durch geringe Kosten und seine Einfachheit in der Verwendung aus. Mehrere Parameter charakterisieren die Leistung des Real Time Positionierung: Verfügbarkeit, Präzision, Genauigkeit, und die Lösungsmethode. In dieser Forschungsarbeit werden die Auswertung von Signal Linear-Kombinationen zur Real-Time Positionierung vorgestellt. Die resultierenden Parameter werden verwendet, um die Real-Time Positionierungsqualität zu beurteilen. Beabsichtigt wird die Positionierungsgenauigkeit zu verbessern und die Verfügbarkeit zu erhöhen, sodass präzise Positionslösungen für Anwender ermöglicht werden.

Diese Arbeit beginnt mit den Untersuchungen zu Linearkombinationen (LC) die sich aus den Signalen der beiden Systeme (GPS und Galileo) ergeben. Einige davon zeigen potenzielle Verbesserungen zur Bestimmung der ganzzahligen Trägerphasenwellenlängen. Für jedes System, wurden verschiedene Trägerphasenkombinationen untersucht und analysiert. Die vielversprechendsten Kombinationen wurden für Auswertung mit Hilfe des Least-Square Ambiguity Decorrelation Adjustment (LAMBDA) verwendet.

Die Ergebnisse der Berechnung mit Hilfe verschiedener Linearkombinationen auf unterschiedlichen Basislinienlängen wurden miteinander verglichen. Sie weisen eine Korrelation zwischen der Anzahl ganzzahlig fixierter Lösungen im Datensatz und der Länge der Basisline, sowie der Wahl der Linearkombination auf. Aus den Signalen mit dem geringsten Signal-Rauschverhältnis wurde eine Real Time Positionierung Referenzlösung erzeugt. Der entwickelte Algorithmus wurde anhand von simulierten GPS und Galileo Daten getestet. Die Daten wurden mit den typischen Fehlereinflüssen wie Mehrwegeeffekten und troposphärischen und ionosphärischen Verzögerungen überlagert. Es wurden Basislinien von 1 km bis 70 km untersucht.

Zusammengefasst zeigen Galileo Signale (speziell E5) hohes Potential zur Steigerung der Positionierungsperformance, sowohl im statischen als auch kinematischen Fall. Da die realen und simulierten Testdatensätze relativ klein waren, werden weitere Untersuchungen mit umfangreichem Datenmaterial angeregt. Abschließend wurden die Daten interpretiert und Anregungen für weitere Arbeiten gegeben.

# 1. Introduction

## 1.1 Research Goals

Over the decades, the GNSS have evolved into a significant tool to meet civilian navigation and positioning requirements worldwide. All GNSS-based positioning techniques operate under a set of constraints. These constraints may be baseline length, attainable accuracy, assured reliability, signal availability, time-to-solution, and so on.

Today, there are various GNSS in operation, like the well-known US system GPS, the Russian Glonass, but also Galileo that has been developed by the European Space Agency. As in all navigation procedures, inaccuracies and even errors impair the measurements in GNSS positioning. To facilitate those limitations of GNSS positioning, one of techniques currently in use is double differencing. This technique is popular because it minimizes errors for short baselines and drastically reduces biases in case of long baselines. The formation of differences is usually performed with respect to a GNSS reference station network installed at known positions. Calculated correction parameters are forwarded to a mobile GNSS rover over radio communication. In order to achieve centimeter-level or even millimeter-level accuracy, the calculation of a real-time position is based on code pseudorange and carrier phase measurements. However, the real-time positioning application is limited by ionospheric errors, tropospheric errors, satellite orbital errors, and multipath.

The focus of this work is to improve positioning performance and ensure reliable and highly accurate position solutions, taking into consideration dual frequency and triple frequency observations. As expected, additional frequencies can enhance precise positioning applications. With dual frequency, a linear combination can be built and with several frequencies included, there can be several IF – LC (ionosphere free linear combination) introduced. Therefore, it is possible to remove the ionosphere delay beside the standard L1/L2 linear combination. Moreover, it is even possible to design triple frequency linear combinations of all frequencies provided by GPS and Galileo.

When forming the commonly used dual frequency IF-linear combination, several literature notices the integer of double difference ambiguities are lost and impossible to recover. Hence, the ionosphere-free linear combination is of no use for fast, precise positioning applications particularly using phase measurements. However, it is possible to estimate integer ambiguities for the ionosphere-free combination as derived from a

model based on uncombined phase observations as described by Odijk (2003). Moreover the ionosphere-free LC can be successfully introduced in conjunction with the WL/NL algorithm. The research addresses the following:

- Investigate the multipath and Signal to Noise Ratio of GNSS signals to provide initial quality checking.
- Investigate the performance of double frequency and triple frequency phase-based positioning algorithms as a function of the length of observation period span ranging from several minutes to 24 hours solutions in static and kinematic mode.
- Investigate the correlation between estimated coordinates, observation time, and ambiguities. Thus, limitations in the coordinate determination resulting from biases are reported.
- Investigate possible LC combinations that can be particularly useful for real-time positioning applications using each system respectively. The LAMBDA method is implemented as integer least-squares technique in the processing.

## 1.2 Motivation

In order to apply GNSS for surveying purposes in an economic manner, relatively short observation time spans are required. The key to precise GNSS positioning is to use carrier-phase observations in a relative measurement setup, such the unknown phase ambiguities become quantities which are known to be integer-valued, instead of real-valued. The integer ambiguities can be determined and be fixed in another standard adjustment, in which the coordinate parameters can be estimated with cm-precision.

The above procedure is currently applied in a successful way to rapid-static and real-time positioning in GNSS surveying. For these types of applications the receiver position needs to be determined in a few minutes or even instantaneously, i.e. using just one epoch of data if possible. However, the distance between the reference receiver and the rover receiver, is usually restricted to about 10-15 km. At longer distance, it is known that errors due to propagation through the atmosphere (ionosphere and troposphere) and orbit errors become significantly present in relative GNSS observations, since these errors tend to decorrelate with the distance. One choice to overcome this problem is error modeling in CORS networks.

The ionospheric errors dominate the atmospheric errors. In the ionosphere (an atmospheric layer between 50-1100 km altitudes), negatively charged particles, the free electrons, influence the GNSS signals. As a consequence, the code range measurements from satellite to receiver become longer than the geometric range. The effect of these ionospheric delays can be estimated (or eliminated by the ionosphere-free combination) from dual-frequency measurements, since the ionosphere is a dispersive medium (Hofmann-Wellenhof et al. 2001). This IF-LC strategy is usually applied for the processing of baselines which may be up to a few thousands of km utilizing very long observation periods.

Whereas research groups and research institutes are expected to pay increasing attention to real-time position and respective scientific applications solve the problem above, the theses specifically keeps the needs of practicing surveyors, particularly to decrease dependency on the CORS (Continuous Operating Reference Stations) and other reference networks in specific areas with limited coverage.

### **1.3 Previous Relevant Works**

Relevant work on real-time GNSS positioning has been carried out over the past decade. There are several publications that are particularly relevant to RTK positioning. These papers sparked the interest in the proposed research.

The theoretical foundation was documented in Odijk (2003). An efficient approach was developed to make the "accuracy achieved with dual-frequency using phase measurement" available to users. Various combinations of phase observations have been established to provide the need for high accuracy positioning. It is preferred to use a dual-frequency combination using of the GPS signals over the triple-frequency of two-combination set L1/L2-L2/L5 GPS, which requires a much longer observation time span and does not improve the float baseline solution much. For Galileo, the dual-frequency ionosphere-free combinations are expected to perform about the same for ambiguity resolution. However, also ambiguity resolution for these Galileo combinations may result in much more precise final coordinate solutions than their ambiguity-float counterparts within the same time span.

Jensen (2002) reported an accuracy up to centimeters for positioning within an RTK network with an increase in the number of required observations. They solve for the parameters of the tropospheric delay on top of the Saastamoinen model. These parameters can also be introduced to numerical weather models. The ambiguity check indicated more ambiguities were solved to correct integer numbers with an improvement of more than 50%. This can also be used in connection with network RTK, where the NWP can be used for developing tropospheric RTK corrections. When GNSS data are affected, for instance by multipath, these errors will propagate into RTK correction. Hence a better estimate for the tropospheric error over the area is expected when using an external data set as numerical weather prediction. And the analysis showed a slightly smaller residual noise which could be neglected for processing.

Schloderer et al. (2010) applied GNSS RTK to build a topographical map and compared their results with a network established by total stations. GNSS-RTK accuracy depends on many factors, which include satellite availability and visibility, signal blockage from trees and buildings, the effects of multipath errors, and the experience of the observers, to just list a few. The results, however, indicate the potential of GNSS-RTK to generate topographical maps capable of supporting the environmental applications, although they must point out, this is not conclusive given the problems of error sources and

limited data. The time taken to perform the survey was much shorter using GNSS-RTK compared with the total station method, where the need for multiple setups and a traverse to establish control on the multiple stations greatly increased the time taken to perform the survey. However, the total station method is still the preferred one for areas with dense tree cover or other obstructions blocking satellite visibility which introduce significant multipath errors. The accuracy achieved by each survey technique was compared against typical accuracies desired for particular survey tasks.

The author noted that the GNSS-RTK method did not meet the required accuracy for cadastral work, utility surveys, land-deformation surveys, or archaeological surveys that require cm–mm level accuracies, but is sufficient for environmental monitoring, such as the mapping of waste disposal areas. In the end, users can achieve a cm level of accuracy and instantaneous results in the field using GNSS-RTK, which requires observation times of only a few seconds at each surveyed point. Compared with conventional equipment and techniques, GNSS-RTK can dramatically decrease the time and manpower needed to complete an environmental monitoring survey of spatial changes at localized levels and which require constant updating of the monitoring data at regular intervals.

On the other hand, Grejner-Brzezinska et al. (2005) was looking at the accuracy and reliability of network RTK as a function of geometry and data processing. It was demonstrated, based on the static data, fair accuracies of about 10 cm in the horizontal components and 20 cm in the vertical one are possible in the fully instantaneous network-based kinematic mode without external atmospheric corrections. These accuracies are achievable within the networks where the baseline length does not exceed 120 km, the baselines are in favorable geometry, and the ionosphere is in undisturbed state. For the centimeter-level accuracy, shorter network baselines (30–40 km) are required or further enhancements to the algorithms are required, such as separating the network solution from the rover positioning step, and using the initial information accumulated in the position estimation process.

Sahmoudi et al. (2010) investigated carrier phase multipath errors as one of the most limiting factors in accuracy and reliability regarding GNSS RTK based positioning and navigation. They are difficult to mitigate since no multipath indicator is available in the literature for each couple of satellite and receiver. The existing methods of carrier phase multipath mitigation are based mainly on previous data processing, multipath modeling or on multiple antennas. The quality of carrier-phase multipath calibration is highly dependent on the ability to separate multipath effects from other errors. For multipath mitigation and ambiguity resolution in RTK positioning, multi GNSS carrier phase measurements are a promising opportunity. With the upcoming modernized GPS, modernized Glonass and the new Galileo, the measurement redundancy will be increased and the satellite geometry will be improved via the composed constellation.

The authors derived a new multipath equality constraint, which is based on the relationship between linear combinations of double differences of three carrier phases and their ambiguities. Then, they incorporated this constraint into the LAMBDA method cost function to mitigate the multipath effect. The multipath free float ambiguities are then fed to the integer ambiguity search step using the LAMBDA method. It is shown that the efficient integration of multi-carriers provides more redundancy in the measurements and better observability for multipath and ionospheric error estimation.

Toho et al. (2012) mentioned that performing single frequency positioning with Galileo E5 could offer a possibility to precise positioning solutions with a moderate budget although the main obstacle with the current GNSS signals remains. The multipath errors introduce a high level noise up to a few decimeters which in the past makes precise single frequency positioning impossible. The authors stated that the E5 Galileo signal experiences a lower multipath influence. The results confirmed that 3D accuracy of a few centimeter could be achieved compared to the L1 and L5 GPS signals. The drawback of this procedure is the long convergence time to get precise positioning.

In the thesis, RTKLIB has been used because the software could support real-time and post-processed positioning. The most important modes of operation tested by the author are static and kinematic.

The measurements for evaluation were obtained from the Global Navigation Satellite System (GNSS) receivers. This receivers provide different types of information, including raw carrier phase measurements. There are several similar researches that previously have been done concentrating on GNSS optimal combinations which can be used as a reference (Eva and Torben, 2007, Richet and El-Sheimy, 2007, Amiri, et al, 2007, Cocard et al, 2008, and de Bakker et al, 2009, 2011).

#### **1.4 The Scope of Research**

This research involves a study and the utilization of existing carrier phase measurements of GPS and Galileo to accomplish centimeter positioning. This study deals with current and planned observation combinations to accomplish the goal. Respective software is used and tested with real and simulated data. In order to facilitate the study, software components developed and modified by other researchers are used.

The scopes of the research conducted here can be summarized as follows:

- A systematic and consistent setup is presented in the relative GNSS phase model.
- The ionospheric error is analyzed from a geometric point of view. Tropospheric delays are neglected in the process, particularly at short baselines and assuming this delay could be eliminated by double differencing.

- The ionosphere-free linear combination model is a very suitable basis for positioning. The LAMBDA method is utilized as an optimum integer search technique.

## **1.5 Thesis Organization**

This thesis consists of seven chapters. Each chapter is outlined as follows:

- In chapter 2, GNSS in general and the signal error sources are discussed and summarized.
- In chapter 3, the mathematical model for the processing of relative GNSS phase and code observations is reviewed. For the sake of simplicity the errors due to the atmospheric propagation are neglected here (discussed in chapter 5) and components of real-time positioning are also summarized. Also data assessment is discussed in this chapter.
- Chapter 4 describes the general way of solving the mathematical model for applications as formulated with the objective, particularly to check multipath and noise on GNSS's signal.
- In chapter 5, the physical background of the propagation of the GNSS signals through the atmosphere is reviewed, with the main focus on the ionospheric error propagation and the comparison between dual- and triple combination.
- In chapter 6, the processing of real and simulated data is described, which includes an analysis of the expected precision of the parameters of interest and an evaluation of the ambiguity success rate and also which linear combination model is applied for fast positioning. Experimental results are shown for some case studies.
- Finally, in chapter 7, the conclusions of this thesis are summarized and recommendations for further research are provided.



## 2. GNSS Overview

The development of satellite-aided positioning or navigation is not yet completed. While the beginning of satellite positioning can be traced back, the Global Positioning System (GPS) has made satellite positioning available to a world-wide community of users since the early eighties and is currently undergoing a modernization phase. Since the 1990-ies also the Russian system Glonass provides a global acting GNSS which was fully recovered a decade ago. Very recently, Galileo was also introduced and begun the deployment of the system that also will offer three open frequencies to all users similar to GPS. Once Galileo fully deployed, both GPS and Galileo will provide users with a multitude of carrier phase observations to be used in precise positioning. Combining the signals of both systems attracted the scientists to explore shortcomings of the individual systems.

In addition to pay attention to the upgrade of the space component of satellite systems and refining positioning algorithms, a complete positioning infrastructure has been developed consisting of worldwide and/or national reference networks, the IGS (refer to IGS in chapter 3), and so on.

This chapter provides background on GPS and Galileo and the various components that are typical and essential for precise positioning. As Glonass data and data of the Chinese Beidou system are not investigated in this research both systems are not further discussed here.

### 2.1 The GPS System

Chapter 2.1 describes the structure of the GPS signals in general. The content is mainly extracted from the Parkinson & Spilker textbook (1996) as well as from Guochang Xu (2007). This section gives an overview of the GNSS signal structure, error sources, and the explanation of the improved characteristics of the new signals.

The GPS constellation nominally consists of 24 satellites arranged in 6 evenly-spaced orbital planes inclined at  $55^\circ$  with respect to the equator. The satellite orbits are circular, with a radius of 26.660 km and an orbital period of 11 hours 58 minutes. GPS satellites have a very stable clock with a fundamental frequency  $f_0 = 10.23$  MHz, which is used to coherently generate the transmitted signals.

Each signal is composed of three parts: a sinusoidal carrier wave at the central frequency modulated by a binary code and a data message. The binary code allows the

receiver to determine the signal travel time, which is the basis of the GPS positioning technique. The data message provides additional information such as satellite ephemerides and clock offsets, UTC-GPST offset, ionospheric model and satellite health data. It takes 30 seconds from receiver cold start to receive all the data necessary for navigation and 12.5 minutes to receive the entire message.

GPS is based on direct sequence-spread spectrum (DS-SS) signaling. An information waveform of low bandwidth (the data message) is modulated by a waveform of high bandwidth (the code) to produce a high-bandwidth signal for transmission. The data message requires a bandwidth of 100 Hz, the spread GPS signal is transmitted with a bandwidth of 20 MHz. Bandwidth is proportional to the chip (bit) rate of the waveform, so the transmission speed of the code must be much greater than for the data message, the data message is transmitted at 50 bps (bits per second), whereas the code on L1 has a rate of 1023 cps (chips per second).

Two types of spreading codes are transmitted: C/A (Coarse/Acquisition) and P (Precision). These are both pseudorandom noise (PRN) codes, i.e. they are designed to look random when taken over their whole period. Each GPS satellite transmits a different version of these codes, which allows the receiver to distinguish between transmissions from different satellites. This technique is called code division multiple access (CDMA).

The C/A-codes are broadcast on L1 and are freely available to civilian users. They are drawn from the family of Gold codes, which have low cross-correlation between members, and are very short at 1023 chips: these properties make it easy for a receiver to acquire the signal. The rate of transmission infers a 1 ms period and 293 meter of wavelength.

The P-code is modulated on both L1 and L2 but is usually encrypted to form the P(Y) code, which is only available to military users. Since the C/A-code is not modulated on L2, it is not possible to obtain this code measurement directly on this frequency. The code and data signals are modulated on the carrier using binary phase shift keying (BPSK). The binary 0's and 1's of the code are represented by multiplying the carrier wave by +1 or -1 respectively, which is the equivalent of leaving the phase unchanged or changing it by 180°, as shown in Figure 2-1. The code and data are modulated together on the same carrier, within one data bit there are exactly 20 C/A-code periods. The data and code bit transitions coincide because the chipping rates of both of these binary codes are coherently related to the same fundamental clock frequency. L1 is modulated by both the C/A-code for civilian users and the P-code for military use.

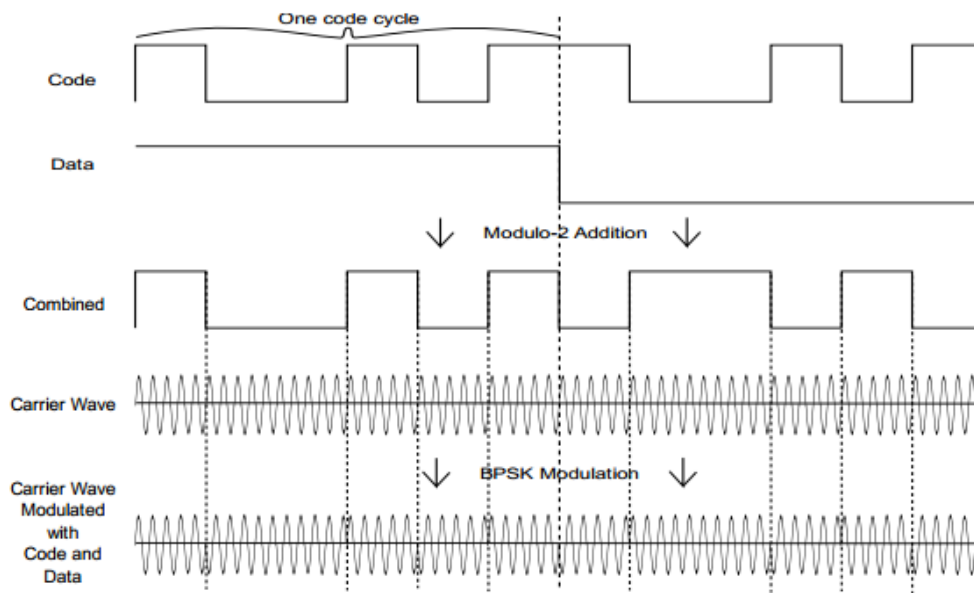


Figure 2-1. Binary phase shift keying modulation of code and data signals (Spilker, 1996)

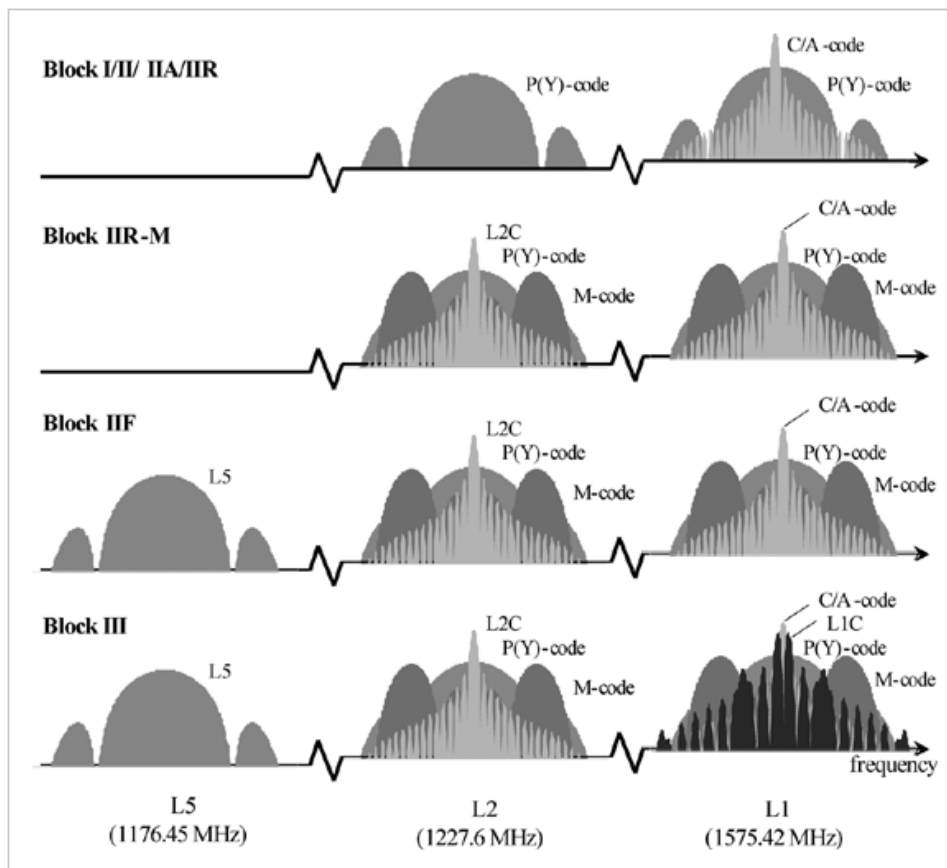


Figure 2-2. GPS signals present and future (Walter et al., 2008)

The next section describes the new civil codes transmitted by the modernized GPS satellites.

### 2.1.1 L2C GPS

Another already available modernized GPS signal is a civil signal on L2, called L2C. There are currently 12 IIR-M and 10 IIF satellites broadcasting L2C, with more being launched as old satellites are decommissioned. The structure of this new signal is specified in IS-GPS-200D. In addition to the new civil signal, the military P(Y)-code will be retained until 2020 and the new military M-code will also be transmitted.

There will be two new sets of PRN codes, time division multiplexed (TDM) chip-by-chip on the quadrature component of the carrier. The first code, Civil Moderate (CM), has a length of 10.230 chips, while the second, Civil Long (CL) has a length of 767.250 chips. The increased length over the C/A-code improves cross-correlation performance: the worst-case cross-correlation performance of the L2C codes is 45 dB, compared to 21 dB for C/A codes.

Both codes (CM, CL) are of even length and perfectly balanced, i.e. sum to exactly zero. This allows the receiver to track each code separately by assuming the bits of the other code average to zero. The chip length is the same for each code, so the signal power is evenly divided; tracking only one code gives a 3 dB power reduction. The minimum received power from the IIR-M and IIF satellites will be -160 dBW, with the civil signal 0-4 dB weaker than the military signal. Overall, L2C will be 2-3 dB weaker than the C/A-code on L1.

The chipping rate and modulation type of the L2C codes is the same as the C/A-code, producing a similar frequency power spectrum. The L2C codes are much longer than the C/A-codes, so the maximum lines have less power, which greatly increases robustness to narrow band interference.

The CL code is a pilot component, which provides a 6 dB improvement to phase tracking threshold. Each code is transmitted at a rate of 511.5 kcps, so the overall speed of the complete TDM L2C signal is the same as the C/A-code at 1.023 Mcps. The clock rate was limited to maintain spectral separation between the civil code and the new military M-code. The CM code have a duration of 20 ms and the CL code 1.5 s, so there are 75 repetitions of the CM code within every CL code cycle.

The length of the CL code is such that it would be very difficult to acquire it directly, so in normal operation the CM code would be acquired using a Costas loop. The receiver could then rapidly search the 75 possible time offsets between the two codes and lock on to the CL code. However, in a difficult environment where acquisition of the CM code is impossible, the CL code could be acquired directly due to its increased length and lack of data modulation. Once the receiver has acquired the CL code from one satellite, the range of possible offsets of this code from the other satellites is limited by the difference in signal travel time from the zenith to the horizon, around 18.7 ms. This

gives a search range of around 19.130 chips, which is about twice the length of the search range for the CM code. It is therefore much easier to acquire the CL codes from subsequent satellites directly. There is little advantage to be gained by tracking both CM and CL codes (Fontana et al., 2001).

### 2.1.2 L5 GPS

The third modernized GPS signal transmitted by the IIF satellites is a completely new signal at L5, with a central frequency of 1176.45 MHz. This is within a protected Aeronautical Radio navigation Service (ARNS) band and is intended for use as a safety-of-life system. This frequency band is also used by aircraft navigation services, such as DME, TACAN and JTIDS, so the noise floor will frequently be higher than the thermal noise. This is compensated for by the high received power of the L5 signal of -154 dBW. The characteristics of this signal are very similar to those of Galileo E5a, with the same code length, code rate, chipping rate and use of tiered codes.

The signal is composed of two QPSK-modulated components with 50% power to each. These components are modulated by unique PRN codes which are broadcast at a rate of 10.23 Mcps, ten times the rate of the L1 C/A and L2C codes. This means that the null-to-null transmitted bandwidth is also ten times greater at 24 MHz, which improves tracking precision and robustness to multipath and RFI, at the expense of increased receiver cost and power usage.

The in-phase component is modulated by a PRN code of 10,230 chips, so the duration is the same as the C/A-code at 1 ms. It is additionally overlaid by a 10-chip long Neumann-Hoffman (NH) code of duration 10 ms, where each chip of the NH code multiplies one whole length of the PRN code. This overlay code improves the cross-correlation properties of the combined code, but the tiered nature allows the receiver to acquire the shorter code before switching to the combined code for tracking. The PRN code is ten times the length of the C/A-code, but the better cross-correlation properties give a four-fold decrease in dwell-time at each potential offset, which mitigates the increase in acquisition time.

The NH code also has the effect of reducing the spacing between the lines in the signal power spectrum from 1 kHz to 100 Hz, which reduces the effect of narrow band RFI. The NH codes also help to increase the robustness of the data bit synchronization, because they are synchronized with the navigation bits. This component of the signal is also modulated by a data channel, at a rate of 50 bps, FEC (1/2) is applied, and hence the data message is transmitted at 100 cps. The FEC provides a 5 dB improvement in the data demodulation threshold.

The quadrature component consists of a different PRN code of the same 10.230 chip length modulated by a 20-chip Neumann-Hoffman sequence. This is a pilot component,

hence is not modulated by a data message. The line spacing in the signal power spectrum for this component is even less at 50 Hz, which further improves the resistance to narrowband RFI. Both of these codes have very low cross-correlation: the quadrature codes are -57 dB or less. Because the codes on each component of the carrier are different, there is a 2 dB improvement for tracking them both at the same time.

### 2.1.3 L1C GPS

The future stages in GPS modernization are the Block III satellites which will feature a new code on L1 and increased transmission power. The L1 band is centered at 1575.42 MHz, which has the advantages of being the GNSS frequency least affected by ionospheric refraction and also within an ARNS protected band. On 26th June 2004, The US and EU signed the "*Agreement on the promotion, provision and use of Galileo and GPS satellite-based navigation systems and related applications*" to ensure the compatibility and interoperability of GPS and Galileo. Part of the agreement was that each system would adopt a signal on L1 with an identical power spectral density (PSD) when computed using all the components of the signal. Initially it was intended to use a BOC (1,1) modulation scheme, but a joint research group has subsequently identified and recommended another candidate modulation scheme, Multiplexed BOC (MBOC), with superior properties as outlined. MBOC is defined in the frequency domain as the sum of 10/11 of the normalized BOC (1,1) PSD and 1/11 of the normalized BOC (6,1) PSD placing some of the signal power into a higher-frequency code improves signal tracking performance and multipath mitigation. This frequency-domain definition of the shared signal allows different implementations in the time domain: L1C will use Time Multiplexed BOC (TMBOC) to achieve the required PSD.

The C/A-code will continue to be broadcast on L1 for backward compatibility, so the GPS III satellites will modulate the C/A, L1C, P (until 2020), and M codes on the same carrier. The technique for doing this has not yet been determined, but will be flexible, with the phase relationship contained in the broadcast navigation message.

The modulating codes have a length of 10.230 chips and are based on Weil sequences; the chipping rate is 1.023 Mcps and the period is 10 ms. The code with the best correlation properties were allocated the pilot component, as code acquisition and tracking will generally be performed on the pilot signal due to the power division. Each pair of pilot/data codes were chosen to have low correlation at zero offset. Each pilot component is additionally modulated by a unique 1,800 chip secondary code at a rate of 100 cps, with duration 18 seconds. This code is modulo-2 added to the spreading code, with each bit of the overlay code applied to a whole cycle of the spreading code, these codes reduce cross-correlation and aid in synchronization to the data message boundary.

## 2.2 The Galileo System

The Galileo system will consist of up to 30 satellites in three circular orbital planes with a semi major axis of about 29600 km and an inclination of  $56^\circ$  with respect to the equator. There will be freely accessible civil signals overlaid on the GPS L1 and L5 frequencies, with very similar characteristics to the GPS signals, called E1 and E5a (Serrano, 2013). In addition there will be another civil signal, E5b, adjacent to E5a at 1207.14 MHz, and an encrypted commercial signal, E6 (not be described here). Galileo does not offer a signal on the current GPS L2 band.

The Galileo system will provide three different services for positioning:

- The Open Service (OS) will use E1, E5a, and E5b and will provide unencrypted data and ranging signals.
- The Commercial Service (CS) will use E1, E5b and E6. Additional data supporting high accuracy positioning and authentication will be transmitted to users. This data will be encrypted and users will have to pay to access it.
- The Public Regulated Service (PRS) will be used by governments and will be transmitted on E1 and E6.

Galileo is designed to be compatible and interoperable with GPS. This section will describe the signal structure of the open service signals. There are currently 7 active Galileo satellites in orbit (3 operational IOV plus 4 FOC) although 2 FOC satellites did not reach their nominal orbits due to a launch failure.

### 2.2.1 E1 Galileo

The Galileo carrier at E1 is modified hexaphase modulated by three signals. There is a military signal (E1a) and two civil components: a data component (E1b) and a pilot component (E1c). As discussed before, due to the agreement between the EU and the US, Galileo E1 and GPS L1C will both use Multiplexed BOC (MBOC), which is defined in the frequency domain as the sum of  $10/11$  of the normalized BOC(1,1) PSD and  $1/11$  of the normalized BOC(6,1) PSD. E1 will use a different modulation scheme to L1C to achieve the MBOC PSD: Composite BOC (CBOC). In this modulation scheme, the BOC(1,1) and BOC(6,1) sub-carriers are linearly combined, and both are present at all times. The use of a different modulation scheme to L1C may complicate receiver design (Julien et al., 2004).

The modulating codes are the same length as L1C at 10.230 chips and the same speed at 1.023 Mcps, but are based on random or memory codes rather than Weil codes. These codes have been designed to achieve the best properties for a given length, and allow more flexibility than conventional codes. They are not generated onboard the satellite in the manner of conventional codes, but rather are stored in memory chips. This allows more flexibility in code design, and has been made possible because of the falling cost of such chips.

The main difference between the GPS L1 and Galileo E1 signals, apart from the different modulation schemes, stems from the provision of encrypted data on the Galileo E1 signal. E1 has a greater proportion of power to the data component (50%, compared to 25% for GPS) and a much higher data rate (250 sps compared to 100 sps). Most receivers will acquire the E1 carrier using only the pilot component, because the high data rate limits the coherent integration time to only 4 ms on the data signal, compared to 10 ms for the C/A-code.

### 2.2.2 E5 Galileo

The Galileo E5 codes are modulated on the carrier using AltBOC modulation, each of the two side-lobes of the BOC modulation has a different code and so can be tracked separately. These two codes are called E5a and E5b, and taken individually are effectively a BPSK (10)-modulated code, with a primary code length of 10.230 chips and a chipping rate of 10.23 Mcps. These codes are overlaid by a longer secondary code and the power is evenly divided between pilot and data components in phase quadrature. When tracked individually, they are very similar in structure and characteristics to GPS L5; the central frequency of E5a is identical to L5 and hence is interoperable without the need for additional front-end hardware. E5a supports the OS and transmits the F/NAV basic navigation message, while E5b supports the OS and CS service and transmits the I/NAV integrity message and encrypted commercial data. The E5b data message is transmitted at 250 cps, compared to 50 cps for E5a. Both of these signals are in the ARNS band, so will be suitable for use in safety-critical applications in conjunction with E1. The greatest advantage of Galileo E5 is realized when E5a and E5b are tracked coherently as a single wide-bandwidth signal. The wide bandwidth produces low code noise and has good potential for advanced multipath mitigation techniques. Moreover, E5a and E5b allow generating ultra wide-lane signal linear combinations.

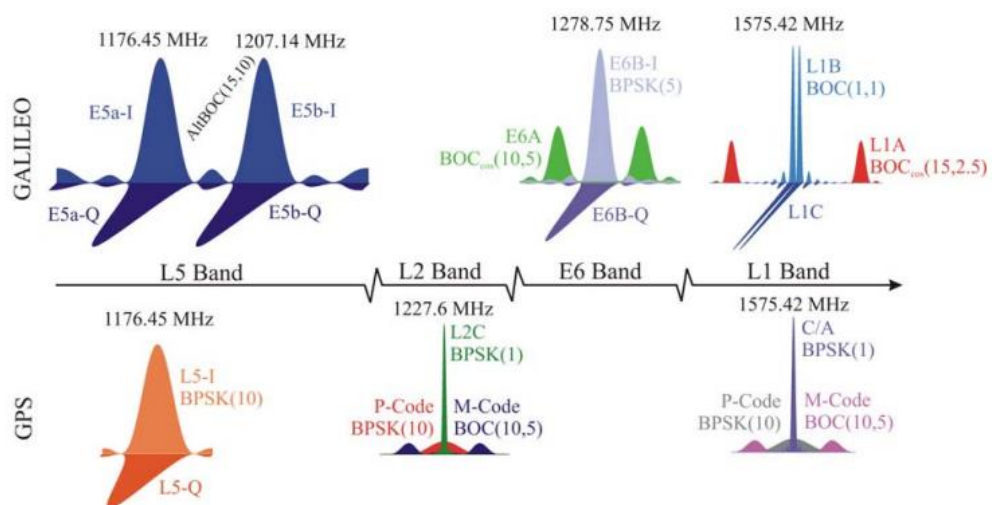


Figure 2-3. Power spectral of Galileo (Wallner et al., 2005)



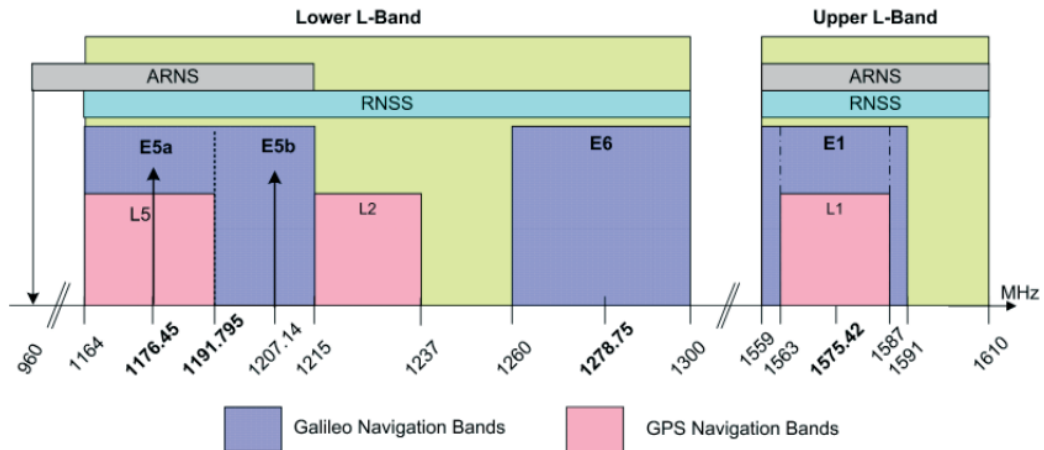


Figure 2-4. Power Spectral and Signal Density of Galileo (European GNSS-Galileo open service, 2010)

## 2.3 Interoperability

Interoperability refers to the ability of GNSS's to be used together or independently without interfering with each other. The methodology for determining the GPS/Galileo radio frequency compatibility was specified as part of the US/EU agreement in 2004 ("Reference assumption or GPS/Galileo compatibility analyses"). The worst-case interference, of GPS L5 on Galileo E5a, is predicted to be 0.6 dB (Wallner et al., 2005). Inter-system interference will be almost undetectable under real conditions. Interoperability refers also to the ability of GNSSs to be used together to provide superior capabilities than each system alone. Interoperability is most important in processing areas dealt with by hardware, where differences significantly increase the cost of using multiple systems. GPS and Galileo will transmit signals with the same central frequency and similar signal structure at L1/E1 and L5/E5a, so it will be easy to track both systems at this frequency; L2 and E5b are not interoperable, because there is no corresponding signal from the other system. The two systems use a different data message structure, but the decoding of this is done in the software and so will have less impact on interoperability.

In contrast, Glonass currently transmits two signals using frequency division multiple access (FDMA) where every satellite transmits on a slightly different central frequency. In the process of waiting for Glonass's CDMA system to become active, interoperability between GPS and Glonass is more complicated and consequently more expensive to achieve, although many modern high-end receivers use both GPS and Glonass. From 2014 onward, Glonass is testing a CDMA signal service broadcasted by its K-type space vehicle services.

### 2.3.1 Reference Frames

Many reference systems and frames have been introduced and made available to users. Examples are WGS-84 and GTRF (as prototype) used by GPS and Galileo respectively for

the broadcast ephemerides. The International Terrestrial Reference System (ITRS) has been established by the International Earth Rotation and Reference Systems Service (IERS). The ITRS realization (ITRF) is frequently updated according to the new data obtained from various geodetic observation systems, thus producing a time series of reference frames. The transformation from one reference frame to another is generally accomplished with a seven-parameter transformation. All present GNSS utilize a more or less close realization of the most recent ITRF.

### 2.3.2 Navigation Message

The modernized signals feature improved navigation message design, both in terms of the structure of the message and the method of transmission. The result is that the data messages can be demodulated at lower  $S/N_0$  levels and the receiver time-to-first-fix is reduced. Forward error correction (FEC) is applied, which adds redundancy to the data transmission and allows the receiver to correct for lost data bits. The data rate is less than the symbol transmission rate, so the data are transmitted more slowly but can be read at a 5 dB lower  $S/N_0$  with the same success rate. Some of the new signals also use block interleaving of the message frames, where the order of data transmission is scrambled, so a burst error does not cause the loss of all data symbols relating to a data bit. However, this causes latency in the data transmission (Luo et al., 2009).

The data rate varies considerably across the new signals. Low data rates are used to improve reception and data demodulation threshold in low  $S/N_0$  environments, while some signals carry high-rate data in order to guarantee the rapid reception of safety-of-life information or to provide encrypted commercial data. The original GPS navigation message modulated on the L1 C/A-code is termed NAV. A new message structure has been designed for use on L2C and L5, called CNAV. This is more compact and flexible than the original NAV message, and the sequence and timing of each component can be specified by the control center. FEC is applied, but not block interleaving. The message structure for L1C will be a further improved design and is termed CNAV-2. The data are divided into fixed (slowly changing) data, such as clock and ephemeris data, and variable data. The broadcast message then defines a period of time over which the fixed message data do not change, allowing the receiver to perform data-wiping on this portion of the message. CNAV-2 will feature a more powerful FEC and block interleaving.

For Galileo there will be three different types of Galileo navigation messages:

- F/NAV, a freely accessible navigation message provided by the E5a signal for the Open Service.
- I/NAV, an integrity navigation message provided by E5b and E1b signals.
- C/NAV, a commercial navigation message type provided by the E6 signal.

### 2.3.3 Time Systems

GPS time (GPST) is steered towards Coordinated Universal Time (UTC), Galileo System Time (GST) will be steered towards International Atomic Time (TAI). By definition, there is an integer number of seconds offset between UTC and TAI. However, even after this has been accounted for, there will still be a difference of the order of tens of nanoseconds between GPST and GST (Moudrak et al., 2004), which will introduce a bias into the combined positioning solution. There are several ways to solve this problem:

The time offset can be computed as an extra parameter in the receiver. This reduces the redundancy of the positioning solution and will therefore reduce the benefit derived from the second system in difficult environments where few additional satellites are visible. However, the time offset only changes slowly, so a previously computed time offset can be used during periods when few satellites are visible.

The uncertainty offset between TAI representations derived from GPS and Galileo broadcast (GPS UTC and Gal UTC respectively) can be expected to be within 28 ns (95%). The GPS-Galileo time offset (GGTO) will represent an important issue for GPS-Galileo interoperability, since it will cause a bias between measurements in combined GPS/Galileo receivers. The characteristics of GPS Time and requirements to GST are summarized in Table 2-1.

Table 2-1. GPS Time and GST (Moudrak et al., 2004)

Property	GPS Time	GST
Type of time scale	Composite clock: average of GPS clocks computed in a Kalman filter	Master clock: steered active H-maser
Produced at	Computations performed at the Master Control Station	Physically produced at Galileo PTF
Access outside the system	Through broadcast corrections to satellite clock	Through direct time transfer or through broadcast corrections to satellite clocks
Steering to TAI	Through USNO	Through time service provider combining several UTC laboratories
Offset from TAI	14 ns	50 ns (95% requirement)
Uncertainty of TAI offset	~9 ns	28 ns (95% requirement)

It has been agreed that GPS and Galileo will broadcast the GPST-GST offset in the navigation message. Applying this correction will reduce the error, but a bias will still remain due to the uncertainty of the correction: this can be solved for as an additional parameter if sufficient satellites are visible and an external provider such as the IGS might compute the clock parameters for GPS and Galileo with respect to a common time scale, therefore eliminating the time offset problem (Moudrak et al., 2004). These products could be available in real time.

## 2.4 Absolute Positioning

In GNSS positioning the basic observable is the distance between the GNSS receiver and the GNSS satellites. Once the distance is determined, the position can be calculated from the “known” position of the satellites as provided by broadcast ephemeris.

This is illustrated in equation (2.1) where  $dist$  is the distance between the receiver and satellite.  $X_{sv}, Y_{sv}, Z_{sv}$ , denotes the position of the satellite,  $X_{rec}, Y_{rec}, Z_{rec}$ , is the position of the receiver, and  $dT$  is the receiver clock offset to GNSS-time, which is explained below, and  $c$  is the speed of light:

$$dist = \sqrt{(X_{sv} - X_{rec})^2 + (Y_{sv} - Y_{rec})^2 + (Z_{sv} - Z_{rec})^2} + c \cdot dT \quad (2.1)$$

With four distances to four different satellites, a set of equation can be established for every epoch and the four unknowns can be estimated. In practice several satellites are observed at the same time whereby it is possible to perform a least squares adjustment after linearization of the observation equations. Systematic signal delays as well as noise from the GNSS receiver itself and from the environment surrounding the GNSS antenna can affect the positioning performance.

## 2.5 Differential Positioning

To obtain positions with improved accuracy, a relative differential technique has to be applied where at least two GNSS receivers are employed. One receiver is located at a reference point with known coordinates and the other receiver, the rover, is located at a point (or moving between points) with unknown coordinates. The position of the rover is then determined relative to the reference point. This can be carried out in real time, utilizing a data link, or in a post processing mode where data is logged by the receivers and processed with software afterwards.

### 2.5.1. Carrier phase observations and error sources

In carrier phase based GNSS positioning, the receiver satellite distance is determined by the carrier wave. In order to use the carrier it must be recovered from all the noise received with the GNSS signals, and also modulated code must be removed before the carrier can be tracked. The actual carrier phase measurement is the difference between the receiver and recovered carrier wave, and a receiver generated copy of the signal. The distance to the satellite can be determined as the full number of cycles between the satellite and the receiver, plus the fractional part of a cycle. When the receiver has locked on to a satellite signal it starts counting the full number of cycles received. The equation below shows the relation between the measured phase (fractional part and counted number of full cycles),  $\Phi$ , and the intended geometric range to the satellite,

$$\Phi = r + dr - d_{ion} + d_{trop} + c(dt - dT) + \lambda N + \varepsilon \quad (2.2)$$

where  $r$  denotes the geometric range (receiver satellite) in meters,  $dr$  is the satellite orbit error in meters,  $d_{ion}$  is the ionospheric signal delay in meters,  $d_{trop}$  is tropospheric delay signal in meters,  $c$  is speed of light given in meters/sec,  $dt$  and  $dT$  are the errors of the satellite and receiver clocks respectively, both given in seconds,  $\lambda$  is the wavelength,  $N$  is the ambiguity (the initial number of cycles), and  $\varepsilon$  is multipath and noise, also given in meters.

The ambiguity is the initial number of cycles i.e. the number of cycles between the satellite and receiver at the initial measurement epoch before the receiver has started counting the number. However, the ambiguity cannot be converted to the receiver-satellite distance by just multiplying with the wavelength, because the ambiguity also contains a receiver dependent oscillator offset and  $N$  in the equation is therefore not necessary a positive integer value as it intuitively would look like. The challenge in connection with carrier phase based positioning is to solve the ambiguous number of cycles. Hence, the distance to the satellite can be determined.

Equation (2.2) indicates that the geometric distance, the ambiguities, and all the errors in the system add up to the observed phase, considering the sign of the various factors. If the influence of the error sources can be minimized, it will be easier to determine the ambiguity and thereby also the distance to the satellite.

### 2.5.2 Double Carrier Linear Combinations

Range errors remaining in differential carrier-phase observations are the inaccuracy in the satellite position and the effect of the atmosphere. These errors are spatially correlated, so when the distance between the two receivers increases, the influence of the errors becomes significant. If the two receivers are located close to each other (closer than 15 km), the influence of the atmospheric error will be almost the same for the two receivers since the signals are transmitted through basically the same parts of atmosphere.

For differential positioning, observation data from at least two receivers and four satellites at the same time epoch in time must be available. The equation can be generated for each receiver-satellite combination, and the observation equations can be differenced. The first step is to generate a single difference equation, i.e. the difference between observation equations for two receivers,  $A$  and  $B$ , observing the same satellite,  $i$ ,

$$\Delta\Phi_{AB}^i = \Phi_A^i - \Phi_B^i \quad (2.3)$$

$$\Delta\Phi_{AB}^i = \Delta r_{AB}^i + \Delta dr_{AB}^i - \Delta d_{ionAB}^i + \Delta d_{tropAB}^i + c(dT_B - dT_A) + \lambda \Delta N_{AB}^i + \Delta \varepsilon_{AB}^i \quad (2.4)$$

$\Delta$  Indicates single difference, the subscript denotes receivers, and the superscript denotes satellites. With single differencing, the satellite clock error cancels out, because it will have the same effect for signals received by both receivers. The influence of the spatially correlated errors is also reduced as noted in equation 2-4.

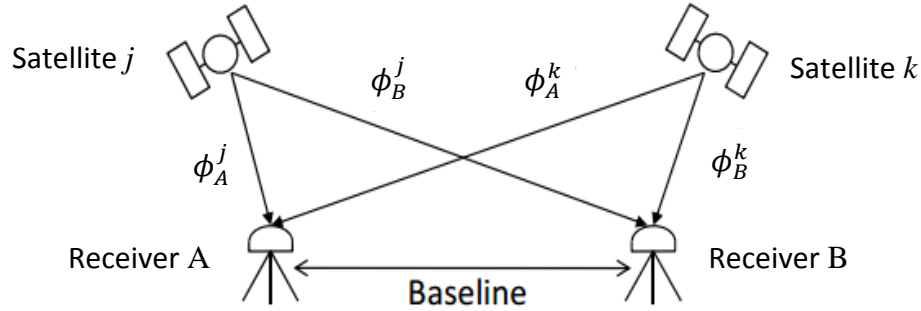


Figure 2-5. Double Difference Observations

The next step is to generate the difference between two single differences i.e. a double difference, where observations from a second satellite,  $j$ , are introduced.

$$\nabla\Delta\Phi_{AB}^{ij} = \Delta\Phi_{AB}^i - \Delta\Phi_{AB}^j$$

$$\begin{aligned} \nabla\Delta\Phi_{AB}^{ij} = & (\Delta r_{AB}^i + \Delta dr_{AB}^i - \Delta d_{ionAB}^i + \Delta d_{tropAB}^i + c(dT_B - dT_A) + \lambda\Delta N_{AB}^i + \Delta\varepsilon_{AB}^i) \\ & - (\Delta r_{AB}^j + \Delta dr_{AB}^j - \Delta d_{ionAB}^j + \Delta d_{tropAB}^j + c(dT_B - dT_A) + \lambda\Delta N_{AB}^j + \Delta\varepsilon_{AB}^j) \end{aligned}$$

$$\nabla\Delta\Phi_{AB}^{ij} = \nabla\Delta r_{AB}^{ij} + \nabla\Delta dr_{AB}^{ij} - \nabla\Delta d_{ionAB}^{ij} + \nabla\Delta d_{tropAB}^{ij} + \lambda\nabla\Delta N_{AB}^{ij} + \nabla\Delta\varepsilon_{AB}^{ij} \quad (2.5)$$

Now also the receiver clock errors have canceled out, the size of  $dr$ ,  $d_{ion}$ , and  $d_{trop}$  is further reduced. For baseline shorter than about 15 km these errors generally cancel out. Omitting the receiver and satellite identifiers, the final double difference expression reads,

$$\nabla\Delta\Phi = \nabla\Delta r + \nabla\Delta dr - \nabla\Delta d_{ion} + \nabla\Delta d_{trop} + \lambda\nabla\Delta N + \nabla\Delta\varepsilon \quad (2.6)$$

The double difference ambiguity is a integer number since the initial receiver phase offset has been eliminated through the double differencing process. In order to obtain position accuracies of a few cm or mm, the correct integer number for the double differenced ambiguity must be determined. This can be a complicated task, but several ambiguity resolution techniques do exist, see for example Frei and Beutler (1990) for the FARA method (Fast Ambiguity Resolution Approach), Teunissen (1993) for the LAMBDA method (Least Square Ambiguity Decorrelation Adjustment). Further methods developed are noted in figure 2-6.

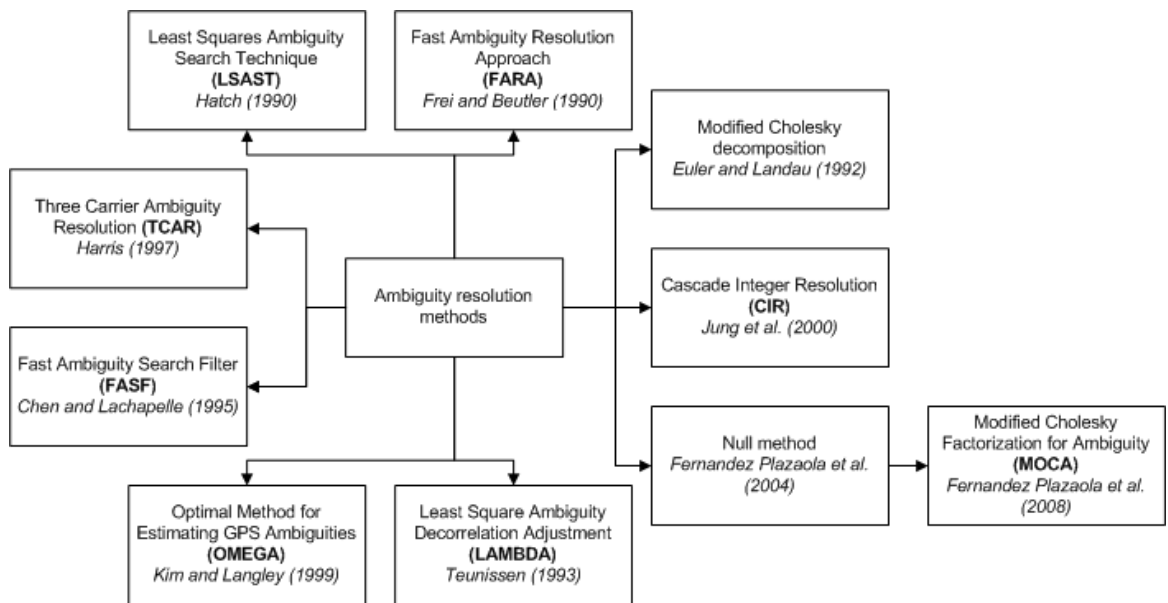


Figure 2-6. Illustration of ambiguity resolution methods (compiled from several sources)

When the correct integer numbers for the ambiguities have been determined, the ambiguities are said to be fixed. If the ambiguity resolution process is not successful, the ambiguities might be fixed to wrong integer numbers, which is in general difficult to discover once it happens in the positioning process. The ambiguities can be also retained as real numbers whereby said to be floating since the constraint introduced by fixing them to integer numbers, is removed.

A position determined on float ambiguities has been very unreliable since all unmodeled errors in the positioning process will propagate into floating ambiguities. However, if a satellite is observed without interruption for longer time intervals, if the noise level in general is low, and if no sudden changes in the receiver-satellite geometry occur, then the floating ambiguities will converge towards the correct integer number, and the accuracy of the resulting position can be as good as a few cm or even better.

## 2.6 GNSS Error Sources

Aside from the effects of the ionospheric bias that will be discussed in detail in the following chapter, also other significant error sources are present in GNSS. The most important of these are outlined below along with methods to mitigate them.

### 2.6.1 Ephemeris Errors

Ephemeris errors are uncertainties in the broadcasted satellite position in space. These uncertainties are then transmitted and used in calculations by the receiver on the ground for position solutions and therefore reduce the quality of the positioning result.

Normally, these errors in the predicted satellite position are in the order of a few meters or less. In single positioning (SPS) the discrepancy is still relatively minute considering the orbital perturbations of the GPS satellites are extremely difficult to measure and predict and often only produce an error on the ground of  $\pm 2.5$  meters or less in field applications (Leick, 2004). However, users are able to acquire precise ephemeris data, for example from IGS (the quality of few cm level) of the actual tracked satellite orbits for use in post processing of the data in office applications. Nowadays also real-time precise orbit information has been made available by various organizations.

### 2.6.2 Satellite Clock Errors

GNSS operates with its own time scale, which is referred to as GNSS time. This time system is based on an atomic time scale, and is in reference to Coordinated Universal Time (UTC). Sources of the clock errors can be due to drifts in either the satellite or receiver oscillators. Errors due to the satellite clock are the offset between the satellite clock and the GNSS system time. This offset arises from the instabilities of the GNSS satellite oscillators. Errors due to the satellite clock are generally less than 1 ms and can be eliminated by differencing the observations between two different receivers with respect to the same satellite (IGS, 2001).

Naturally, any errors in the satellite clock corrections will introduce errors into the position calculated. These errors can contribute up to and around a  $\pm 2$  meters shift in position (Leick, 2004). These errors are also common to all users observing the same satellite and can be removed through differencing between the receivers.

The satellite clock correction is reflected by the broadcast coefficients as part of the navigation message with a typical accuracy in the range of 5 ns. The satellite clock error also can be estimated more accurately and provided by the IGS network. The predicted clock errors by IGS are accurate to 3 ns over 12 hours, which is equivalent to 90 cm in range (IGS, 2002). The accuracy of the computed precise clocks in post-mission by IGS can be accurate to 0.1 ns, which is 3 cm in range (IGS, 2002). The offset between the receiver clock and the GNSS system time produces the receiver clock error. Temporal variations of this error depend on the type of receiver oscillator. The magnitude of the receiver clock error ranges from 200 ns to several ms and depends on the receiver internal firmware (IGS, 2002). It can be eliminated by differencing the observations of the same receiver between two different satellites.

### 2.6.3 Troposphere

Satellite signals travel through the atmosphere which affects the state of the signals. These are divided into two effects, tropospheric and ionospheric. Each effect influences the satellite signals differently. The lowest region of the atmosphere, extending to a maximum of about 16 km above the earth's surface, is known as the troposphere. The



neutral atmosphere may be considered to include the stratosphere, extending the altitude of the area considered to approximately 50 km (Brunner and Welsch, 1993). However, since the majority of the neutral atoms and molecules are located below 16 km it is usual to refer to the delay induced as the tropospheric delay. This area of the atmosphere is electrically neutral and is non-dispersive at GNSS frequencies. Since the troposphere is a non-dispersive medium for microwaves, tropospheric refraction causes an identical effect on both code and phase modulation. The troposphere causes a signal delay of up to 2.5 m in the vertical direction and up to 30 meters for a horizontal signal path (Hofman-Wellenhof, 2001). Therefore, the effect from the troposphere is considered one of the major sources of errors imposed on the satellite signals.

The neutral atmosphere can normally be divided into two components, the hydrostatic (dry) and wet portions of the troposphere. The hydrostatic component consists of mostly dry gases (normally referred to the dry part), whereas the wet component is a result of water vapor. The hydrostatic fraction contributes approximately 90% of the total tropospheric refraction (Leick, 1995). For high accuracy positioning, correcting the delay of radio signals as they traverse the neutral atmosphere is necessary.

Generally speaking, the tropospheric delay depends on temperature, pressure, humidity as well as the location of the GNSS antenna. The tropospheric delay can be written as (Xu, 2007):

$$\delta = \int (n - 1) ds \quad (2.7)$$

where  $n$  is the refractivity index of the troposphere. The integration is along the signal transmitting path, simplified as the geometric path. Scaling of the refractivity index is made by,

$$N^{trop} = (n - 1) \cdot 10^6 \quad (2.8)$$

where  $N$  is called tropospheric refrativity.  $N$  can be separated into wet (10%) and dry (90%) parts:

$$N^{trop} = N_w^{trop} + N_d^{trop} \quad (2.9)$$

Therefore the tropospheric delay can be rewritten as:

$$\delta = 10^{-6} \int_{path} (N_d^{trop} + N_w^{trop}) ds \quad (2.10)$$

$$\delta = 10^{-6} \int_{path} N_d^{trop} ds + 10^{-6} \int_{path} N_w^{trop} ds \quad (2.11)$$

$N_d^{trop}$  and  $N_w^{trop}$  correspond to tropospheric refractivity of the hydrostatic and the wet

components. In 1974, Thayer expressed the refractivity  $N_T$  in terms of absolute temperature and partial pressure of the dry gases ( $P_d$ ) and of water vapor pressure ( $e_0$ ) (e.g., Mendes, 1999):

$$N_T = K_1 \frac{P_d}{T_0} Z_d^{-1} + \left[ K_2 \frac{e_0}{T_0} + K_3 \frac{e_0}{T_0^2} \right] Z_w^{-1} \quad (2.12)$$

The constant coefficients  $K_1$ ,  $K_2$ , and  $K_3$  are empirically determined.  $T_0$  is absolute temperature in Kelvins at the tracking station.  $Z_d$  and  $Z_w$  are corresponding compressibility factors for dry air and water vapor, which account for the departure of the air behavior from that of the ideal gas and rest on the partial pressure due to dry gases and temperature. The first term on the right side of equation (2.12) refers to  $N_d^{trop}$ , whereas the terms in brackets refer to  $N_w^{trop}$ . The frequently used sets of refractivity constants are given in Table 2-2.

Table 2-2. Frequently used refractivity constants (Langley, 1996)

Refractivity coefficients	Smith and Weintraub [1953]	Thayer [1974]
$K_1$ (K/mb)	77.61±0.01	77.604 ± 0.014
$K_2$ (K/mb)	72 ± 9	64.79 ± 0.08
$K_3$ (K <sup>2</sup> /mb)	(3.75 ± 0.03) 10 <sup>5</sup>	(3.776 ± 0.004) 10 <sup>5</sup>

Normally the wet and dry refractions are related to the refraction of a particular elevation angle by the mapping function. Much research has been focused on modeling water vapor content. The water vapor pressure  $e_0$  can be calculated from a priori knowledge of environmental information such as relative humidity and temperature at the tracking station. Water vapor pressure in millibars is modeled as recommended in the IERS Conventions (1996) is,

$$e_0 = 0.0611RH 10^{\frac{7.5(T_0-273.15)}{237.3+T_0-273.15}} \quad (2.13)$$

where RH is the relative humidity at the observing station in percent.

To model the troposphere delay directly along the signal path, various tropospheric models such as Saastamoinen, Hopfield, have been developed to approximate the integrated tropospheric delay. In general, surface meteorological parameters, such as pressure, temperature, and humidity are required input for these models.

The hydrostatic delay can be modeled with an accuracy better than 1%, where in some cases temperature, and hydrostatic equilibrium is assumed. The zenith wet delay contributes to about 10% of the total delay, but cannot be modeled exactly. The wet component depends on water vapor, which is highly variable with space and time.

A modified Saastamoinen model reads (Shrestha, 2003, Victoria, 2005),

$$\delta = \frac{0.002277}{\cos z} \left[ P + \left( \frac{1255}{T} + 0.05 \right) e - B \tan^2 z \right] + \delta R \quad (2.14)$$

where  $z$  is the zenith angle of the satellite,  $T$  is the temperature at the station in Kelvin unit,  $P$  is the atmospheric pressure in millibar unit,  $e$  is the partial pressure of water vapor in millibar,  $B$  and  $\delta R$  are the correction terms that depend on  $H$  and  $z$  respectively.  $H$  is the height of the station and  $\delta$  is the tropospheric path delay in meters. Finally,

$$e = R_h \exp(-37.2475 + 0.213166T - 0.000256908T^2) \quad (2.15)$$

where  $R_h$  is the relative humidity (in %) and the height dependent values of pressure, temperature, and humidity may be obtained by the equations,

$$P = P_o [1 - 0.000226 (H - H_o)]^{5.225} \quad (2.16)$$

$$T = T_o - 0.0065 (H - H_o) \quad (2.17)$$

$$R_h = R_{ho} \exp[-0.0006396(H - H_o)] \quad (2.18)$$

where  $P_o$ ,  $T_o$ ,  $R_{ho}$  are called standard pressure, temperature, and humidity at the orthometric reference height  $H_o = 0$  m. The values are dependent on the geographic position on the station. The remaining tropospheric delay can also be estimated as tropospheric parameters on top of an a priori model.

The Hopfield model (1969) can be expressed as the sum of two components (Ueno, 2001),

$$\Delta_d^{trop}(E) = \frac{10^{-6}}{5} \frac{77.64 \frac{P}{T}}{\sin \sqrt{E^2 + 6.25}} H_d^e \quad (2.19)$$

$$\Delta_w^{trop}(E) = \frac{10^{-6}}{5} \frac{-12.96T + 3.718 \cdot 10^5}{\sin \sqrt{E^2 + 2.25}} \frac{e}{T} \cdot 11000 \quad (2.20)$$

where  $H_d^e = 40136 + 148.72 (T - 273.16)$ ,  $H_d^e$  is the height above sea level, in kilometers. Most of the parameters are the same as in the formula of the Saastamoinen model.  $E$  is the elevation angle in degrees. The Hopfield model uses the refractivity constant from Smith and Weintraub (1953).

In summary, the tropospheric delays are not frequency dependent for the GNSS signals like ionospheric delays. Thus, the carrier phase and code measurement are affected by

the same delay. As a consequence, the tropospheric delays cannot be removed by linear combination of dual-frequency. To mitigate the tropospheric delays, a tropospheric correction model such as Saastominen or Hopfield can be applied to estimate the tropospheric correction from observation data. Fortunately, most of the delay comes from the predictable hydrostatic component and can be corrected in short- and medium-baseline calculations with an accuracy of centimeter to decimeter level.

#### 2.6.4 Ionosphere

This thesis's approach relies on the use of the frequencies used by Global Navigation Satellite Systems (GNSS), i.e. Galileo and modernized GPS for TEC reconstruction. As TEC is the key parameter for the mitigation of ionospheric effects on different space based systems, in particular on GNSS, a precise TEC reconstruction would allow to improve the precision and the reliability of many GNSS navigation and positioning techniques.

The ionosphere affects GNSS signals travelling through a dispersive atmosphere to the antenna. The effect inversely varies with the square of frequency of the signals. Having dual-frequency observations, ionospheric range errors can be removed to a large extent from observation data.

Ionospheric range delays are directly proportional to the total electron content (TEC), which varies along the transmission path and can be defined as:

$$TEC = \int_{path} N_e(s) ds \quad (2.21)$$

where  $N_e$  is the local electron density (electrons/m<sup>3</sup>). The TEC represents the total number of free electrons contained in a column with cross-sectional area of 1-square meter along the path of signal between satellite and receiver. The TEC is in units of  $el/m^2$ . The Total Electron Content Unit (TECU) is defined as  $TECU = 1.10^{16} el/m^2$ . Transforming the time delay of a code delay or the phase advancement to the corresponding distance (in meters), leads to:

$$I_{k,f,p}^p = \frac{40.28}{f^2} TEC = \frac{40.28}{f^2} \int_{path} N_e ds \quad (2.22)$$

$$= \frac{40.28 c}{f^2} \int_{path} N_e ds \quad (2.23)$$

The above equation is the ionospheric range delay or advance between receiver  $k$  and satellite  $p$  for the carrier frequency  $f$ ,  $c$  is the speed of light. The corresponding time delay or advance follows as:

$$v_f = \frac{I_{k,f,p}^p}{c} = \frac{40.3 TEC}{cf^2} \quad (2.24)$$

Whereas the first-order range error in GNSS applications can be completely eliminated by a linear combination of dual frequency measurements at the two frequencies, e.g. GPS L1 and L2, higher order terms of the refractive index  $n$  given in equation 2.25 cannot be mitigated in a linear approach (Warnant et al., 2009).

$$n \approx 1 - \frac{f_p^2}{2f^2} \mp \frac{f_p^2}{2f^3} \cos \theta - \frac{f_p^4}{8f^4} \quad (2.25)$$

Here  $f$  denotes the signal frequency,  $f_p$  the plasma frequency ( $f_p < 25$  MHz),  $\theta$  the angle between the Earth's magnetic field vector and the propagation vector.

Depending on information on the ray path geometry, the electron density distribution and the shape of the geomagnetic field it is possible to correct the higher order effects with an accuracy of about 1 mm. Yet, the knowledge of the actual electron density distribution is rather poor in operational GNSS applications. Thus, correction formulas taking into account the ionosphere could be of practical importance.

The correlation between the first, the second, and third order ionospheric error term for carrier phase measurements after applying appropriate scaling factors for each error term respectively can be written more compactly as (for details see Elmas et al., 2011),

$$\delta\rho = -Ion1 - \frac{Ion2}{2} - \frac{Ion3}{3} \quad (2.26)$$

$$Ion2\rho_{g,i} = \frac{\kappa e B_0 \cos \theta}{\pi m f_i^3} STEC \quad (2.27)$$

and,

$$Ion3\rho_{g,i} = \frac{3\kappa^2}{2f_i^4} \eta N_{max} STEC \quad (2.28)$$

$\rho_{g,i}$  is the total delay due to the ionosphere effect at the respective signal (i),  $\kappa$  is a constant (40.3),  $e$  is the electron charge,  $f$  is the signal frequency,  $N$  is the electron density along the signal path,  $B_0$  is the magnitude of the geomagnetic field at the ionospheric pierce point (IPP) where the signal penetrates the ionosphere,  $\theta$  is the angle between signal wave vector and geomagnetic field vector at the IPP, and  $\eta$  is shape parameter, which can be detailed as,

$$\eta = \frac{\int_{rec}^{sat} N^2 ds}{N_{max} \int_{rec}^{sat} N ds} \quad (2.29)$$

Converting (2.27) and (2.28) in meters reads:

$$d_{igr}^2 = \frac{11.28 \times 10^7}{f^3} TEC \quad (2.30)$$

$$d_{igr}^3 = (1602.81 N_m + 2.37 \times 10^{14}) \frac{TEC}{f^4} \quad (2.31)$$

with TEC in electrons/m<sup>2</sup>, f in Hz, N<sub>m</sub> is measured in e/m<sup>3</sup>, if the vertical TEC is known, N<sub>m</sub> can be calculated by the following expression (Hoque and Jakowski, 2007, 2012),

$$VTEC = 4.13 H N_m \quad (2.32)$$

where VTEC is TEC in vertical direction and H is the atmospheric scale height.

As more than two frequencies are available in modernized GPS or Galileo, higher order effects can directly be mitigated by using more frequency combinations. Although the standard dual frequency method is able to correct for the majority of the ionosphere induced delay or phase advance, the most accurate positional determination (1 cm accuracy or better) requires a more precise ionospheric correction.

By determining the higher order errors accurately for any GNSS satellite to receiver path, these errors can be subtracted from the total phase advance so that only the f<sup>-2</sup> (second term of ionosphere) dependence remains which can be eliminated using the dual frequency method. On the other hand, the f<sup>-3</sup> (third term of ionosphere) error is very small (less than 2 cm) and superimposed by a number of other error sources.

Chapter 5 will describe more detailed the ionosphere-free linear combinations that were applied in data processing.

### 2.6.5 Multipath

A multipath effect emerges when the transmitted signal is received by the GNSS receiver from more than one path (a direct or indirect path). This can result in an incorrect position calculation if proper planning or corrective techniques are not employed (Parkinson & Spilker, 1996). The multipath effect is often of most concern in urban environments or environments with highly reflective and elevated surfaces of which are easy for the signal to refract off.

The nature of the localized terrain determines the composition of the radio frequency environment. To understand this multipath environment, it is necessary to consider not only physical relationship of the GNSS receiver to the surrounding terrain but also the propagation of the terrain.

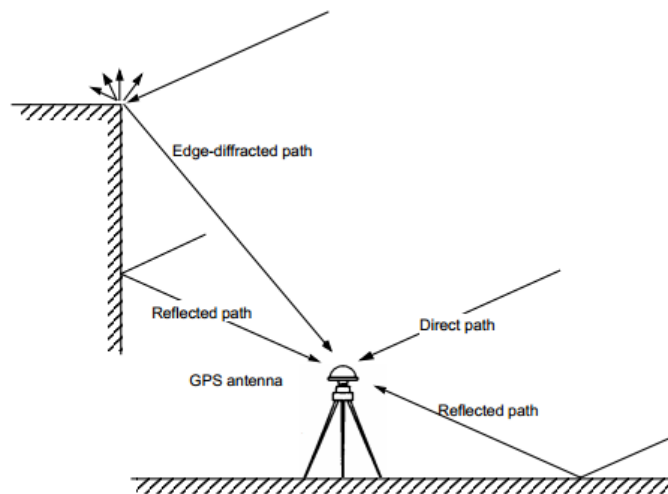


Figure 2-7. Multipath Environments (Hannah, 2001)

The term multipath obviously describes the separate propagation paths taken by reflected/diffracted signals. Since the multipath signals travel additional distances, they are delayed relative to the line of sight signal. In addition to the relative time delay, multipath is characterized by its amplitude, phase, and phase rate of change, all relative to the line of sight signal (Hannah, 2001). Multipath on code and phase degrades the performance of positioning, especially when using low elevation satellites. For phase measurements, the multipath errors contribute up to a quarter cycles ( $\approx 5$  cm) while for code this effect can cause range errors of tens of meters. A much more detailed discussion about multipath is provided in chapter 4.

#### 2.6.6 Antenna Phase Center Variation

The internal components of the GNSS equipment can also introduce an error into a position calculation in the area of a few centimeters (El-Rabbany, 2002). This error comes from the location offset between the geometric center of the GNSS unit and the electronic sensor within the device that actually receive the satellite signal. This is called the antenna phase center variation or PCV. This centimeter level systematic error can be eliminated by calibration of the GNSS control unit and software used to account for the offset.

The GNSS antenna phase center is neither a single well-defined physical point, nor stable spot, but rather varies with the changing direction of the incoming satellite signal. However, practically, users assume that the received signal point stays constant over the observation period, which is often referred to as the phase center of the antenna.

Dawidowicz (2010) experimented with a series of tests using baselines to study relative antenna phase center position with respect to the reference antenna. But, absolute antenna calibrations have not been clearly demonstrated. For very short baselines using identical antennas at the opposite ends, the phase center variations should cancel out and no effect is seen. On the other hand, when different antenna types are used and these variations are disregarded, the baseline solution will be the weighted average of the individual phase centers of the two antennas. Neglecting antenna phase center offset may infer significant vertical positioning errors of up to 10 cm and sub-centimeter in the horizontal. Normally, PCV is a function of both elevation and azimuth. However, it is not easy to model PCV variations due to high temporal correlation with signal reflection multipath and specific antenna. As a matter of simplicity by assuming azimuthal symmetry, one simple model is rather to assume that the phase center varies as a function of satellite elevation angle only.

#### 2.6.7 Phase Wind-up

The phase wind-up problem is associated with the antenna orientation, both at the satellite and at the receiver. This is due to the electromagnetic nature of circularly polarized waves intrinsic in the GNSS signals. Ideally, at the receiver the measured angle of carrier phase equals the geometric angle between the instantaneous electric field and a reference direction at the receiving antenna. Thus, when the antenna orientation changes, also measured phase changes. Likewise, the change of satellite antenna orientation changes the direction of the electric field at the transmitting antenna and, as a result, changes the measured phase at the receiving antenna.

Wu et al. (1993) derived formulas to account for the phase wind-up correction for a crossed dipole antenna. A crossed dipole antenna consists of two equal-gain dipole elements perpendicular to each other. Let  $x$  and  $y$  be the unit vectors in the directions of the two dipole elements at the receiver antenna (horizontal plane), see Figure 2-8. Similarly, let  $x'$  and  $y'$  be the unit vectors in the directions of the two dipole elements at the transmitting antenna. Symbol  $\theta$  is an azimuth angle from the receiver antenna  $x$ -dipole direction to the satellite and  $\vartheta$  is a satellite zenith angle. Angles  $\theta'$  and  $\vartheta'$  are at the satellite, measured similar to that at the receiver. At the receiving antenna, let the phase signal from the  $x$ -dipole be received  $90^\circ$  earlier relative to that from the  $y$ -dipole element. The signals from both dipoles are added to form the antenna output.



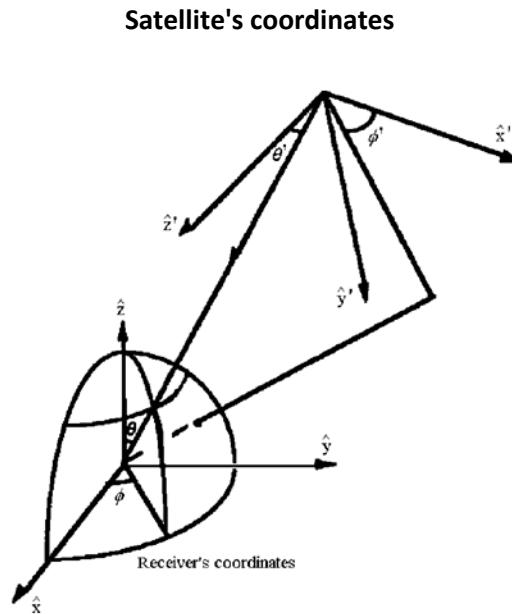


Figure 2-8. Geometric Effects on Phase (Wu et al. 1993)

### 2.6.8 Receiver Errors

Receiver error refers mainly to the quality of the hardware processing. This is in regard to its ability to accurately track and process the satellites signals and to measure the differences in time. Previously receiver processors relegated these tasks very few processor pipelines/channels which resulted in concerns tracking the minimum of four satellites, but receivers are now equipped with a multitude of processing channels, speed and precision levels there is a negligible effect on the position solution (Parkinson & Spilker, 1996). Some of these error sources can be eliminated by implementing dual-frequency receivers and techniques using a single advanced GNSS unit. However, with other error sources this approach is not viable as a means of correction so another technique is used to eliminate or account for much if not all of these sources of error with differential positioning. The up to date receiver noise of code measurements account up to  $\pm 3$  decimeters, while the phase noise is well below  $\pm 2$  mm.

## 3. Real-Time Positioning and RTKLIB software

In order to achieve centimeter- or even millimeter-level accuracy, the calculation of a position is based on code pseudoranges and carrier phase measurements. However, as already mentioned in chapter 2 several error sources affect the quality of GNSS positioning, like ionospheric errors, tropospheric delays, orbital errors, and multipath.

By means of GNSS reference stations installed at known positions, range corrections can be calculated in real-time and forwarded to a GNSS rover. Lachapelle et al., (2000) mentioned during periods of extremely high ionospheric activity, the maximum distance of the rover (user) from the reference station shall be less than 20 km to ensure a successful ambiguity resolution at the rover station.

### 3.1 Real-Time Positioning

Real-time positioning is a system that allows for centimeter level accuracy positioning in real time through efficiently differencing away correlated errors that are caused by atmospheric effects and GNSS satellite orbit errors and clock biases. In the mid 1990's investigations related to real-time positioning began, focusing on an optimal way of processing reference receiver data and then in real-time, providing correction information to users. Today, phase-based real-time positioning (RTK) is a common surveying and navigation technique using a static base station at a known spot and for real-time data collection utilizes a mobile rover unit at the point of interest. Data from the reference station are combined and processed at the rover position.

The reference station as well as the rover station is commonly equipped with a dual frequency receiver. Within the initialization procedure, the rover receiver calculates the unknown number of phase-ambiguities between the rover and the reference site and the tracked satellites on double difference level.

This process is known as "ambiguity resolution". The rover receiver delivers centimeter level positions once ambiguities have been resolved. Once a successful initialization has been performed, the rover is free to move when collecting accurate 3 dimensional data in real-time. Any loss of lock on the satellites will require the receiver to undergo this initialization procedure again.

Today, the joint use of GPS and Galileo has attracted an increased interest among the navigation community because of the firm progress in the development of the Galileo

system. Combined GPS/Galileo navigation can offer many benefits for users, such as enhanced availability, improved accuracy and integrity, especially in environments with limited satellite visibility such as in urban areas. Navigation users will benefit significantly from the combined use of GPS and Galileo. However, aside of the position, an additional unknown has to be solved for as there is a system time difference between GPS and Galileo. As a result, an observation to a further satellite of the second system is necessary for the achievement of a navigation solution. This intersystem bias can also be broadcasted via the navigation message, but not at the required accuracy.

The advantages of combining GPS with Galileo are:

- There are two independent systems.
- There is a significant increase in redundancy with the increase in the number of available satellites, and therefore more checks on the integrity/quality of the position solution can be carried out.
- An increase in the number of satellites results in a valid position being computed in more situations, for example, when the antenna experiences uneven masking such as by motion, in the forest, and due to buildings.
- The geometry of the constellation (PDOP) usually improves as the number of available satellites increases.

### 3.1.1 Integer Ambiguity Resolution for Real-Time GNSS Positioning

The determination of integer uncertainties in GNSS carrier measurements and their successful resolution is an important and challenging undertaking at the same time, in particular regarding real-time positioning. Carrier phase measurements are extremely ambiguous since the phase measurements are simply modulo  $2\pi$  numbers. With no additional information, such measurements determine merely the fractional part of the pseudorange when measured in carrier wavelengths. Further measurements are necessary to allow for ambiguity resolution, in which the integer number of wavelengths can be decided. The integer ambiguity problem can be attended to, to some extent, with sophisticated statistical methods that compare the measurements from the code signals and by comparing the resulting ranges between multiple satellites.

The calculation efficiency is of major importance, due to the speed and memory limits. In order to reach accurate and dependable position solutions under different conditions and navigation environments, the system entails a certain number of procedures. These main procedures are: inter-ambiguity resolution in real-time, message decoding, GNSS positioning, navigation and augmentation data availability monitoring, data correction and position calculation. The following three performance parameters are most significant: ambiguity resolution initialization time, ambiguity resolution reliability, and accuracy, which are all related to each other.

Nonetheless, it is still a challenge for the single-frequency case to resolve the ambiguities rapidly and reliably because of variations in the ionospheric propagation delay of the code and carrier. Furthermore, it is practically impossible to obtain ambiguity resolution at zero-difference level known as integer fixed PPP-AR (Precise Point Positioning). Consequently, carrier phase measurements are almost always relegated to high-accuracy applications in which errors of such kind are cancelled out by differential operations with a supplementary receiver (base-station). One example of real-time GNSS positioning by Real Time Kinematic (RTK) can be seen in figure 3.1,

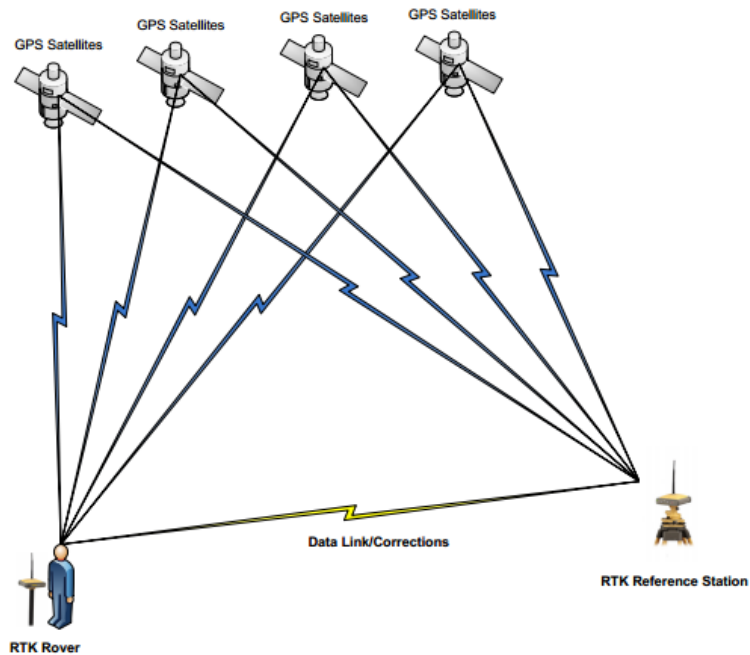


Figure 3-1. RTK System utilizing GPS signals

GNSS ambiguities connected to Double Difference (DD) carrier phase observations are generally resolved in GNSS data processing schemes. The double-difference technique efficiently alleviates common errors brought in by the receiver and satellite hardware, together with satellite clocks and the receiver, and also the Earth's atmosphere. By subtracting two inter-station single difference observations, double-difference observations can be shaped. Moreover, the interstate single-difference is derived, by subtracting measurements to the same satellite observed simultaneously at two stations. The double-difference observations involve reference station *B*, rover station *A*, and at least two GNSS satellites (Petovello and Takac, 2009), as shown in Figure 3.1.

### 3.1.2 Network Real Time Kinematic (Network - RTK)

This thesis mainly focuses on single baseline real-time positioning. However, when real-time positioning requested over the distances more than 20 km inducing range biases of the order of magnitude of a half wavelength, it can be difficult to determine the correct

phase ambiguity. As dense GNSS reference station networks used for RTK over long distances became popular over the past years, NRTK is explained here as overview. Network RTK GNSS increases the positioning accuracy by precisely modeling the errors that depend on the distance at the rover position using the raw measurements of an array of Continuously Operating Reference Stations (CORS) neighboring the rover site (Wanninger, 2008), as shown on figure 3.2,

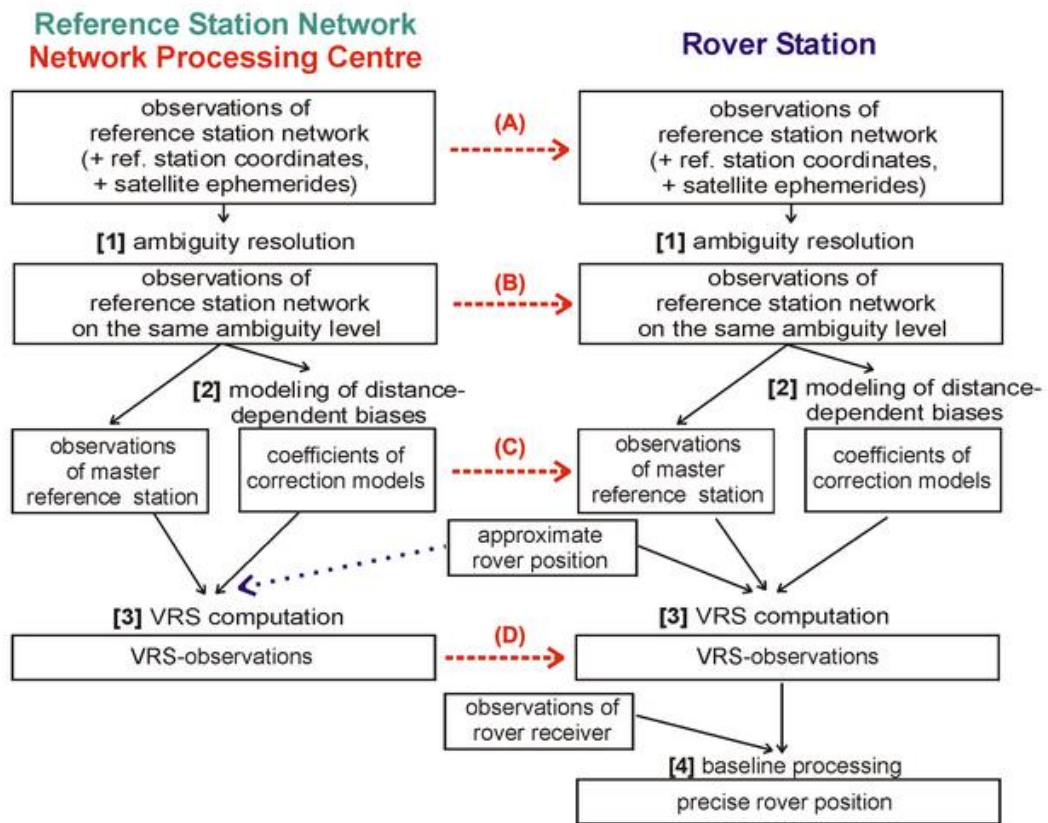


Figure 3-2. Network RTK Data Processing Steps (Wanninger, 2008)

NRTK technology was accepted and became a confirmed technology that is extensively employed today in a great amount of installations all around the world. There are many developments over the past years (Paziewski and Wielgosz, 2014, Schuler, 2007, Vollath et al., 2004, 2001, Chen et al., 2004). By contrast to traditional single base real-time positioning technology, NRTK removes a noteworthy quantity of spatially correlated errors because of the troposphere, ionosphere and satellite orbit errors, hence permits performing RTK positioning in reference stations networks with distances of 40 km or more from the next reference station while supplying the performance of short baseline positioning (Landau et al., 2004).

In comparison to a standard differential GPS system, the accuracy attained when using joined GNSS differential stations was favorably. In these cases, dual-frequency

measurements can be used to remove the first order ionospheric effects, thus resulting in better positioning accuracy. Naturally, the more reference and rover stations track satellites, the faster the ambiguity resolution gets and the performance of NRTK solutions in terms of accuracy, availability, reliability improves.

The typical NRTK model comprises of three or more permanent reference stations connected to a central processing facility that estimates the distance dependent errors across the network. Corrections for these errors are combined with raw reference station observations and distributed to users in the field. The most popular concepts for establishing and forwarding error models in NRTK are VRS (Virtual Reference System), FKP, and MAL.

The information from the network helps to diminish the distance dependent errors viewed at the rover, resulting in more homogenous position accuracy within the region surrounded by the reference stations. On the other hand, the network software might not be able to supply with corrections for all satellites in sight. A usual case is low elevation satellites for which the network software has not resolved the corresponding ambiguities. Nonetheless, the raw reference observations still contain valuable information that can be useful for real-time positioning.

In NRTK, the determined corrections need to be interpolated to the user's location to correct the observations and to position the rover. The interpolation method is the most important step of network RTK, as it has the greatest effect on positioning accuracy (Dai et al., 2004). The numerous interpolation methods used are,

- The distance dependent linear interpolation for the dispersive and non-dispersive correction uses the distance from the reference stations to set weights for the interpolation process. Closest reference station corrections would have the largest weights as an inverse of the distance is used.
- The linear interpolation method is one of the most commonly used interpolation techniques and is based on obtaining two coefficients or more which represent the spatial extent of the errors. With this method at least three reference stations are required in order to obtain the unknown coefficients, which means one master station differenced with respect to two other reference stations.
- Low-order surface fitting is used to describe the distance dependent errors, as well as location dependent errors like multipath. The coefficients of this method for more than three reference stations are obtained using a least-square adjustment. This method is based on a second-order Taylor expansion of the GPS error model.
- The least-squares collocation method makes use of the covariance matrices to predict distance dependent errors at the user's location. In terms of performance least-squares collocation method performs at a similar level as the second-order surface fitting and linear combination interpolation methods.

To summarize the mentioned interpolation methods commonly used in network RTK, table 3-1 shows the main advantage and disadvantage for each technique and displays the relative performance of each method.

Table 3-1. Interpolation methods of network RTK (Dai et al., 2004)

<b>Interpolation Method</b>	<b>Advantage</b>	<b>Disadvantage</b>	<b>Performance</b>
Distance dependent linear interpolation	Simple	Inaccurate	Below average
Linear interpolation	Two baselines needed	Inaccurate over long baselines (>30 km)	Average
Low order surface fitting	Capable of higher order surface fitting	Inaccurate over long baselines (>30 km)	Average
Least square collocation	rigorous	Requires more Computations	Good

### 3.1.3 Message Decoding

The Radio Technical Commission for Maritime Services (RTCM) has established a binary standard format for GNSS code and phase correction data. This format is supported by all receiver types and usually forwarded via internet protocol (Ntrip).

Several message types are considered while decoding the RTCM messages, containing pseudorange corrections (PRC), along with the rate of change for the pseudorange corrections (RRC) for visible healthy satellites observed at the corresponding DGNSS reference station. In addition, another message type is considered for obtaining ECEF coordinates of the corresponding GNSS station.

RTCM messages are made of a number of blocks known as RTCM words; every word is 30-bit length (five RTCM bytes), containing 24 data bits and 6 parity bits. Each RTCM message consists of a body and a header. While the body keeps data for each corresponding message type, the header contains in the first and second RTCM words, the message type, reference time, reference station identification, time, and length of message as shown in Figure 3-3,

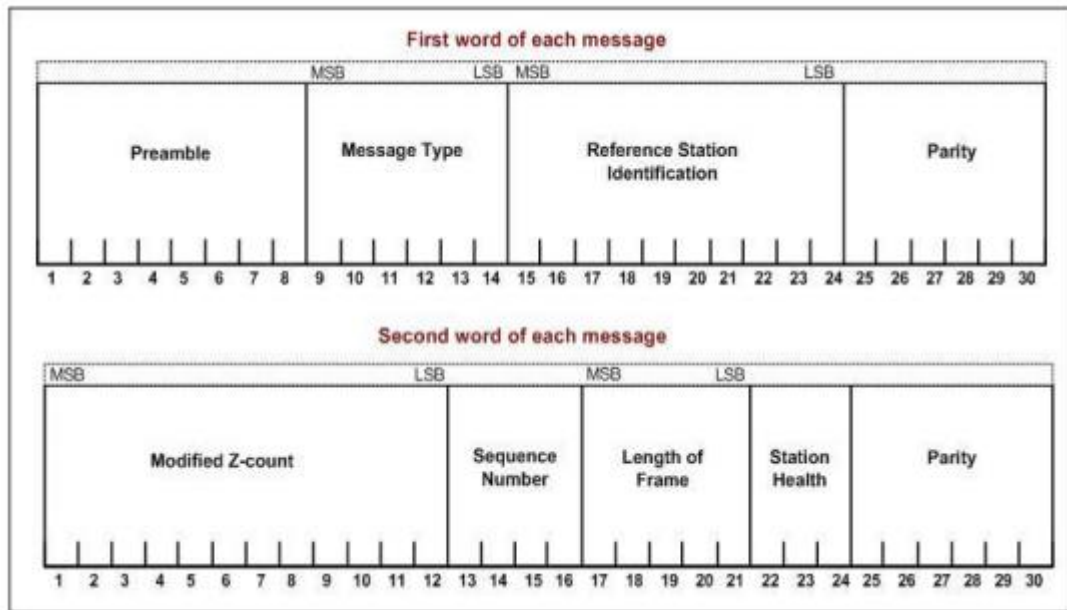


Figure 3-3. RCTM Message

The navigation message includes a number of data pages, of which each holds five sub-frames. Each and every frame has two data words of 30 bits. In order to extract pertinent information about each observed satellites with respect to the users measurement the following sub-frames are considered in the decoding process:

- Sub-frame 1, containing the Satellite Vehicles (SVs) clock parameters. This information is utilized to correct the code phase time received from the SVs, with respect to the relativistic effects.
- Sub-frames 2 and 3 consist of ephemeris parameters which are used to determine the SVs orbits within two hours interval.
- Sub-frame 4 holds the ionospheric delay coefficients needed for computing the ionosphere delay at the time of measurements by using an embedded ionospheric model.

Before the coordinates are processed, the decoded correction information passes through the integrity monitoring and baseline estimation procedures for reliability and validity inspection at the rover site.

An RTCM message length depends on the number of covered and correct satellites. Nevertheless, an integer value in the second RTCM word (Length of Frame) indicates, at all times, the total number of RTCM words that compiles the message. Several versions of RTCM SC-104 data format have been made available since 1990:

- RTCM 2.0: is only used for DGPS applications (without RTK).
- RTCM 2.1: is comparable to version 2.0 but it also contains new messages for carrier phase data and RTK corrections.



- RTCM 2.2: additionally to the above, it composes of GNSS data and associated information which is carried by newly added messages 31-36.
- RTCM 2.3: consists of the antenna types in message 23 and ARP information in message 24 as well.
- RTCM 3.0: supports network RTK messages and also accommodates message types for new GNSS systems that are under development, such as Galileo.
- RTCM 3.1: incorporates network corrections which enable a mobile receiver to obtain accurate RTK information valid over a large area. In addition a new GNSS messages provide orbital parameters to assist rapid acquisition and supports also PPP.
- RTCM 3.2: is the recent version, for carrier and code differential corrections for high precision with Multiple Signal Messages for generic inclusion of new constellations and signals. Supports GPS, GLONASS, GALILEO, QZSS, BeiDou, and SBAS.

RTCM supports Networked Transport of RTCM via Internet Protocol (Ntrip), designated as RTCM Standards 10410.1. This standard defined by RTCM's Special Committee 104 (SC104), along with other things and supplies a protocol for streaming differential correction data to stationary or mobile users through the Internet. Usually, differential correction have been broadcasted over the radio links from either a single or networked reference stations situated in familiar settings to improve the mobile receivers (rovers) real-time accuracy.

The design of Ntrip is to allocate the GNSS streaming data to mobile or stationary clients through the Internet, allowing simultaneous PC, PDA or receiver connections to a broadcasting host. Through the mobile IP networks, such as GSM, GPRS, EDGE, UMTS or HSDPA, Ntrip can support the wireless Internet access.

### **3.2 RTKLIB software**

Since a few years ago, RTKLIB has developed a compact and portable software library for real-time GNSS positioning. RTKLIB provides simple functions for carrier-based relative positioning and RINEX file handling for post processing which is in line with this research purpose to test the GNSS data using post-processing under similar conditions as in real-time positioning.

From the version 2.4.2 onwards, RTKLIB is an open source program package under the GPLv3 license. The package of RTKLIB consists of user executable binary APs on Windows and whole source programs of the library and the APs. Users can freely download the program package, use the APs, install or link the library to the user own AP and modify the source codes according to the requirements for user applications.

The console APs in RTKLIB were also written in standard C and standard libraries. These APs can be built on many environments. The GUI APs in RTKLIB were written in C++ to utilize environment-dependent GUI (graphical user interface) libraries. The distribution package of RTKLIB already contains the entire pre-built user executable binary APs for Windows PC, which were built by free edition Borland Turbo C++ (Takasu and Yasuda, 2007).

For this thesis, all tests were conducted using RTKLIB, in order to mimic a real-time positioning system. Nevertheless, the performance of real data and simulated data processing are evaluated in post-processing mode.

### 3.2.1 RTKLIB Algorithm

This section briefly introduces the positioning algorithm used in RTKLIB. The text is extracted from the RTKLIB manual (Takasu, 2013). For carrier based relative positioning with a short length baseline between rover *A* and base station *B*, the following measurement equations for carrier base and pseudorange are commonly used. In these equations, satellite and receiver clock-biases, and atmospheric effects are eliminated by double differencing,

$$\Phi_{AB}^{ij} = \rho_{AB}^{ij} + \lambda(B_{AB}^i - B_{AB}^j) + \varepsilon_{\Phi} \quad (3.1)$$

$$P_{AB}^{ij} = \rho_{AB}^{ij} + \varepsilon_P \quad (3.2)$$

Where  $()^{ij}$  and  $()_{AB}$  represent single-difference between satellite and between receivers, respectively,  $\rho$  is the geometric range,  $\lambda$  is the carrier wave length and  $\varepsilon$  is the measurement error.  $B_{AB}^i$  is the single-difference of carrier phase ambiguities in cycles. The unknown state vector  $x$  for RTK reads:

$$x = (r_A^T, B_{Li}^T, B_{Lj}^T)^T \quad (3.3)$$

$$B_{Lj} = (B_{AB,Lj}^1, B_{AB,Lj}^2, \dots, B_{AB,Lj}^m)^T \quad (3.4)$$

where  $r_A$  is the rover antenna position in ECEF frame. RTKLIB employs single-difference instead of double difference for carrier phase ambiguities to avoid the hand over problem of reference satellites. The measurement vector  $y_k$  at the epoch  $t_k$  is defined with double differenced carrier phase and pseudorange measurements as:

$$y_k = (\Phi_{Li}^T, \Phi_{Lj}^T, P_{Li}^T, P_{Lj}^T)^T \quad (3.5)$$

$$\Phi_{Lj} = (\Phi_{AB,Lj}^{12}, \Phi_{AB,Lj}^{13}, \Phi_{AB,Lj}^{14}, \dots, \Phi_{AB,Lj}^{1m})^T \quad (3.6)$$

$$P_{Lj} = (P_{AB,Lj}^{12}, P_{AB,Lj}^{13}, P_{AB,Lj}^{14}, \dots, P_{AB,Lj}^{1m})^T \quad (3.7)$$

By using the Extended Kalman Filter (EKF), the state vector  $x$  and its covariance matrix  $P$  can be estimated by:

$$\hat{x}_k(+) = \hat{x}_k(-) + K_k(y_k - h(\hat{x}_k(-))) \quad (3.8)$$

$$P_k(+) = (I - K_k H(\hat{x}_k(-)))P_k(-) \quad (3.9)$$

$$K_k = P_k(-)H(\hat{x}_k(-))(H(\hat{x}_k(-))P_k(-)H(\hat{x}_k(-))^T + R_k)^{-1} \quad (3.10)$$

where  $h(x)$ ,  $H(x)$ , and  $R_k$  are the measurement model vector, the matrix of partial derivatives and the covariance matrix of measurement errors, respectively. These matrices are defined as:

$$h(\hat{x}_k) = (h_{\phi,Li}^T, h_{\phi,Lj}^T, h_{P,Li}^T, h_{P,Lj}^T) \quad (3.11)$$

$$h_{\phi,Lj} = \begin{pmatrix} \rho_{AB}^{12} + \lambda(B_{AB}^1 - B_{AB}^2) \\ \rho_{AB}^{13} + \lambda(B_{AB}^1 - B_{AB}^3) \\ \vdots \\ \rho_{AB}^{1m} + \lambda(B_{AB}^1 - B_{AB}^m) \end{pmatrix}, h_{P,Lj} = \begin{pmatrix} P_{AB}^{12} \\ P_{AB}^{13} \\ \vdots \\ P_{AB}^{1m} \end{pmatrix} \quad (3.12)$$

$$H(\hat{x}) = \frac{\partial h(x)}{\partial x} \Big|_{x=\hat{x}} = \begin{pmatrix} -DE & 0 & \lambda_{Li}D & 0 \\ -DE & 0 & 0 & \lambda_{Lj}D \\ -DE & 0 & 0 & 0 \\ -DE & 0 & 0 & 0 \end{pmatrix} \quad (3.13)$$

$$R_k = \text{diag}(DR_{\phi,Li}D^T \quad DR_{\phi,Lj}D^T \quad DR_{P,Li}D^T \quad DR_{P,Lj}D^T) \quad (3.14)$$

$$\rho_A^i = \|\hat{r}_A - r^i\|, \rho_B^i = \|\hat{r}_B - r^i\|, E = (e_A^{1T}, e_A^{2T}, \dots, e_A^{mT})^T \quad (3.15)$$

$$R_{\phi,Lj} = 2\text{diag}(\sigma_{\phi,Lj}^{1^2} \quad \sigma_{\phi,Lj}^{2^2} \quad \dots \quad \sigma_{\phi,Lj}^{m^2}) \quad (3.16)$$

$$R_{P,Lj} = 2\text{diag}(\sigma_{P,Lj}^{1^2} \quad \sigma_{P,Lj}^{2^2} \quad \dots \quad \sigma_{P,Lj}^{m^2}) \quad (3.17)$$

$$D = \begin{pmatrix} 1 & -1 & 0 & \dots & 0 \\ 1 & 0 & -1 & \dots & 0 \\ \vdots & \vdots & \vdots & \ddots & \vdots \\ 1 & 0 & 0 & \dots & -1 \end{pmatrix} \quad (3.18)$$

where  $r^i$  is satellite  $i$  position in ECEF frame,  $r_B$  is the base station antenna position,  $e_A^1$

is the line of sight vector from antenna to satellite. For weighting the carrier phase and pseudoranges, RTKLIB employs an a priori elevation dependent model with user defined parameters. The time update of the state vector and its covariance matrix from epoch  $t_k$  to epoch  $t_{k+1}$  is expressed as:

$$\hat{x}_{k+1} = F_k^{k+1} \hat{x}_k(+) \quad (3.19)$$

$$P_{k+1} = F_k^{k+1} P_k(+) F_k^{k+1 T} + Q_k^{k+1} \quad (3.20)$$

where  $F$  is the state transition matrix and  $Q$  is the covariance matrix of system noise. In the kinematic mode, a noise model should be assumed for the rover antenna as:

$$F_k^{k+1} = \text{diag}(0_3 \quad I \quad I), Q_k^{k+1} = \text{diag}(\infty \quad I \quad I) \quad (3.21)$$

where the carrier-phase ambiguities are assumed to be stationary. Instead of the pure kinematic model expressed by (3.21), RTKLIB resets the states of the rover antenna position to the single point solution at every epoch considering numerical stability. In this scheme, the iteration of the filter due to the nonlinearity of the measurement equations also can be avoided for efficient computation. In the static positioning mode, RTKLIB uses just a simple state transition model defined as  $F=I$  and  $Q=0$ . The current version supports only the kinematic mode or the static mode, where any receiver dynamic are not incorporated in. To detect cycle-slips, RTKLIB monitors the jump of the geometry-free LC (linear combination) of L1 and L2 carrier-phase as well as LLI (loss of lock indicator) and lock-time provided by the receiver (Takasu and Yasuda, 2008).

### 3.2.2 Integer Ambiguity Resolution

Once the estimated states obtained, the float carrier-phase ambiguities should be resolved into integer values in order to improve accuracy and convergence time. In RTKLIB, the float solution of the rover position and the single-differenced carrier-phase ambiguities are transformed to a double-differenced form by:

$$\hat{x}'_k = G \hat{x}_k(+) = (r_A^T, N_A^T)^T \quad (3.22)$$

$$P'_k = G P_k(+) G^T = \begin{pmatrix} Q_R & Q_{NR} \\ Q_{RN} & Q_N \end{pmatrix}, G = \text{diag}(I_3 \quad D \quad D) \quad (3.23)$$

the double-differenced carrier-phase ambiguities, which should be integers by canceling the receiver initial phase terms. In this form, the best integer vector is searched to satisfy the condition of ILS (integer least square) problem as:

$$\tilde{N} = \text{argmin}(N - \hat{N})^T Q_N^{-1} (N - \hat{N})^T \quad (3.24)$$

To solve the problem, the well-known efficient strategy LAMBDA and its extension MLAMBDA (Chang et al., 2005) are employed in RTKLIB. After the validation by the simple ratio-test, "FIX" solution of the rover antenna position is obtained by solving the following equation.

$$\check{r}_r = \hat{r} - Q_{RN} Q_N^{-1} (\hat{N} - \check{N}) \quad (3.25)$$

### 3.3 Data Sources

According to the International GNSS Service (IGS), 2009, this service generates precise ephemerides for the satellites together with by-products such as Earth rotation parameters (ERP) and GNSS clock corrections. The IGS service is built upon a global network of permanent tracking stations and provides information and data products from computational centers to all GNSS users through data archive and exchange centers. The IGS Analysis Centers make use of the global tracking data and establish a suite of so-called products as listed in table 3.3 and table 3.4.

Table 3-2. Data Sources (IGS, 2009)

<b>IGS Station Network</b>	
Global Data Centers:	
CDDIS	- Crustal Dynamics Data Information System (US-MD)
SOPAC	- Scripps Orbit and Permanent Array Center (US-CA)
IGN	- Institut National De L'Information Geographique et Forestiere (FR)
KASI	- Korea Astronomy and Space Science Insitute (SK)
Analysis Centers:	
CODE	- Center for Orbit Determination in Europe, Switzerland (TBC)
EMR	- Natural Resources Canada, Canada (TBC)
ESA	- European Space Operations Centre (ESOC), ESA, Germany
GFZ	- GeoForschungsZentrum/Potsdam, Germany (TBC)
GRGZ	- Groupe de Recherche de Géodésie Spatiale - CNES/CLS, Toulouse, France
JPL	- Jet Propulsion Laboratory, USA
MIT	- Massachusetts Institute of Technology, USA
NGS	- National Geodetic Survey, NOAA, USA
SIO	- Scripps Institution of Oceanography, USA (TBC)

The tracking data are available at various Data Centers, the individual orbits determined by the Analysis Centers at the Global Data Centers, and the official IGS orbits are combined at the Central Bureau and the Global Data Centers (IGS, 2009). Table 3-2 provides the IGS components/structure, beginning with the IGS station network which rigorously applies IGS standards for station monument/hardware, data quality, submission formats, and delivery delays.

Normally, the high-quality GNSS data is online within one day and data products are online within one day up to two weeks of observations. The IGS global network of permanent tracking stations, each equipped with a GPS receiver or multi GNSS receiver, generates raw orbit and tracking data. The Operational Data Centers, which directly contact the tracking sites, store the receiver data in Receiver INdependent EXchange format (RINEX) (Gurtner, 2009) and then forward these data to the Regional or Global Data Centers.

Table 3-3. IGS Products – GPS and GLONASS Satellite Ephemerides. (IGS, 2009)

**GPS Satellite Ephemerides / Satellite & Station Clocks**

Type		Accuracy	Latency	Updates	Sample Interval
Broadcast	orbits	~100 cm	real time	--	daily
	Sat. clocks	~5 ns RMS ~2.5 ns SDev			
Ultra-Rapid (predicted half)	orbits	~5 cm	real time	at 03, 09, 15, 21 UTC	15 min
	Sat. clocks	~3 ns RMS ~1.5 ns SDev			
Ultra-Rapid (observed half)	orbits	~3 cm	3 - 9 hours	at 03, 09, 15, 21 UTC	15 min
	Sat. clocks	~150 ps RMS ~50 ps SDev			
Rapid	orbits	~2.5 cm	17 - 41 hours	at 17 UTC daily	15 min
	Sat. & Stn. clocks	~75 ps RMS ~25 ps SDev			5 min
Final	orbits	~2.5 cm	12 - 18 days	every Thursday	15 min
	Sat. & Stn. clocks	~75 ps RMS ~20 ps SDev			Sat.: 30s Stn.: 5 min

**GLONASS Satellite Ephemerides**

Type	Accuracy	Latency	Updates	Sample Interval
Final	~3 cm	12 - 18 days	every Thursday	15 min

**Geocentric Coordinates of IGS Tracking Stations**

Type		Accuracy	Latency	Updates	Sample Interval
Final positions	horizontal	3 mm	11 - 17 days	every Wednesday	weekly
	vertical	6 mm			
Final velocities	horizontal	2 mm/yr	11 - 17 days	every Wednesday	weekly
	vertical	3 mm/yr			

For efficiency and to reduce electronic network traffic, the Regional Data Centers collect data from several Operational Data Centers before transmitting them to the Global Data Centers. Data not used for global analyses are archived and available online at the Regional Data Centers. The Global Data Centers archive and provide online access to tracking data and data products which normally must be available to users for at least 60 days.

Table 3-4. IGS Products – GNSS Earth Rotation and Atmospheric Parameters (IGS, 2009)

**Earth Rotation**

Polar Motion (PM) Polar Motion Rates (PM rate) Length-of-day (LOD)

Type		Accuracy	Latency	Updates	Sample Interval
Ultra-Rapid (predicted half)	PM	~200 $\mu$ as	real time	at 03, 09, 15, 21 UTC	daily integrations at 00, 06, 12, 18 UTC
	PM rate	~300 $\mu$ as/day			
	LOD	~50 $\mu$ s			
Ultra-Rapid (observed half)	PM	~50 $\mu$ as	3 - 9 hours	at 03, 09, 15, 21 UTC	daily integrations at 00, 06, 12, 18 UTC
	PM rate	~250 $\mu$ as/day			
	LOD	~10 $\mu$ s			
Rapid	PM	~40 $\mu$ as	17 - 41 hours	at 17 UTC daily	daily integrations at 12 UTC
	PM rate	~200 $\mu$ as/day			
	LOD	~10 $\mu$ s			
Final	PM	~30 $\mu$ as	11 - 17 days	every Wednesday	daily integrations at 12 UTC
	PM rate	~150 $\mu$ as/day			
	LOD	~10 $\mu$ s			

**Atmospheric Parameters**

Type	Accuracy	Latency	Updates	Sample Interval
Final tropospheric zenith path delay	4 mm	< 4 weeks	weekly	2 hours
Ultra-Rapid tropospheric zenith path delay	6 mm	2-3 hours	every 3 hours	1 hour
Final ionospheric TEC grid	2-8 TECU	~11 days	weekly	2 hours; 5 deg (lon) x 2.5 deg (lat)
Rapid ionospheric TEC grid	2-9 TECU	<24 hours	daily	2 hours; 5 deg (lon) x 2.5 deg (lat)

To perform the computations discussed in chapter 5, several data from the IGS station network were extracted. The data are mainly available in Rinex format and has either 30 seconds or 1 second sampling rate, as the GNSS observation provides information that can be used for real time positioning. Furthermore, precise satellite orbits are required to fully exploit the potential of the GNSS observations corresponding with the main intention of this thesis. And, an ionospheric model correction from IGS is used to mitigate the ionospheric errors in GNSS observations in real time positioning.

To exploit the RTK-performance when processing signal linear combinations in chapter 6, a high sampling rate (1 second) Rinex data was requested. Due to the site and infrastructure requirements, the baseline length needs to be less than 70 km and both stations collecting GPS and Galileo data.

## 4. Signal to Noise Ratio and Code Multipath

GNSS signal power or SNR (Signal Noise Ratio) is related to the carrier phase multipath parameters. The receiver determines the power of the carrier, not code or data, and generally expresses it as ratio of average signal power to noise power spectral density or  $C/N_0$  (Parkinson and Spilker, 1996).

Multipath is correlated with the surrounding terrain (geometry) and also with the propagation characteristic. Signal propagation effects are reflected by SNR. A higher SNR usually indicates less signal attenuation and thus less path delay. SNR is a quantity measured by the receiver and used for data quality checking. A low SNR indicates a large tracking error caused by diffracted signals.

In precise applications, multipath errors dominate the total positioning error (Smyrniotou et al., 2013). Despite the different approaches developed, several aspects of multipath propagation are still not fully understood. Furthermore, the site-dependent characteristics of multipath correlates with the errors caused by multipath propagation, path geometry, the signal characteristics, the diffraction, and reflection effects. In the observation domain, multipath errors are not constant in time. They show a sinusoidal behavior which can be noticed in carrier-phase residuals or  $C/N_0$  time series. The  $C/N_0$  observable is the only GNSS observation type in which multipath propagation effects are directly visible without any sophisticated data pre-processing.

On the other side, the code and carrier phase measurement noise depends on different factors (Luo et al., 2009) like the signal power, the method used for the analog-to-digital conversion, the correlation process, the design of the antenna, etc. Multipath and signal noise are independent for each receiver and for each signal, and cannot be removed by differential techniques (differences between receivers or satellites) or by combinations of measurements.

### 4.1 SNR( $C/N_0$ ) on GNSS Observations

Concerning satellite configuration, site-specific factors as well as atmospheric effects, the quality of GNSS observations may become inconsistent and affecting SNR. In addition, observation weighting plays a dominant role when GNSS receivers calculate positions by measuring pseudo-distances to transmitting satellites. A GNSS receiver performance mainly depends on the signal power in the receiver's tracking loops (Langley, 1997).



There are several methods to measure the GNSS signal strength. However, as the data sent by GNSS are through radio signals, it is a known fact that radio signals cannot maintain their strength for longer distances. The GNSS system employs phase modulation to superimpose data on the radio signals for better reception by the GNSS receiver and the manufacturers employ different algorithms to retrieve the data from the signals for offering the desired data.

All the factors correlating with the elevation angle of the transmitted GNSS signals like the SNR normally grow with increasing satellite elevation angle. SNR is usually expressed in decibels and it refers to the ratio of the signal power and noise power in a given bandwidth. Due to the fact that noise and signal are amplified in the same way, these ratios can be expressed as (Rost and Wanninger, 2009):

$$\frac{C_{ant}}{N_{ant}} \approx \frac{S_{corr}}{N_{corr}} \approx S \quad (4.1)$$

Signal to noise ratio can usually be found in the context of signal baseband of the modulated signal at correlator output ( $S_{corr}$ ). The quality of a received GNSS signal is commonly described by carrier to noise ratio of the modulated carrier at the receiving antenna ( $C_{ant}$ ). The system noise affects the signal quality and the noise and signal are amplified in the same way in the antenna ( $N_{ant}$ ) and at the correlator output ( $N_{corr}$ ). As the system noise is several magnitudes smaller than  $C_{ant}$  and  $S_{corr}$ , therefore the values are normally converted to decibels (dB) to represent a specific bandwidth, thus:

$$S(dB) = 10 \cdot \log_{10}(S) \quad \text{and} \quad (4.2)$$

$$SNR(dB) = S/N \quad (4.3)$$

Assuming the GNSS signal strength is  $S$  and the noise level is  $N$ , the basic formula to measure the GNSS signal strength is  $S/N$ . If the carrier waves facing obstructions,  $S$  will get affected by attenuation.  $S/N$  is being normalized to a specific bandwidth. Hence the system noise  $N$  is substituted by the product of noise power density  $N_0$  and loop bandwidth  $B_L$ :

$$N = N_0 \cdot B_L \quad (4.4)$$

because many signals have a very wide dynamic range and are expressed using the logarithmic decibel scale, signal and noise may be expressed in decibels (dB) as using equations 4.2 and 4.4. Assuming the system noise ( $N_0$ ) is several magnitudes smaller than the signal strength ( $S$ ), the normalized signal quality is (Butsch, 2002):

$$SNR (dBHz) = S - N = 10 \cdot \log_{10}(S)(dB) - (N_0 \cdot B_L)(dBHz) \quad (4.5)$$

The user should be careful when comparing different GNSS receivers, particularly for older models e.g. Trimble that provided the signal quality in “arbitrary manufacture unit” (AMU). AMU units are dependent and need to be converted by a conversion formula because the value can differ by up to 3 dB from the original value (Butsch, 2002). Different generations of GNSS satellites have inherently different signal strengths, which could cause different SNR values with nothing wrong at all.

As the RTKLib processed the signal at the specific bandwidth, a more technically precise and common measurement of GNSS signal strength is known as  $C/N_0$ .  $C/N_0$  is the SNR (usually in dB) in a 1Hz bandwidth and  $C/N_0$  is expressed in decibel hertz (dBHz) and refers to the ratio of the carrier. The  $C/N_0$  can be expressed as follows (Joseph, 2010):

$$C/N_0 = C - (N - BW) = C - (N_0) = SNR + BW \quad (4.6)$$

where  $C$  is the carrier power in dBW,  $N$  is the noise power in dBW,  $N_0$  is the noise power density in dBW-Hz, and  $BW$  is the bandwidth of signal observation.

The  $C/N_0$  values are only approximate and do not really determine the ability of a receiver to track and measure signals. That ability is more dependent on integration times, loop bandwidths, and receiver design.

## 4.2 Multipath Line of Sight

Multipath propagation occurs when environmental features cause combinations of reflected and diffracted signals to arrive at the receiving antenna. The multipath signals can cause distortion of the receiver function and hence errors in the range estimation. To understand multipath mitigation, it is imperative to understand the multipath propagation environment and the resultant error effect.

Unlike the code multipath, the carrier phase multipath error is always less than 1/4 of the carrier wavelength as long as the multipath signal is weaker than the direct signal (Xu, 2007). The carrier phase multipath error is not spatially correlated for two receiver sites that are in different environment and the differential multipath error is therefore always less than 1/2 of the carrier phase wavelength.

The purpose of this section 4.2 is to give a short overview how the multipath propagation arrived at the antenna. Some propagation situation scenarios have been developed using simple ray-based geometry (Hannah, 2001), formulate equations for the defining multipath parameters. There are forward scatter geometry and back scatter geometry.

The forward-scatter problem confined to a two dimensional domain with a flat reflecting lower boundary, the GNSS antenna is located at point  $P$ , at a distance  $d$  from

left-hand boundary and height  $h$  above the reflecting surface with a LOS (line of sight) signal propagating into the domain at angle  $\theta$ , as shown in figure 4.1,

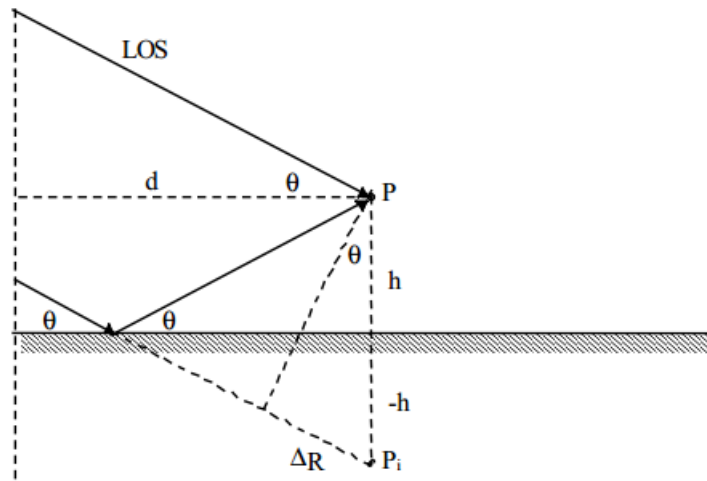


Figure 4-1. Forward scatter geometry (Hannah, 2001)

Using image theory, the reflected signal travels an additional distance  $\Delta R$  to the image point  $P_i$ . This additional path length is given by,

$$\Delta R = 2h \sin \theta \quad (4.7)$$

Also the length of propagation of the LOS signal into the domain ( $D_P$ ) is given by,

$$D_P = \frac{d}{\cos \theta} \quad (4.8)$$

Consider the backscatter problem caused by a reflecting surface forming at the right side boundary,

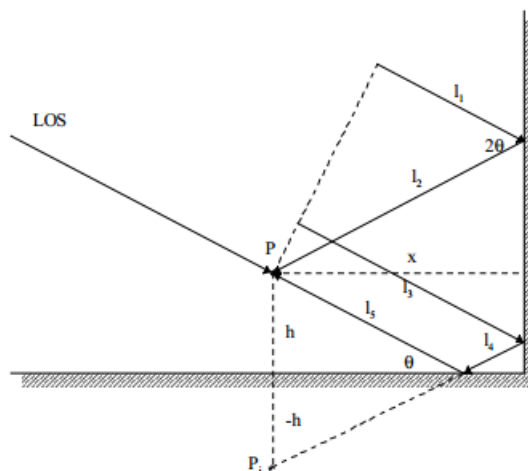


Figure 4-2. Back scatter geometry from above (Hannah, 2001)

the geometry equations read,

$$x > \frac{h}{\tan\theta} \quad (4.9)$$

The individual path lengths are then,

$$l_1 = \frac{x \cos 2\theta}{\cos\theta}, l_2 = \frac{x}{\cos\theta}, l_3 = 2h \sin\theta + \frac{x \cos 2\theta}{\cos\theta}, l_4 = \frac{x}{\cos\theta} - \frac{h}{\sin\theta}, l_5 = \frac{h}{\sin\theta} \quad (4.10)$$

and the total path length differences relative to the line of sight for two multipath propagations are,

$$\Delta R_a = 2x \cos\theta \quad (4.11)$$

and

$$\Delta R_b = 2h \sin\theta + 2x \cos\theta \quad (4.12)$$

$R$  is the length of propagation of the LOS signal and the subscripts  $a$  and  $b$  represent the multipath, either arriving from above (a) or below (b) the horizontal plane containing the antenna. In detail, the correlation between geometric delays and phases are shown in table 4.1

Table 4-1. Geometry Delays and Phases (Hannah, 2001)

Path	Amplitude	Relative time delay	Total Phase
Line of sight	$E_0$	$\frac{1}{c} \left( \frac{d}{\cos\theta} \right)$	$\frac{2\pi d}{\lambda \cos\theta}$
Forward scatter	$\rho_g E_0$	$\frac{1}{c} (2h \sin\theta)$	$\phi_g + \frac{4\pi h}{\lambda} \sin\theta$
Backscatter (above)	$\rho_r E_0$	$\frac{1}{c} (2x \cos\theta)$	$\phi_r + \frac{4\pi x}{\lambda} \cos\theta$
Backscatter (below)	$\rho_r \rho_g E_0$	$\frac{1}{c} (2h \sin\theta + 2x \cos\theta)$	$\phi_r + \phi_g + \frac{4\pi}{\lambda} (h \sin\theta + x \cos\theta)$

In table 4-1, the GNSS antenna is assumed to be located at a point  $P$ , at a distance  $d$  from left-hand boundary and height  $h$  above the reflecting surface with a LOS (line of sight) signal propagating into the domain at angle  $\theta$  and  $x$  is the horizontal distance from the reflector to the antenna location. The speed of propagation is given as the reference speed of light  $c$ . The reflection coefficients are  $\rho_g, \phi_g, \rho_r, \phi_r$ . The phase terms are all assumed to be  $\pi$ .

### 4.3 Code and Phase Multipath on GNSS Observations

In order to understand the effect of multipath in any given environment, the user needs to understand how the ranging receivers operate and how multipath distortion results in ranging errors. Hereafter, code measurements (abbreviated expressions),

$$P_i = R + I_i + MP_i \quad (4.13)$$

$$P_j = R + I_j + MP_j \quad (4.14)$$

and phase measurement,

$$L_i = R - I_i + N_i + mp_i \quad (4.15)$$

$$L_j = R - I_j + N_j + mp_j \quad (4.16)$$

are defined.

R denotes the geometric terms, P and L represent code and phase ranges in meters, *i* and *j* represent the introduced carriers, I the ionosphere delay, N the phase ambiguity (converted to meters), MP and mp represent code multipath and phase multipath which is assumed to be negligible in comparison with code multipath (MP >> mp).

MP<sub>*i*</sub> can be derived by forming the appropriate linear combination (Ray, 2000, Xu, 2007):

$$P_i - L_i = 2I_i + MP_i - N_i \quad (4.17)$$

$$L_i - L_j = I_j - I_i + N_i - N_j = I_i \times (\alpha - 1) + N_i - N_j$$

$$2I_i = \frac{2}{\alpha-1} \times (L_i - L_j) + 2 \times \frac{(N_j - N_i)}{\alpha-1} \quad (4.18)$$

with

$$\alpha = \left( \frac{f_i}{f_j} \right)^2 \quad (4.19)$$

Therefore the expression for MP<sub>*i*</sub> reads,

$$MP_i - \left\{ N_i - \frac{2}{\alpha-1} \times (N_j - N_i) \right\} = P_i - \left( \frac{2}{\alpha-1} + 1 \right) \times L_i + \frac{2}{\alpha-1} \times L_j \quad (4.20)$$

A very similar derivation for code multipath  $MP_j$  yields,

$$MP_j = P_j - \left(\frac{2\alpha}{\alpha-1}\right) \times L_i + \left(\frac{2\alpha}{\alpha-1} - 1\right) \times L_j \quad (4.21)$$

For carrier phase multipath, the following equations can be derived,

$$mp_i = 2I_i + MP_i - N_i \quad (4.22)$$

$$mp_j = 2I_j + MP_j - N_j \quad (4.23)$$

Introducing equations (4.18) and (4.21), leads to:

$$\begin{aligned} mp_i &= \frac{2}{\alpha-1} \times (L_i - L_j) + 2 \times \frac{(N_j - N_i)}{\alpha-1} + P_i - \left(\frac{2}{\alpha-1} + 1\right) \times L_i + \left(\frac{2}{\alpha-1}\right) \times L_j - N_i \\ &= P_i + \frac{2}{\alpha-1} \times (N_j - N_i) - L_i - N_i \end{aligned} \quad (4.24)$$

and

$$mp_j = P_j + \frac{2\alpha}{\alpha-1} \times (N_i - N_j) - L_j - N_j \quad (4.25)$$

#### 4.4 Signal to Noise Ratio and Code Multipath Data Processing

In this section, the proposed algorithm will be tested using several datasets. The performance of the GNSS signal will be discussed based on the criteria defined in section 4.1 and 4.3. The following steps are carried out:

- L1C (BPSK(1)), L2C(BPSK(10)), L5X(BPSK(10)) GPS signal and E1X(BOC(1,1)), E5X(BPSK(10)), E7X(BPSK(10)), and E8X(AltBOC(15,10)) Galileo signals are looked at.
- Use code and phase data to extract the SNR and code multipath/noise residuals.
- SNR was calculated using equations in section 4.1 for the determined GNSS signals. Insufficient availability of the modernized GNSS signals may cause further problems.
- Epoch to epoch code multipath calculations were carried out for each signal and are compared.

In order to determine the SNR and code multipath/noise residual, test calculations were carried out using real data from different sources, e.g. from BKG and IGS, 24 hours Rinx data with 30 seconds sampling rate were retrieved. The purpose of this process was to determine the signal strength and raw quality of the perspective GNSS signal. Several stations collecting multi-GNSS signals were selected. Calculations were carried out for

Galileo signals during similar periods with approximately equal satellite geometry and according to the formulas in section 4.1 using the RTKLIB software.

By taking a large number of observations, the random error becomes minimal as the measurement quantity increases. Assuming the data was collected correctly following the standard procedure, its quality is affected by the receiver, the antenna, and the signal itself. Table 4.2 provides an overview of the stations which data has been investigated.

Table 4-2. Site Information, DOY 081, 2014

Station	Rec/ver		Antenna	Approx. Position			Antenna Offset		
				X (m)	Y (m)	Z (m)	H (m)	E (m)	N (m)
CHPG	TRIMBLE	NETR9 4.70	TRM59800.00	4163480.735	-4163816.902	-2444513.197	0.425	0.000	0.000
CPVG	TRIMBLE	NETR9 4.81	TRM59800.00	5626898.121	-2380937.028	1824483.527	0.430	0.000	0.000
DLF1	TRIMBLE	NETR9 4.81	LEIAR25.R3 LEIT	3924697.780	301125.130	5001905.290	0.000	0.000	0.000
FAA1	SEPT	POLARX4 2.5.2	LEIAR25.R4	-5246415.000	-3077260.000	-1913842.000	0.126	0.000	0.000
GOP7	JAVAD	TRE_G3TH DELTA3.5.1	LEIAR25.R4 LEIT	3979319.260	1050312.880	4857064.480	0.065	0.000	0.000
KIR8	TRIMBLE	NETR9 4.80	LEIAR25.R3 LEIT	2248127.371	865685.468	5886424.301	0.003	0.000	0.000
MAR7	TRIMBLE	NETR9 4.80	LEIAR25.R3 LEIT	2998198.758	931449.710	5533392.638	0.003	0.000	0.000
NNOR	SEPT	POLARX4 v2.5.1-patch1	SEPCHOKE_MC	-2414151.446	4907778.504	-3270645.187	0.112	0.000	0.000

Several stations from IGS network which is distributed around Europe were collected to obtain SNR and code multipath. The selected test stations allow processing of a range of different signals on GNSS (modernized GPS and Galileo). The data collection time was chosen to maximize the number of visible modernized satellites of GPS and Galileo.

These stations were chosen as most of the GNSS receivers and antenna are made of same brands. Hence, the test results expected to yield similar results. And the results from each station signal datasets will be compared.

#### 4.4.1 SNR and Code Multipath on GNSS signals

For all figures in section 4.4.1, RTKLIB extracts SNR data from RINEX files and computes a simple azimuth and elevation angle for easy reading and plotting into other programs, i.e. Matlab. The output format is: time, satellite number, azimuth angle in degrees, elevation angle in degrees, and SNR in dBHz. Then, the code multipath is calculated according the equation 4.21 in section 4.3 using a differencing method applied to the code and the phase measurements.

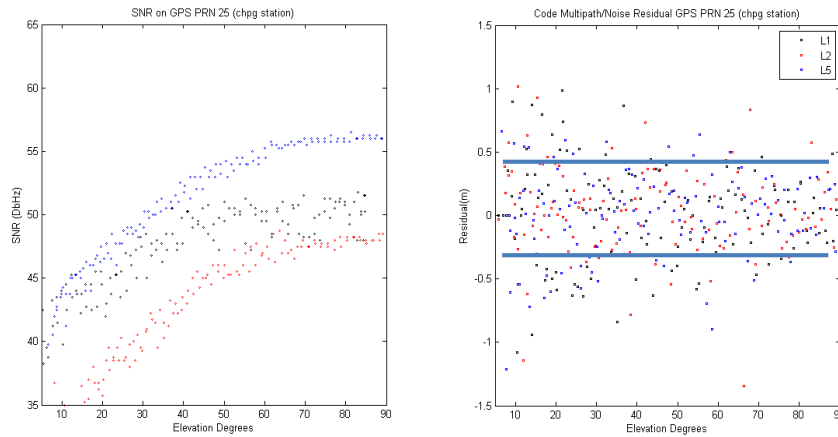


Figure 4-3. SNR and Multipath at CHPG station (Trimble NetR9, TRM59800) w.r.t. elevation of GPS PRN25

By example, figure 4-3 displays a slight difference at CHPG station in the signal strength between the L1, L2, and L5 GPS signals as well as residual errors due to multipath (GPS satellite PRN 25). The different signal strength values vary by approximately 10 dBHz when the satellite moves from low elevation to high elevation. The L5 GPS offers a better power than the legacy signals known as L1 and L2 GPS. Although L5 GPS provides a better signal strength, the code multipath/noise residuals on L5 GPS are similar to L1 and L2 GPS signal. L1 and L2 GPS signals have code multipath/noise residuals of about 30 to 40 cm with a maximum residual up to 1 meter at low satellite elevations (refer to blue line in figure 4-3).

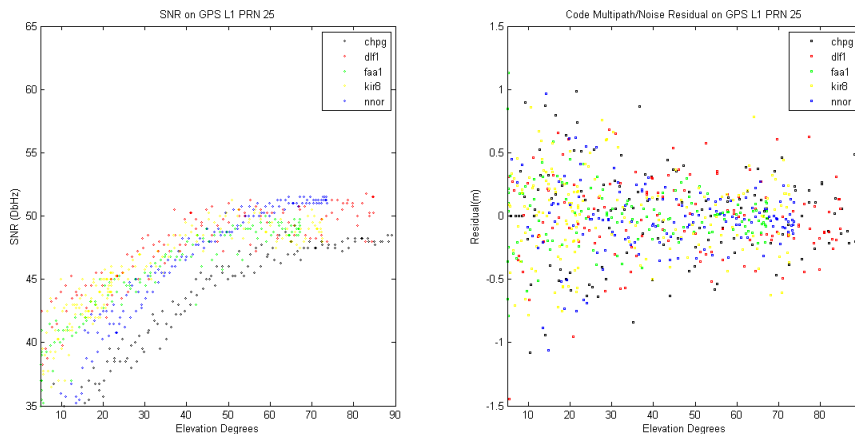


Figure 4-4. SNR and Code Multipath/Noise Residuals of L1 GPS signals of various IGS stations w.r.t. elevation of GPS PRN25



Comparing SNR and code multipath residuals on L1 and L5 GPS on various stations shows no significant differences (refer to figure 4.4 and figure 4.5). Looking at the distribution epoch-by-epoch result of code multipath/noise residuals on each station, i.e. CHPG, DLF1, FAA1, KIR8, and NNOR, L1 and L5 GPS offers similar SNR and code multipath residuals. The L5 GPS signal has offered the best signal strength compared to the L1 GPS on PRN 25. The difference is up to 5 dBHz.

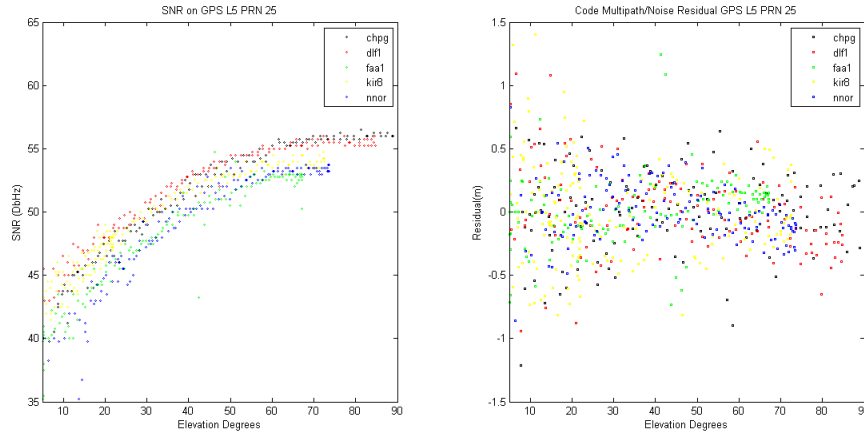


Figure 4-5. SNR and Code Multipath/Noise Residuals of L5 GPS signals of various IGS stations w.r.t. elevation of GPS PRN25

A comparison between L1 and L5 GPS confirms the L5 GPS signal intends to increase the precision and robustness of the navigation solution and seems to offer a similar characteristic to E5a (or part of E5) Galileo despite having similar signal strength with L1 GPS below 20 degrees elevation. L5 GPS can be implemented to enhance the mitigation design with higher signal strength compared to the existing GPS signals to mitigate the multipath/noise errors or the ionospheric error.

Using the same procedure as before, Galileo signals are generated and processed. The performance of Galileo signals is illustrated in figure 4.6, 4.7, and 4.8 which were computed by a subtractive combination of code range and carrier phase measurements to obtain the code multipath/noise residual and portrays the values of E1, E5, E5a, and E5b signals collected from the Galileo satellites.

Comparing the GPS results and Galileo results confirmed that the Galileo signals provide a more powerful signal strength, in particular the E5 Galileo signal (see figure 4-6). Comparing L1 GPS and E1 Galileo, the signal strength of Galileo differs up to 3-5 dBHz, although the same receiver and antenna was used. It shows a slight attenuation affecting the signal strength with respect to the satellite elevation.

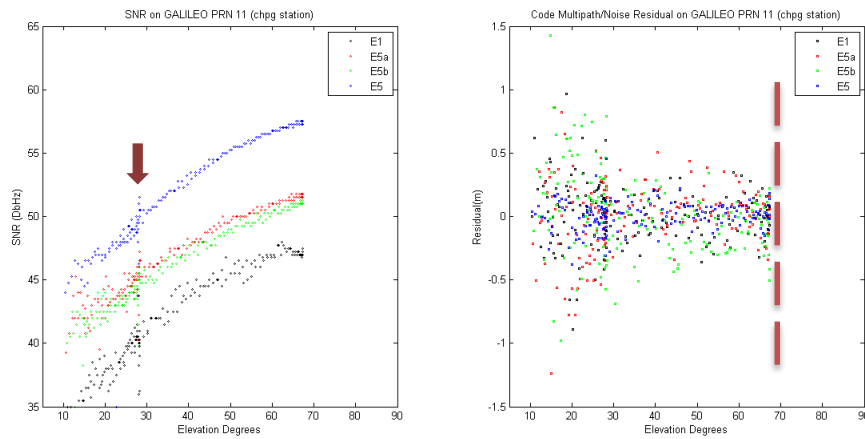


Figure 4-6. SNR and Code Multipath/Noise at CHPG (Trimble NetR9, TRM59800) w.r.t. elevation of Galileo E11

However, in figure 4-6 the displays code multipath/noise residuals show an unusual variation, particularly in low elevations (at 30 degrees satellite elevation and lower). They may be affected by internal problems of the data recording process. This effect does not appear at the other stations using the same receiver and antenna with Galileo PRN11 satellite signals (refer to figure 4-7). Unfortunately, SNR and code multipath/noise residual could not be calculated at high elevations as Galileo data were only available up to 70 degrees from horizon (see vertical line in figure 4-6).

The code multipath/noise residuals for E5 Galileo are smaller than for E1 Galileo. On average, the E5 provides 10 cm error standard deviation compared to E1 Galileo 25 cm standard deviation on code multipath/noise residuals. These characteristics open the possibility of performing code-range measurements using E5 Galileo at the decimeter level and enable a better mitigation of multipath effects. Moreover, E5 Galileo allowed more accurate combined code-and-carrier observable to mitigate ionospheric errors because it has the strongest signal strength of the modernized GNSS signals tested.

In the figure 4.7, the E5a and E5b Galileo signals show only slight differences of 1-2 dBHz in signal strength. Hence, these signals do not changes significantly for Galileo signals while on acquisition and tracking. As a whole, E5 (with E5a) Galileo signals provides best performance as they are more resistant against multipath/noise.

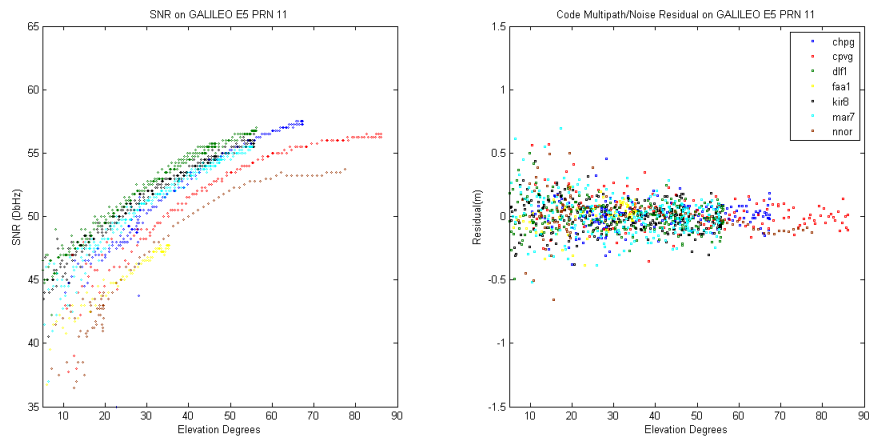


Figure 4-7. SNR and Code Multipath/Noise Residuals of Galileo signals of various IGS stations w.r.t. elevation of E11

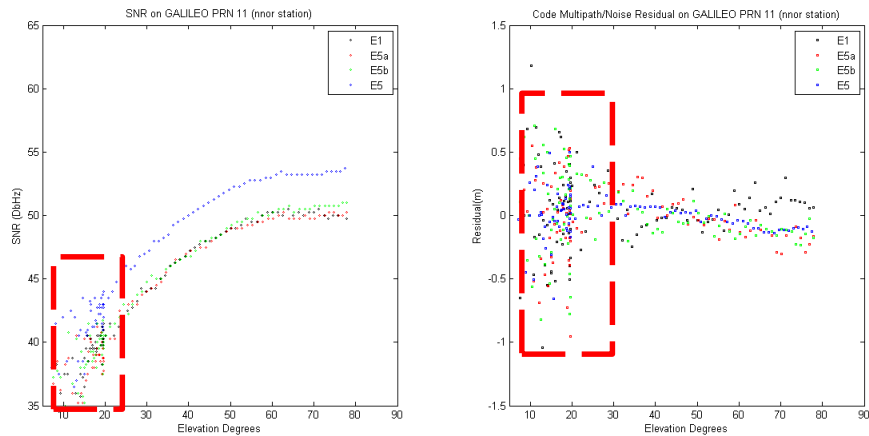


Figure 4-8. SNR and Code Multipath/Noise at NNOR (Sept Polar X4, Sepchoke\_MC) w.r.t. elevation of Galileo E11

Some stations displayed in figure 4-7 seem to be affected by equipment/internal problems when recording data below 30 degrees satellite elevation (refer to figure 4-6). One of them is displayed in the figure 4.8 (refer to red box). In detail, the residual at the NNOR station provide a small standard deviation of up to 0.15 m at higher satellite elevation. However, below 30 degrees there is no difference (up to 0.5 m) compared to the CHPG station. At 30 degrees elevation, all Galileo signals residuals seem to be random and show an unusual deviation that suddenly dissipate when the satellite elevation gradually going higher.

The E1, E5a, and E5b Galileo signals deliver on average residuals of about 0.18 m to 0.25 m. Moreover, the E5 Galileo signal provides highest signal strength and provides the lowest code multipath/noise residual. The E1, E5a, E5b Galileo signals are affected by

almost equal noise values. Different antenna or receiver types distinguish by signal acquisition and tracking.

Back again with the GPS signals results, the GPS data processing shows high- and low-SNR values affected by antenna and receiver algorithm. To further analyze, the SNR values obtained for the same time and same satellite tracking with respect to satellite elevation on each signal were separately analyzed (figure 4-9, figure 4-10, and figure 4-11).

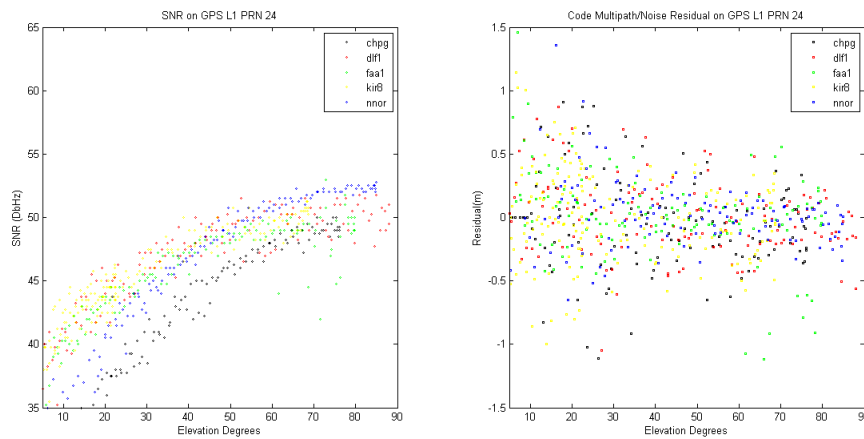


Figure 4-9. SNR and Code Multipath/Noise Residuals of L1 GPS signal of various IGS stations w.r.t. elevation of PRN24

By using the same acquisition and calculation methods as before, the SNR values of the L1 signal vary in the figure 4-9 although using the same antenna and receiver type. The differences of signal strength and range residuals are not significant with a deviation of about 2-3 dBHz at all stations. This statement is also valid for the L5 GPS signal. Compared to the other figures, SNR obtained from L2 GPS signal in figure 4.10 varied up to 5 dBHz.

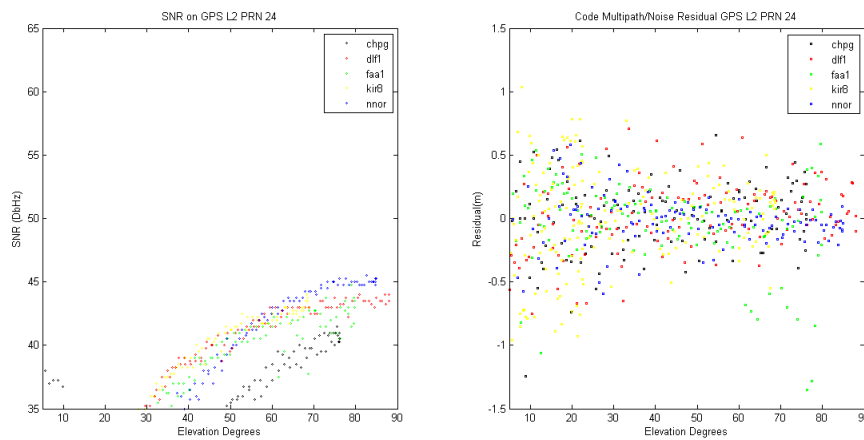


Figure 4-10. SNR and Code Multipath/Noise Residuals of GPS L2 signal of various IGS stations w.r.t. elevation of PRN24

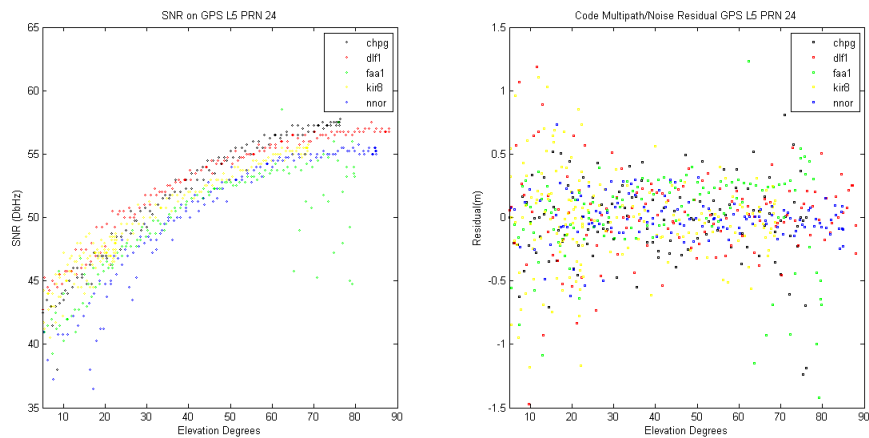


Figure 4-11. SNR and Code Multipath/Noise Residuals of GPS L5 signal of various IGS stations w.r.t. elevation of PRN24

There is an average residual deviation up to 0.4 m pattern in the code multipath/noise residuals at all stations. Comparable results are achieved at all stations using same antenna. It seems to be an indication of the systematic pattern due to un-modeled phase center variations, since phase center variations of the antennas were assumed. Moreover, the code multipath/noise residuals in L1, L2, and L5 GPS signals are affected similar by un-modeled phase center variations.

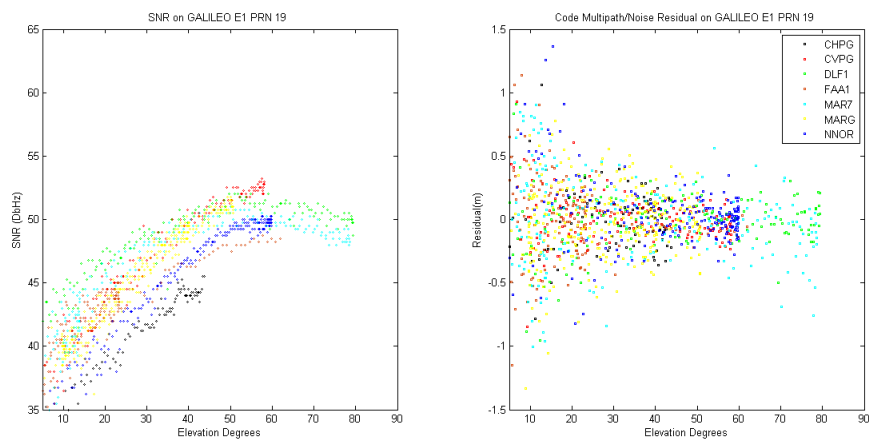


Figure 4-12. SNR and Code Multipath/Noise Residuals of E1 Galileo of various IGS stations w.r.t. elevation of E19

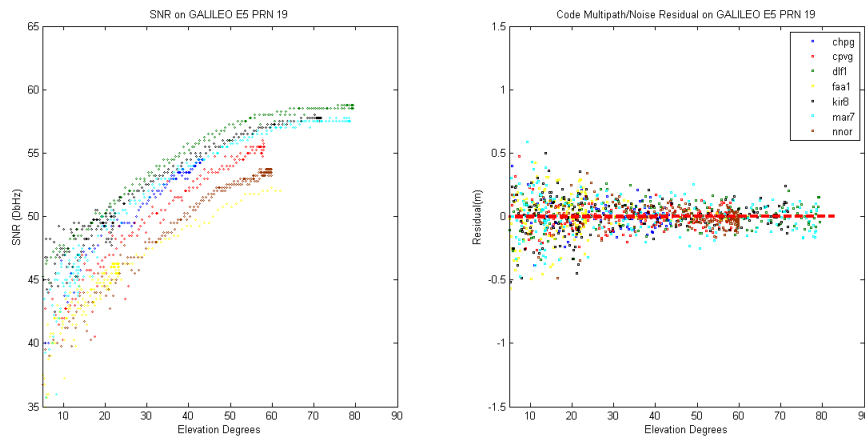


Figure 4-13. SNR and Code Multipath/Noise Residuals of E5 Galileo of various IGS stations w.r.t. elevation of E19

A different result for stations that using the same antenna and receiver is visible in figure 4.12 and 4.13. The E5 Galileo signal from several IGS stations provides a high SNR results with the difference up to 5 dBHz and a low code multipath/noise residuals less than 0.5 m compared with other GNSS signals (refer to figure 4-9, 4-10, and 4-11). However, from the practical point of view, is not feasible to predict the GNSS signals quality purely from SNR and the code multipath/noise residuals as there are many possibilities to obtain a better raw GNSS signal with different results.

In case of the E1 Galileo signal, the SNR and the code multipath/noise residual seems to perform better than the L1 GPS (up to 1-2 dBHz for signal strength and up to 0.1 m for residual difference). On the other hand, E5 Galileo performs best in SNR and code multipath/noise residuals at every station tested. When selecting promising signals for future real-time positioning, the combined E5 Galileo signal emerges as the best alternative (better than E5a or E5b).

#### 4.4.2 Conclusions on SNR and Code Multipath

In order to analyze the behavior of SNR and code multipath/noise, observations from the 5 stations i.e. CHPG, DLF1, FAA1, NNOR, and KIR8 were processed. Code range residuals were ordered in separate elevation degrees. By using an epoch by epoch method, each epoch was processed to get SNR and code range residuals and then an averaging method was adapted to get mean values for the 5 stations. 6 GNSS signals were processed from 5 stations i.e. L1 (C/A), L2C (M+L) GPS – civil-moderate code (M) and civil-long code (L), L5 (I+Q) GPS and E1 (B+C), E5b (I+Q), E5a (I+Q), E5 (I+Q) Galileo.

The code range residuals and the SNR are displayed in table 4-3 and 4-4.

Table 4-3. Code Range Residuals (m) of GNSS signals, DOY 081, 2014

GNSS Signal	Satellite Elevation (deg)								
	<10	10-20	20-30	30-40	40-50	50-60	60-70	70-80	80-90
<b>L1(C/A) GPS</b>	0.32	0.33	0.26	0.21	0.19	0.18	0.17	0.18	0.15
<b>L2C(M+L) GPS</b>	0.40	0.32	0.25	0.19	0.18	0.16	0.16	0.16	0.12
<b>L5(I+Q) GPS</b>	0.37	0.28	0.22	0.20	0.19	0.18	0.22	0.31	0.13
<b>E1(B+C) GAL</b>	0.36	0.24	0.18	0.14	0.14	0.12	0.11	0.09	NaN
<b>E5a(I+Q) GAL</b>	0.36	0.27	0.22	0.16	0.13	0.12	0.13	0.05	NaN
<b>E5b(I+Q) GAL</b>	0.37	0.30	0.25	0.18	0.14	0.13	0.13	0.08	NaN
<b>E5(I+Q) GAL</b>	0.16	0.13	0.10	0.07	0.06	0.05	0.05	0.03	NaN

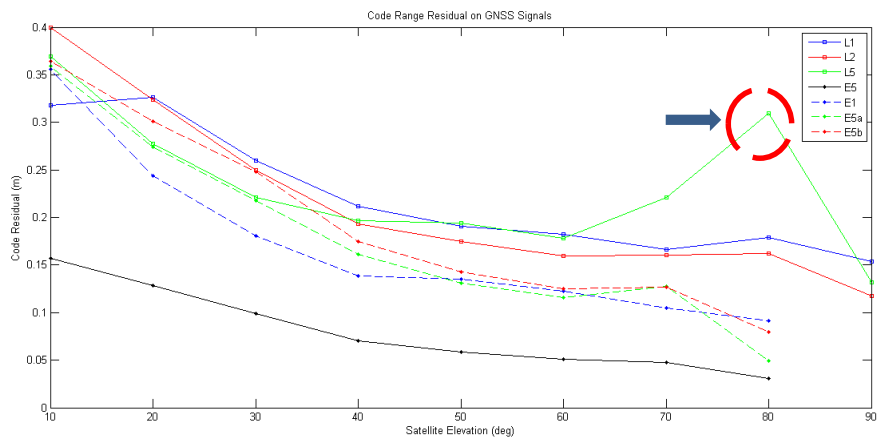


Figure 4-14. Code Range Residuals (m) of GNSS signals, DOY 081, 2014

As shown in table 4-3 and figure 4-14, the E5 Galileo signal performs best compared to the other signals. In case of the number of satellites at high elevation, notably for the L5 GPS signal, the insufficient number of satellites affects the statistic and cause high code multipath/noise residual (refer to the spike in figure 4-14). Yet, when looking at signal strength, the E5 Galileo signal performs best in combination with lowest multipath residual values at every station tested. Hence the value should be considered as preliminary as the number of data samples was small.

In table 4-4 and figure 4-15, the E5 Galileo signal provides the highest SNR for every satellite elevation angle compared to the other GNSS signals even though the E5 Galileo signal SNR is only slightly higher than the L5 GPS signal. As L1 GPS, E1, E5a, and E5b Galileo are within a similar range of SNR with a difference of approximately 1-2 dBHz and rising up following the satellite elevation. On the other hand, the L2 GPS signal shows the lowest SNR with a difference between 15-20 dBHz compared to other GNSS signals which can affect the signal performance for real-time positioning.

Table 4-4. SNR of GNSS signals, DOY 081, 2014

GNSS Signal (dBHz)	Satellite Elevation (deg)								
	<10	10-20	20-30	30-40	40-50	50-60	60-70	70-80	80-90
<b>L1(C/A) GPS</b>	36.9	40.9	43.8	46.2	47.9	48.4	48.8	48.6	47.9
<b>L2(M+L) GPS</b>	20.4	23.7	28.6	33.4	36.8	38.6	40.3	40.7	39.7
<b>L5(I+Q) GPS</b>	41.0	45.1	48.0	50.6	52.7	53.9	54.7	54.7	55.0
<b>E1(B+C) GAL</b>	37.3	40.9	43.3	45.9	47.1	48.2	48.7	49.9	NaN
<b>E5a(I+Q) GAL</b>	38.0	41.7	44.0	46.5	48.0	49.4	50.6	51.4	NaN
<b>E5b(I+Q) GAL</b>	37.6	41.4	43.8	46.3	47.8	49.3	50.5	52.0	NaN
<b>E5(I+Q) GAL</b>	41.8	45.7	48.4	51.2	52.9	54.6	55.6	57.7	NaN

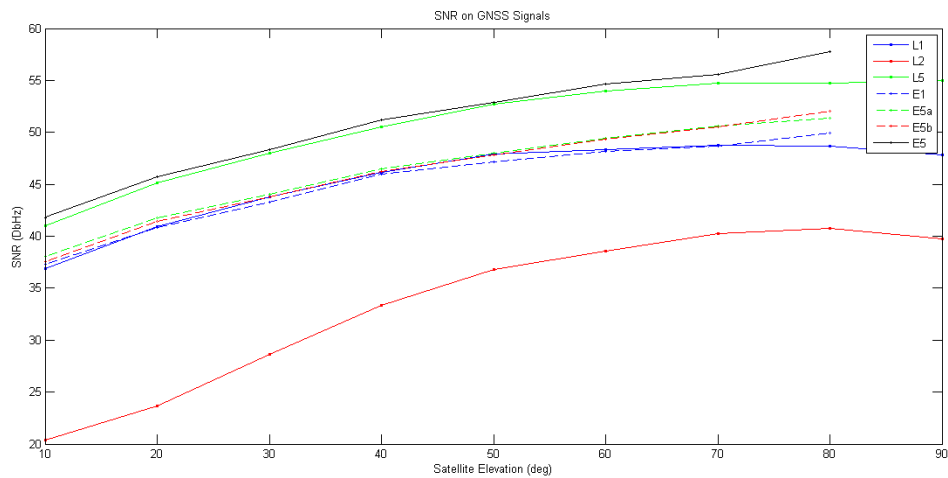


Figure 4-15. SNR of GNSS Signals, DOY 081, 2014

Finally, different GNSS receivers with the same antenna i.e. CHPG, DLF1, and KIR8 tracking the same satellite at the same time may provide different SNR values. This differences could be from band limitation or processing algorithms. In case of independent acquisition and tracking algorithms used by a receiver, the values could be considered to indicate the quality of the received signal when antenna and receiver type, design, and performance are neglected. Hence the SNR depends on the receiver bandwidth, signal acquisition and tracking parameter.

Because multipath errors are site-specific and particularly affect the code ranges, the use of E5 Galileo provides an advantage, as this signal shows a low multipath/noise residual behavior compared to all other GNSS signals. Moreover, due to its higher signal strength, the E5 Galileo signal is preferable for positioning because the signal is more resilient against outside interference than other GNSS signals and offers advantages to mitigate multipath/noise and ionospheric errors.



## 5. GNSS Carrier-Phase Linear Combinations

In this chapter, a general form of phase linear combinations is developed and the features of a variety of specific phase linear combinations are studied and compared. The chapter begins with the search for an optimal linear combination for GNSS RT-positioning over short and medium baselines by deriving the multi-frequency combinations characteristics and then selecting the combinations which have the most desirable characteristics. As the basics of dual frequency linear combination are explained in chapter 2, the next paragraph starts with a description of triple linear combinations.

### 5.1 Triple Carrier Linear Combinations

Based on double differences (Urquhart, 2009), a number of linear combinations of the phase measurements can be generated. These can be helpful in the ambiguity estimation process for baselines longer than 15 km, where the influence of the spatially correlated errors is significant.

The derivation of triple frequency carrier phase combinations of GNSS data can be performed in general for both the GPS and Galileo systems. For GPS the carriers L1, L2, and L5 are utilized. The simplified carrier phase observation at frequency  $n$  (in units of length) is displayed in equation 5.1 where ( $m$ ) represents units of meters:

$$L_n(m) = \rho + \lambda_n N_n - I_n \quad (5.1)$$

$\rho$  represents the geometric range and contains clock and troposphere terms,  $\lambda_n$  is the wavelength,  $N_n$  is the ambiguity, and  $I_n$  is the ionospheric propagation delay on the signals of the frequencies (e.g. L1, L2, and L5). A linear combination of the three carrier phases can be formed by:

$$LC(m) = \alpha L1 + \beta L2 + \gamma L5 \quad (5.2)$$

Equation 5.2 can be expanded to:

$$LC(m) = \rho (\alpha + \beta + \gamma) + \alpha \lambda_{L1} N_{L1} + \beta \lambda_{L2} N_{L2} + \gamma \lambda_{L5} N_{L5} - \alpha I_{L1} - \beta I_{L2} - \gamma I_{L5} \quad (5.3)$$

In order to obtain a combination to be useful for ambiguity resolution, an integer ambiguity should be constrained. To keep the geometric portion unchanged, the equation reads:

$$N = \frac{\alpha\lambda_{L1}N_{L1}}{\lambda} + \frac{\beta\lambda_{L2}N_{L2}}{\lambda} + \frac{\gamma\lambda_{L5}N_{L5}}{\lambda} \quad (5.4)$$

In order that N shall be an integer, the coefficients  $i, j, k$  can be defined as:

$$i = \frac{\alpha\lambda_{L1}}{\lambda}, j = \frac{\beta\lambda_{L2}}{\lambda}, k = \frac{\gamma\lambda_{L5}}{\lambda} \quad (5.5)$$

By arranging the equations in terms of  $\alpha, \beta, \gamma$  the coefficients can be calculated:

$$\alpha = \frac{i\lambda}{\lambda_{L1}}, \beta = \frac{j\lambda}{\lambda_{L2}}, \gamma = \frac{k\lambda}{\lambda_{L5}} \quad (5.6)$$

The wavelength for the new linear combination can be formed from equation  $\alpha+\beta+\gamma = 1$ , which is the geometric constraint (Odijk, 2003), to yield:

$$\lambda = \frac{(\lambda_{L1}\lambda_{L2}\lambda_{L5})}{(i\lambda_{L2}\lambda_{L5} + j\lambda_{L1}\lambda_{L5} + k\lambda_{L1}\lambda_{L2})} \quad (5.7)$$

The frequency can be formed from equation:

$$f = if_{L1} + jf_{L2} + kf_{L5} \quad (5.8)$$

To obtain the linear combination parameterized in units of cycles, each frequency is divided by its wavelength and combined:

$$\Phi_{i,j,k}[cy] = \frac{\rho}{\lambda} + iN_{L1} + jN_{L2} + kN_{L5} - \frac{I_{L1}}{\lambda_{L1}} - \frac{I_{L2}}{\lambda_{L2}} - \frac{I_{L5}}{\lambda_{L5}} \quad (5.9)$$

### 5.1.1 Noise and Multipath Observation

A small signal noise of the introduced linear combination in addition to a long wavelength is prerequisite for a fast ambiguity resolution. The observation noise can be calculated following the law of error propagation,

$$\sigma_{\Phi_{i,j,k}}[cy] = \sqrt{i^2\sigma^2_{\Phi_{L1}} + j^2\sigma^2_{\Phi_{L2}} + k^2\sigma^2_{\Phi_{L5}}} \quad (5.10)$$

and in meters:

$$\sigma_{\Phi_{i,j,k}}[m] = \sqrt{\alpha^2\sigma^2_{\Phi_{L1}} + \beta^2\sigma^2_{\Phi_{L2}} + \gamma^2\sigma^2_{\Phi_{L5}}} \quad (5.11)$$

The white noise of our basic phase observations can be assumed to be at the 1.5 mm level.

According to Hofmann-Wellenhof (2001), the error due to multipath is at its maximum  $\frac{1}{4}$  of the total wavelength. Multipath is not a random error, but a systematic one. The effect of multipath on the linear combination can be calculated according to:

$$mp_{\Phi_{i,j,k}}[cy] = i mp_{\Phi_{L1}} + j mp_{\Phi_{L2}} + k mp_{\Phi_{L5}} \quad (5.12)$$

$$mp_{\Phi_{i,j,k}}[m] = \alpha mp_{\Phi_{L1}} + \beta mp_{\Phi_{L2}} + \gamma mp_{\Phi_{L5}} \quad (5.13)$$

As we make use of the wide-lane linear combination, ionosphere linear combination, and multipath linear combination in GNSS point positioning, this chapter also discusses in more detail their characteristics.

### 5.1.2 Wide-lane Combination

The advantage of the dual-carrier wide-lane measurement built from GPS L1 and L2 signals is the longer wavelength (0.86 m) that makes it easier to solve ambiguities. To define a wide-lane triple linear combination, the equation can be as follows if:

$$\frac{\lambda_{L1}\lambda_{L2}}{i\lambda_{L2}\lambda_{L5}+j\lambda_{L1}\lambda_{L5}+k\lambda_{L1}\lambda_{L2}} > 1, \text{ there exist } \lambda > \lambda_{L5} \quad (5.14)$$

where  $\lambda_{L5}$  is the wavelength of L5 GPS. By rearranging the inequality and using the identities  $r = \frac{f1}{f5}$  and  $t = \frac{f2}{f5}$  we obtain:

$$1 - ir - jt > k > -ir - jt \quad (5.15)$$

Since the range of inequality is one, there can only be one value of k for any combination of i and j.

$$k = \text{ceil}(-ir - jt) \quad (5.16)$$

By substituting this equation for k into equation  $\lambda$ , the expression for the wavelength as a function of i and j reads:

$$\lambda(i, j) = \frac{\lambda_{L5}}{ir+jt+\text{ceil}(-ir-jt)} \quad (5.17)$$

To minimize the noise of the wide-lane, the absolute values of i and j should be minimized to be (Henkel and Gunther, 2007),

$$i \in [-57, 57], j \in [-11, 11] \quad (5.18)$$

Table 5-1. Optimal Wide Lane Combinations (Urquhart, 2009)

LC	$\lambda_1$	$\lambda_2$	$\lambda_5$	$\lambda(m)$	$\lambda/\text{noise}$
	0	-1	2	0.266	0.086
ML	1	0	-1	0.751	0.136
WL	1	-1	0	0.862	0.136
	1	-2	1	1.011	0.079
	1	-5	4	2.093	0.030
HR	1	-6	5	3.256	0.025
	3	1	-5	4.187	0.033
EW	0	1	-1	5.861	0.137
HR	1	-7	6	7.326	0.021
	-3	1	3	9.768	0.044
HR	3	0	-4	14.653	0.038
HR	4	-8	3	29.305	0.020

These combinations in table 5-1 were chosen because they have an extremely large wavelength and minimize the error sources while maintaining the wide-lane combination. We have always to keep in mind that the noise and ionospheric error amplification can also affect the chances of a successful ambiguity resolution. The most common LC shown in table 5-1 is the extra wide-lane (EW), wide-lane (WL), and middle-lane (ML) with wavelengths of approximately 5.86 m, 0.86 m, and 0.75 m respectively. However, a drawback of these combinations, i.e. WL [1,-5,4] is that the noise amplification considerable and could degrade the precision of the solution.

### 5.1.3 Melbourne-Wübbena Combination

The Melbourne-Wübbena Linear Combination based on dual-frequency signals is a linear combination that eliminates the ionospheric delay, the geometry, the clock, and the tropospheric delay. The combination is given by (Xu, 2007, Davaine, 2011),

$$MW = \frac{1}{f_i - f_j} (f_i L_i - f_j L_j) - \frac{1}{f_i + f_j} (f_i P_i - f_j P_j) \quad (5.19)$$

Equation 5.21 can be noted in terms of integer ambiguities N,

$$MW = \lambda_w \left( N_{1,i}^k - N_{2,i}^k + \frac{\beta_1^k}{\lambda_1} - \frac{\beta_2^k}{\lambda_2} \right) + f(\epsilon_{1,i}^k, \epsilon_{2,i}^k, \eta_{1,i}^k, \eta_{2,i}^k) \quad (5.20)$$

with the wide-lane wavelength  $\lambda_w$  and the combined noise term  $f$ ,

$$\lambda_w = \frac{1}{\frac{1}{\lambda_1} - \frac{1}{\lambda_2}} \quad f(\epsilon_{1,i}^k, \epsilon_{2,i}^k, \eta_{1,i}^k, \eta_{2,i}^k) = \frac{f_1 \epsilon_{1,i}^k - f_2 \epsilon_{2,i}^k}{f_1 - f_2} - \frac{f_1 \eta_{1,i}^k - f_2 \eta_{2,i}^k}{f_1 + f_2} \quad (5.21)$$

$\beta_i^k$  is the difference between the phase clock offset on  $f_1$  and ionosphere-free phase clock offset for user  $i$  and satellite  $k$ ,  $\epsilon$  is phase noise including multipath, and  $\eta$  is pseudorange noise including multipath.

The wavelength of the Melbourne-Wübbena combination corresponds to the wide-lane linear combination (in case GPS L1 and L2, 86.2 cm).

$L_i$  and  $L_j$  in equation 5.19 (expressed in meters) are assumed to be equally accurate and uncorrelated. Note that the noise level of the MW linear combination is pre-determined exclusively by the quality of the code data considered.

#### 5.1.4 Ionosphere linear combination

Another important linear combination is the ionosphere free (IF) linear combination,

$$\Phi_{IF} = \Phi_{L1} - \frac{f_2}{f_1} \Phi_{L2} \quad (5.22)$$

The advantage of the ionosphere-free combination is that the first order ionospheric effect is removed. The disadvantage is that the double difference ambiguity is not an integer, so it is more sensitive to noise, and it is difficult to test whether it is solved correctly. However, Odijk (2003) shows that it is possible to rewrite the equation to obtain an expression with an integer property of the ionosphere-free double differenced ambiguities.

When using  $\Phi_{IF}$  most of the ionospheric errors are removed, but higher order effects must be taken into account and are still in. For baselines longer than 50 - 100 km these higher order terms must be included in data processing.  $\Phi_{IF}$  can be useful in the ambiguity resolution where  $\nabla\Delta N_{L1}$  and  $\nabla\Delta N_{L2}$  can be resolved easier after  $\nabla\Delta N_{IF}$  have been determined. A major disadvantage is the noise, which is amplified by the linear combination.

In case of available observations of (at least) 3 frequencies the ionospheric delay can be mitigated. It is necessary to write the ionospheric delay on each frequency in terms of the delay experienced by the L1 GPS frequency. From equation (5.22), the ionospheric delay for a linear combination of the 3 GPS frequencies in unit meters is noted as:

$$I_{LC} = \alpha I_{L1} + \beta I_{L2} + \gamma I_{L5} \quad (5.23)$$

Then relating the expressions for each order terms with respect to the delay experienced by just the L1 term, the equation can be reformulated as (Urquhart, 2009):

$$\begin{aligned}
I_{LC}^{1st}[m] &= I_{LC}^{1st} \left( \alpha + \beta \frac{f_1^2}{f_2^2} + \gamma \frac{f_1^2}{f_5^2} \right), I_{LC}^{1st}[cyc] = \frac{I_{LC}^{1st}}{\lambda_{L1}} \left( i + j \frac{f_1}{f_2} + k \frac{f_1}{f_5} \right) \\
I_{LC}^{2nd}[m] &= I_{LC}^{2nd} \left( \alpha + \beta \frac{f_1^3}{f_2^3} + \gamma \frac{f_1^3}{f_5^3} \right), I_{LC}^{2nd}[cyc] = \frac{I_{LC}^{2nd}}{\lambda_{L1}} \left( i + j \frac{f_1^2}{f_2^2} + k \frac{f_1^2}{f_5^2} \right) \\
I_{LC}^{3rd}[m] &= I_{LC}^{3rd} \left( \alpha + \beta \frac{f_1^4}{f_2^4} + \gamma \frac{f_1^4}{f_5^4} \right), I_{LC}^{3rd}[cyc] = \frac{I_{LC}^{3rd}}{\lambda_{L1}} \left( i + j \frac{f_1^3}{f_2^3} + k \frac{f_1^3}{f_5^3} \right)
\end{aligned} \tag{5.24}$$

The first order term of the ionospheric delay is by far the largest,

$$\left| \alpha + \beta \frac{f_1^2}{f_2^2} + \gamma \frac{f_1^2}{f_5^2} \right| \approx 1 \text{ and in cycles } \left| i + j \frac{f_1}{f_2} + \gamma \frac{f_1}{f_5} \right| \approx 1 \tag{5.25}$$

The simplest method to find all those combinations that satisfy this inequality is to create a loop to run through the coefficients of i, j and k and this leaves an enormous number of possibilities. To further refine the search, the possibilities based on the other characteristics such as wavelength and noise amplification factors can be narrowed down.

Selecting an optimal linear combination can be a difficult task. Depending on the conditions at a given site the linear combination that will provide the best result will vary temporally. Further to take into account is a consideration how to choose a reasonable wavelength so the ambiguities can be resolved.

It is not always necessary or advantageous to completely eliminate the ionospheric delay. When choosing a combination that will significantly reduce ionospheric delays, the combination may be able to less susceptible to noise and multipath effects or have a larger wavelength. Other research has typically resulted in wavelengths of about 0.10 meters. It has been shown that even with wavelengths of about 0.10 meters it is still possible to properly solve for the ambiguities (Richert, 2007). Unfortunately, orbital errors and tropospheric delays are independent of frequency, so the IF-LC cannot reduce these effects. Table 5-2 shows the theoretical results using the coefficients of i, j, k to calculate the optimal IF-LC for GPS signals.

Table 5-2. Optimal Combination for GPS (Urquhart, 2009)

i	j	k	$\lambda(m)$	Amplification (cycle)					Amplification (meter)				
				Noise	mp	I <sup>1st</sup>	I <sup>2nd</sup>	I <sup>3rd</sup>	Noise	mp	I <sup>1st</sup>	I <sup>2nd</sup>	I <sup>3rd</sup>
4	1	-4	0.1062	5.715	2.25	-0.073	-1.53	-3.49	3.177	5.02	-0.04	-0.85	-1.95
4	0	-3	0.1081	4.982	1.75	-0.017	-1.38	-3.2	2.824	3.98	-0.01	-0.78	-1.82
4	-1	-2	0.1102	4.572	1.75	0.0384	-1.23	-2.92	2.642	4.05	0.022	-0.71	-1.69
5	-5	1	0.1028	7.105	2.75	-0.078	-1.44	-3.17	3.828	5.94	-0.04	-0.78	-1.71

Table 5-2 outlines the theoretical characteristics for each selected combination of GPS carriers L1, L2, L5 including the wavelength ( $\lambda$ ), noise amplification (noise) and higher order ionospheric delay amplification I<sup>1st</sup>, I<sup>2nd</sup>, and I<sup>3rd</sup> in units of cycles and meters.

## 5.2 Calculation Tests of Linear Combinations

Table 5-3. Scenario for Post-processing Calculations

<b>Parameter</b>	<b>1st Scenario</b>	<b>2nd Scenario</b>
	<b>setting</b>	<b>Setting</b>
<i>System</i>	GPS	<b>GPS, Galileo</b>
<i>Frequency</i>	L1, L2	<b>L1, L2, L5, E1, E5 (E5a, E5b)</b>
<i>Positioning Mode</i>	Static	<b>Static, Kinematic</b>
<i>Integer Ambiguity Res.</i>	Continuous	<b>Continuous, fix and hold</b>
<i>Error Sources</i>	Atmospheric, Clock	<b>Atmospheric, Clock</b>
<i>Troposphere Correction</i>	Saastamoinen	<b>Saastamoinen</b>
<i>Ionosphere Correction</i>	Broadcast/NL	<b>WL/MW/IGS</b>
<i>Satellite Ephemeris</i>	IGS	<b>Broadcast/UltraRapid (IGS)</b>
<i>Elevation Mask</i>	5/10/15 degrees	<b>5 degrees</b>
<i>Observation Time</i>	Long Observation (24 h)	<b>short Observation (5/10/15/30/60 minutes)</b>

The following calculations were carried out using data from different sources, i.e. 24 hours of observation Rinx data from BKG with 30 seconds sampling rate. Calculations were also carried out with Galileo signals (if available) during similar observation periods in equal satellite geometry. Integer ambiguities are estimated and resolved on an epoch-by-epoch basis in kinematic positioning mode. A summary of the general parameter setting is given in table 5-3.

The initial scenario assumes all the observations are processed in difference mode. Hence, the atmospheric errors and clock errors are almost canceling. To create a scenario with different lengths of baselines, the data were sorted out by the stations to arrange the conditions required. As the local time and the location of the test are essentially affecting the results due to variations in the ionosphere and troposphere activity, calculations of the measurement effect on morning and afternoon sessions were performed.

Mask angles of five degrees, ten degrees, and fifteen degrees were selected. The receiver noise level was neglected, and when required, IGS precise orbit corrections were used. Tropospheric effects are also independent of frequency. Hence a Saastamoinen model was used as the standard model correction.

Furthermore, baseline observations were grouped in short-term observations (less than and equal to 60 minutes) for positioning in particular to study with the impact of temporal variability and long-term observations (24 hours and 30 seconds sampling rate) for static and kinematic positioning.

In order to analyze the multi-signal performance dual- and triple-difference observations were processed and the results from the carrier phase observable among GPS and Galileo are compared. The first step was to apply the linear combination to both systems. For the analysis, it is necessary to choose data which cover visible satellites for the entire simulation. Additionally, since most observation data covers satellites with low elevation angles, observation to satellites which are below 5 degrees are removed to minimize the influence of errors in the data processing.

To test which ionosphere corrections are an optimum, several sources, i.e. broadcast, IGS model correction, Narrow-Lane Linear combination, and Wide-Lane linear combination were introduced to check how the ionosphere correction can improve the ambiguity fixing for GNSS positioning. The IGS stations used in the data processing are listed in table 5-4.

Table 5-4. List of Test Stations

<i>POINT</i>	<i>SIGNAL</i>			<i>Epoch (s)</i>	<i>Network</i>	<i>DOY/Year</i>
	<i>GPS</i>	<i>Glonass</i>	<i>Galileo</i>			
<b>ARIF</b>	L1, L2	-	-	30	Other	240/2014
<b>AXPV</b>	L1, L2, L5	G1,G2	E1, E5	30	IGS	240/2014
<b>PBRT</b>	L1, L2	-	-	30	Other	240/2014
<b>CEBR</b>	L1, L2, L5	G1,G2	E1, E5	30	IGS	240/2014
<b>CREI</b>	L1, L2	G1,G2	-	30	IGS	240/2014
<b>GANP</b>	L1, L2, L5	G1,G2	E1, E5	30	IGS	240/2014
<b>KRA1</b>	L1, L2, L5	G1,G2	-	30	IGS	240/2014
<b>MARS</b>	L1, L2, L5	G1,G2	E1, E5	30	IGS	240/2014
<b>MLVL</b>	L1, L2	G1,G2	-	30	IGS	240/2014
<b>SMNE</b>	L1, L2, L5	G1,G2	E1, E5	30	IGS	240/2014
<b>TLMF</b>	L1, L2, L5	G1,G2	E1, E5	30	IGS	240/2014
<b>TLSE</b>	L1, L2, L5	G1,G2	E1, E5	30	IGS	240/2014
<b>VILL</b>	L1, L2, L5	G1,G2	E1, E5	30	IGS	240/2014

Processing the data from table 5-4 was conducted to fix the ambiguity problem and to study the success rates of the various linear combinations. All the data used in chapter 5.2 are 24 hours long observations with 30 seconds. Furthermore, several of IGS stations have 1 hour short observation with 1 second sampling rate.



### 5.2.1 The effect of baseline length on ambiguity resolution

Table 5-5. Ambiguity Resolution using L1 GPS at DOY 240, 2014.

Baseline	Distance (km)	AMBIGUITY FIX (%)					
		iono (broadcast), orbit (broadcast)		iono (broadcast), orbit (IGS)		iono (IGS), orbit (IGS)	
		L1(%)	$\sigma$ (m)	L1(%)	$\sigma$ (m)	L1(%)	$\sigma$ (m)
ARIF - PBRT	0.2	99.9	0.01	92.1	0.29	92.5	0.01
TLMF - TLSE	8.7	95	0.05	99.4	0.02	97.3	0.01
MLVL-SMNE	11.9	100	0.02	100	0.03	100	0.01
AXPV - MARS	23.7	92.5	0.22	94.9	0.05	100	0.04
VILL - CEBR	35.3	85.9	0.19	78.6	0.15	99.9	0.03
MLVL - CREI	47.2	82.8	0.14	87.6	0.47	89.1	0.05
GANP - KRA1	118.4	10.2	1.99	4.4	1.37	12	3.18

When processing just GPS L1 data, the success rate of ambiguity resolution on baselines more than 20 km is below 90%. Utilization of orbit corrections (Ultra rapid correction from IGS) and ionospheric corrections (from IGS) on L1 GPS data processing can improve the ambiguity resolution success-rate on baselines more than 20 km. On the other hand, it becomes quite clear at baselines longer than 100 km, ambiguity fixing with just GPS L1 data is not possible.

Table 5-6. Ambiguity Resolution using L1 and L2 GPS at DOY 240, 2014

Baseline	Distance (km)	AMBIGUITY FIX (%)									
		iono (broadcast), orbit (broadcast)		iono (IGS), orbit (IGS)		Widelane, orbit (IGS)		Narrowlane, orbit (IGS)		Melbourne-Wubben, orbit (IGS)	
		L1/L2(%)	$\sigma$ (m)	L1/L2(%)	$\sigma$ (m)	L1/L2(%)	$\sigma$ (m)	L1/L2(%)	$\sigma$ (m)	L1/L2(%)	$\sigma$ (m)
ARIF - PBRT	0.2	100	0.01	100	0.01	92.5	0.29	99.9	0.01	97.9	0.25
TLMF - TLSE	8.7	99.4	0.02	94.9	0.02	98.5	0.02	85.2	0.12	82.5	0.72
MLVL-SMNE	11.9	99.3	0.02	99.5	0.02	99.6	0.03	98.4	0.03	90.2	0.38
AXPV - MARS	23.7	94.9	0.06	86.6	0.03	86.7	0.04	77.6	0.04	91.2	0.54
VILL - CEBR	35.3	93.5	0.06	82.8	0.03	95.9	0.02	33.1	0.08	89.9	0.25
MLVL - CREI	47.2	66.7	0.15	91.5	0.03	95.9	0.02	3.2	0.42	99.4	0.06
GANP - KRA1	118.4	26.9	0.44	94.4	0.03	94.8	0.04	1.9	0.53	82.8	0.05

When comparing table 5-5 and table 5-6, ambiguities with GPS L1/L2 data were fixed almost 100% with only using ionospheric correction from broadcast data at very short baselines. The success rate of ambiguity fixing then gradually declines about 80-90% when the length of baselines becomes more than 20 km. In case of medium baselines (more than 20 km), the success rate using only broadcast data corrections for orbit errors and ionosphere delay is below 70% with decimeter-level of standard deviation (refer to MLVL-CREI and GANP-KRA1 baselines). Utilizing IGS corrections (orbit and ionospheric) exhibit higher success rates on short and medium baseline (equal and more than 90% success rate).

Of course, narrow-lane ambiguities cannot be resolved at a high level on baselines longer than 40 km i.e. VILL-CEBR baseline. The Melbourne-Wübbena linear combination, gives a promising high success rate result of about 90% at varying test baselines. As also visible in table 5-6, IGS corrections can correct ionospheric errors and allow for resolving almost all the ambiguities even at medium baselines with a standard deviation up to 3 cm which is acceptable for real-time positioning.

Table 5-7. The cut-off Angle effect on Ambiguity Resolution at DOY 240, 2014

Baseline	Dist.	Cut off 10				Cut off 15			
		(iono + orbit broadcast)				((iono + orbit - broadcast)		IF – LC (narrow lane)	
		L1	$\sigma$ (m)	L1+L2	$\sigma$ (m)	L1+L2	$\sigma$ (m)	L1+L2	$\sigma$ (m)
ARIF-PBRT	0.2	99.9	0.01	99.9	0.01	100	0.01	97.9	0.14
SMNE -MLVL	11.9	91.7	0.02	85.1	0.02	86.4	0.02	96.0	0.21
AXPV-MARS	23.7	65.9	0.12	53.0	0.10	56.2	0.10	75.4	0.36
VILL-CEBR	35.3	65.4	0.09	32.1	0.12	32.3	0.15	98.6	0.36

Table 5-7 displays the cut-off angle effects and contributes to the success rate of ambiguity resolution, although it is only a slight improvement up to 5% when the masking angle was changed from 10 degrees to 15 degrees. The standard deviation of the coordinate solution shows only a slight variation up to 1 cm when using L1/L2 GPS with a different cut off angle for baselines under 20 km and varies when the length of the baseline becomes more than 20 km (up to 15 cm). On the other hand, even though the success-rate using the narrow-lane linear combination indicates a high percentage, the standard deviation is poor. As the standard deviation could be one of the key parameters to check the quality results, a standard deviation more than 10 cm is assumed to be not acceptable for positioning.

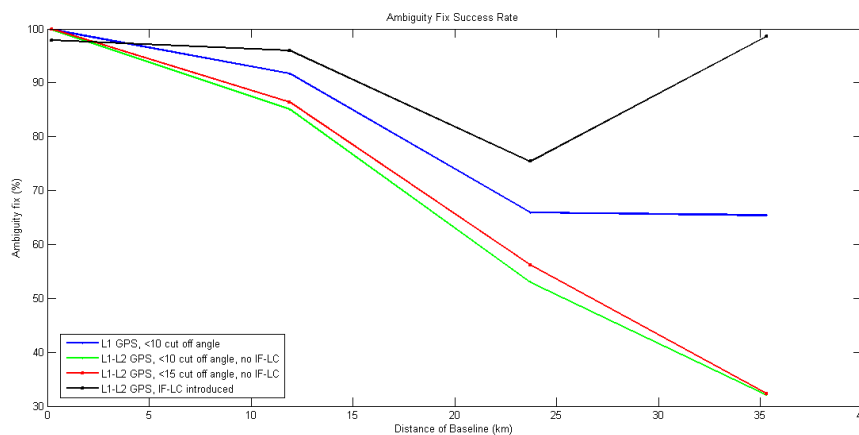


Figure 5-1. Ambiguity resolution success-rate

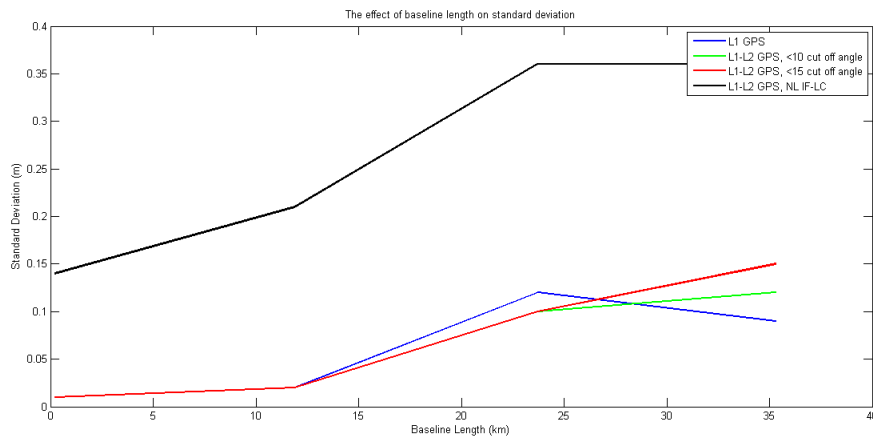


Figure 5-2. The effect of baseline length on coordinate standard deviation

The interesting part in table 5-7 is that the success rate of ambiguity resolution using just L1 GPS is sometimes better than using L1/L2 GPS linear combinations. When an ionosphere free linear combination of the observations was processed, all the ambiguities are solved even in baselines longer than 30 km, concerning the increased coordinate standard deviation we have to take into account the increased noise level of the ionosphere-free linear combination. Another problem might be from the RTKLIB assumption that a baseline up to 100 km is still considered as a medium baseline and this needs further investigation. The content of table 5-7 is illustrated in figures 5-1 and 5-2.

Another area of interest and evaluation is the influence of varying cut-off angles. The purpose of the elevation mask is to control the field of view. This is done to eliminate satellites which are too low at the horizon or to have more control over the satellite geometry used in the positioning solution. For a better illustration, please refer to figure 5-1, figure 5-2 (please check the appendix for the different baseline lengths).

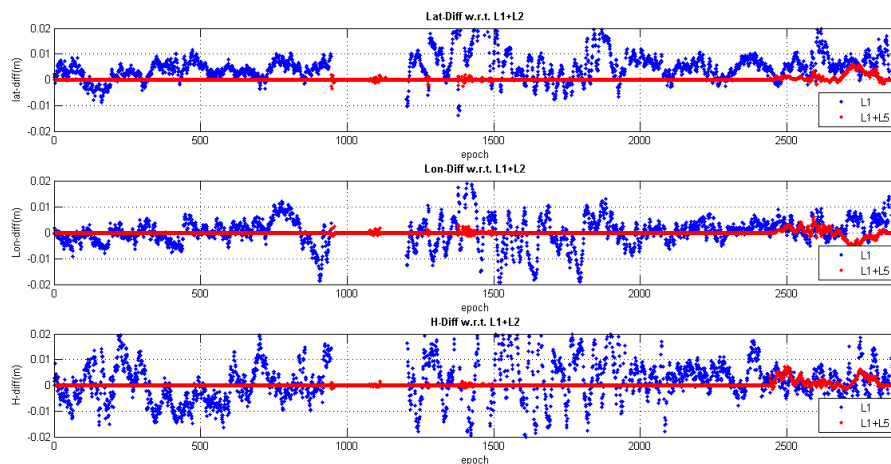


Figure 5-3. L1 GPS and L1/L5 GPS position biases w.r.t. L1/L2 GPS solution (reference); TLMF-TLSE baseline (8.7 km)

As only 5 GPS satellites provide the L5 observable signal within 4-5 hours observation time (depending on station site), the use L2 GPS signal is assumed as the substitute and used simultaneously in case of insufficient L5 GPS observations for data processing. As the consequence, the results have no difference with L1/L2 GPS result when L5 GPS signal not available.

In case of a single frequency to handle the ionosphere errors, a linear combination model of L1 GPS code and carrier phase data and external source i.e. IGS are used which diminishes the ionosphere errors and the code noise. Over short baselines, the results were obtained using single frequency (L1 GPS) as the ionospheric effects of a short baseline are very similar and cancel in differencing process and the noise is less than dual frequency linear combination.

Table 5-8. Coordinate differences and standard deviation w.r.t. L1/L2 GPS solution; TLMF-TLSE baseline (8.7 km)

	$\Delta n$ (m)	$\Delta e$ (m)	$\Delta u$ (m)	$\sigma n$ (m)	$\sigma e$ (m)	$\sigma u$ (m)
<b>L1</b>	0.01	0.02	0.02	0.01	0.02	0.02
<b>L1/L5</b>	0.01	0.01	0.01	0.01	0.01	0.01

In figures 5-3 and 5-4, coordinate biases up to  $\pm 2$  cm between L1 GPS (blue line) and L1+L5 GPS (red line) in latitude, longitude, and height are displayed. However, when computing the standard deviation of the coordinates, the result from L1 GPS have more biases than L1/L5 GPS result which is expected and can be from the effect of multipath interference and ionosphere errors. The utilization of L2 GPS as substitute signal in case of insufficient L5 GPS signal affects the result. Hence, the solution and standard deviation using L1/L5 have similar values w.r.t. L1/L2 GPS (refer to table 5-8 and 5-9).

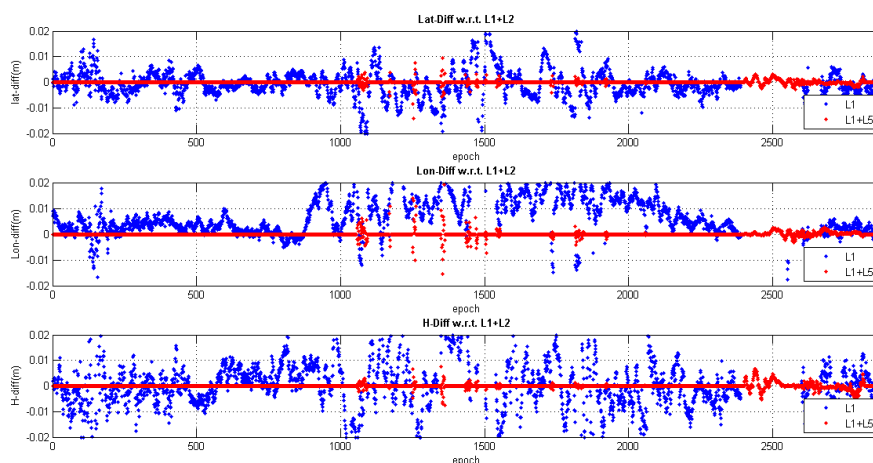


Figure 5-4. L1 GPS and L1/L5 GPS position biases w.r.t. L1/L2 GPS solution (reference); AXPV-MARS baseline (23.7 km)

Table 5-9. Coordinate differences and standard deviation w.r.t. L1/L2 GPS solution;  
AXPV-MARS baseline (23.7 km)

	$\Delta n$ (m)	$\Delta e$ (m)	$\Delta u$ (m)	$\sigma n$ (m)	$\sigma e$ (m)	$\sigma u$ (m)
<b>L1</b>	0.02	-0.01	0.03	0.02	0.01	0.03
<b>L1/L5</b>	0.01	0.01	0.01	0.01	0.01	0.01

From the figures 5-3 and 5-4, it can be concluded that there is no a significant effect on the position if the length of baseline is less than 30 km. The standard deviation of the position differences using dual frequencies over several minutes of data (up to 60 minutes) w.r.t. L1 GPS seems to deviate against the  $\pm 1.5$  cm level. On the other hand, the L1/L5 GPS solution is very close to the L1/L2 GPS. Hence, the L5 GPS signal can be used as a reliable signal and provide a sufficient performance in positioning, although it is currently only available for a few hours (3-4 hours and 5 available satellites were collected at DOY 240, 2014).

In accordance with the increased baseline length, a poorer result is expected in the figure 5-5. The coordinates standard deviation is up to more than 10 cm (see table 5-10). The L1/L5 GPS combination provides a comparable solution to L1/L2 GPS. Hence, it is recommended to correct both the orbit and ionospheric errors using precise orbit and ionospheric correction from IGS when calculating a position from only L1 GPS observations at baseline more than 30 km.

Table 5-10. Coordinate differences and standard deviation w.r.t. L1/L2 GPS solution;  
VILL - CEBR baseline (35.3 km)

	$\Delta n$ (m)	$\Delta e$ (m)	$\Delta u$ (m)	$\sigma n$ (m)	$\sigma e$ (m)	$\sigma u$ (m)
<b>L1</b>	0.02	0.01	0.02	0.08	0.05	0.10
<b>L1/L5</b>	0.01	-0.02	0.06	0.03	0.02	0.05

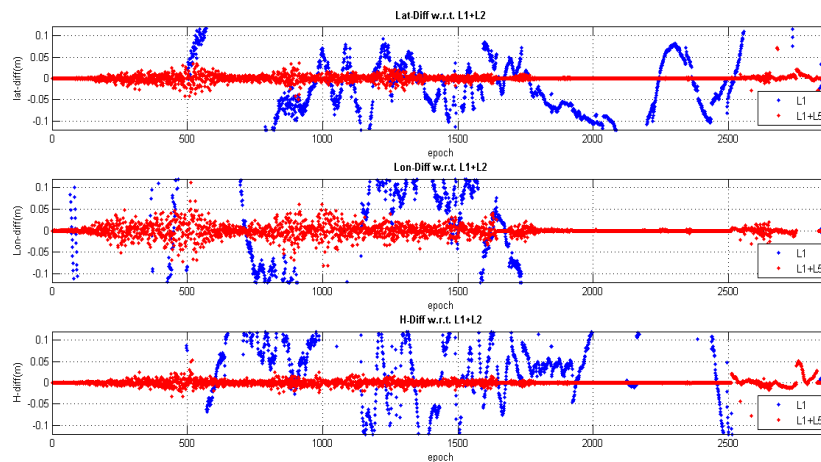


Figure 5-5. L1 GPS and L1/L5 GPS position biases w.r.t. L1/L2 GPS solution (reference);  
VILL-CEBR baseline (35.3 km)

The L1 GPS time series position in figure 5-6 exhibits atmosphere errors mainly from ionosphere biases. At baselines over 30 km, atmospheric errors cannot be mitigated only using an orbit correction from IGS, however, by introducing orbit and ionosphere corrections, the ambiguity fixing problems can be limited.

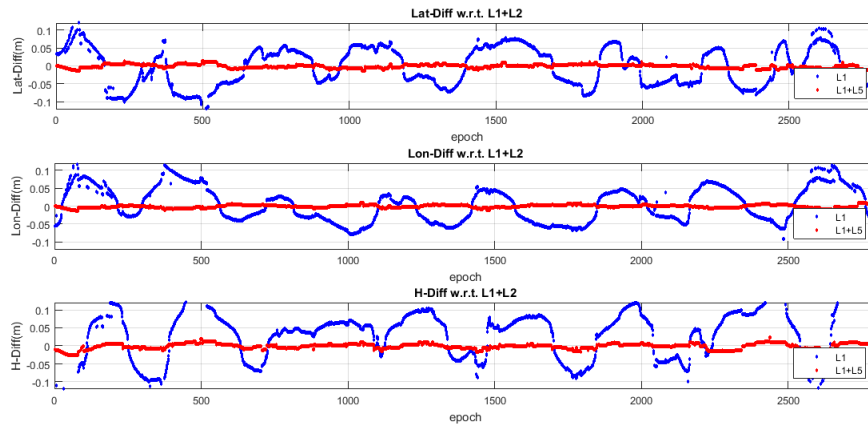


Figure 5-6. L1 GPS and L1/L5 GPS position biases w.r.t. L1/L2 GPS solution (reference); GANP-KRA1 baseline (>100 km)

Table 5-11. Coordinate differences and standard deviation w.r.t. L1/L2 GPS solution; GANP-KRA1 baseline (>100 km)

	$\Delta n$ (m)	$\Delta e$ (m)	$\Delta u$ (m)	$\sigma n$ (m)	$\sigma e$ (m)	$\sigma u$ (m)
<b>L1</b>	-0.06	-0.16	-0.08	0.06	0.06	0.09
<b>L1/L5</b>	0.01	-0.02	0.04	0.04	0.05	0.05

Figure 5-6 shows unexpected results because the L1 GPS and L1/L5 GPS have a good result with respect to the reference. To be noted, the L1 GPS solutions on long baselines with external corrections from IGS i.e. orbit information and ionospheric corrections delivers an adequate position comparable to the L1/L5 GPS results. Moreover, the ambiguity fixing of the L1/L5 GPS IF-LC which determined by the availability of data (only a few of L5 GPS observation in the GANP-KRA1 baseline) can be improved by introducing external corrections i.e. orbit information and ionospheric corrections.

To improve the coordinate solutions even on medium and long baselines, we may utilize three GNSS signals of the same system (please refer to figure 5-7) or an additional signal such as Galileo signals. As Tiberius et al. (2002) mentioned, with the capability of instantaneous resolving the carrier phase ambiguities correctly, using a combined GNSS system, it clearly prevails over present dual-frequency GPS operations.

On a short baseline, very high ambiguity success-rate levels can be obtained, using even a single epoch of data and atmosphere biases are assumed zero, Galileo offers better solutions as longer wavelengths can be established by forming wide-lane combinations.

On a medium baseline, typically 20–30 km or longer, when corrective information is used from a network of active GNSS reference stations, a success-rate at the level of 95% can be achieved using combined GNSS systems. Nevertheless, on a long baseline, up to 100s km, the success-rate is still too low for practical purposes.

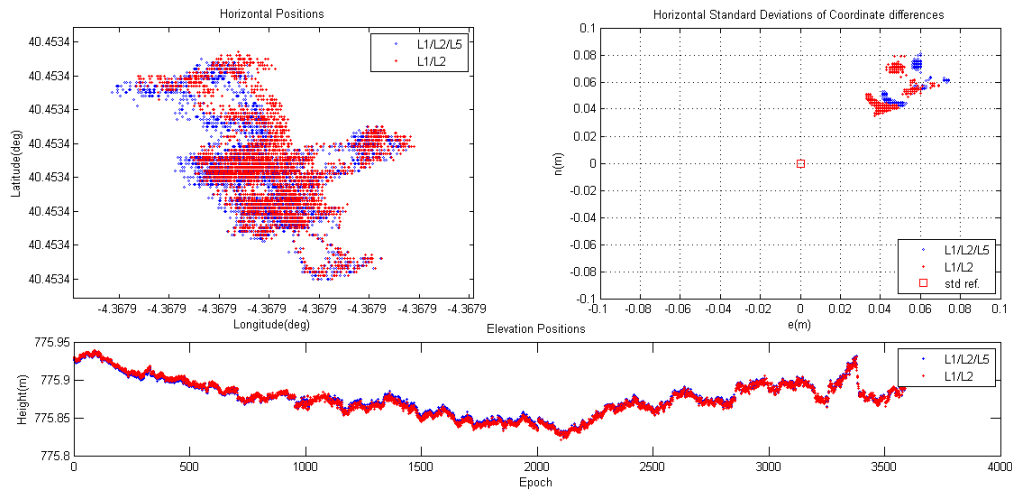


Figure 5-7. GPS solutions calculated from L1/L2 GPS and L1/L2/L5 GPS on VILL-CEBR baseline at DOY 240, 2014 (35.3 km)

Figure 5-7 shows a comparison of coordinate time series calculated from a dual signal combination and triple signal combination in the case of a medium baseline (more than 20 km). The GPS satellite constellation is used since Galileo observables are not available for data processing at DOY 240, 2014. As can be seen from the top left and the top right panel of figure 5-7, the effect from adding a third frequency signal is almost negligible even on medium baselines. On the medium baseline the ambiguity success-rate reduces from 97% to 91%, yet only affecting a bias of position from 1 to 3 cm and introducing a similar bias of about 5 cm for both L1/L2 GPS and L1/L2/L5 GPS solutions with respect to the reference coordinates.

From figure 5-7, we learn that introducing a third frequency, i.e. using L5 GPS instead solely using dual frequency brings no significant changes of the estimated position and the ambiguity resolution success-rate but can reduce fixing times. When carrier phase ranging is carried out simultaneously on two frequencies, an idea of forming ionosphere-free linear combinations is carried out and the ambiguities have to be resolved. And, when three carriers are employed, all three ambiguities need to be resolved. One has to consider the overall ambiguity resolution success-rate is taking into account the measurement precision, observation scenario, modeling aspects, and how efficiently this model can be used.

In most positioning applications, the relative receiver-satellite geometry will not change too much over small periods of time. The ambiguity transformation computed for one period will be a good approximation to the ambiguity fixing. The performance study is

restricted to the standard model used for short- and medium- baseline applications. The method, however, is generally applicable and not restricted to the single-baseline case, thus can also be applied when additional parameters are introduced.

In terms of receiver-satellite geometry, a small change of geometry will not result in large changes in the solution. A short length of baseline would indicate that the solution is resistant to atmospheric errors, multipath errors, and orbit errors. In the double differencing process, when neglecting ionospheric biases, the signal from satellites provides a good precision. Therefore, the relative satellite-receiver geometry is determining the precision of estimated positions. On the other hand, utilization of atmospheric correction, orbit correction, and signal selection in medium baselines should be taken into account as these parameters affect both the position and its precision.

The geometry of multiple satellites in view of a receiver determines the level of precision of the receiver position. When visible navigation satellites are close together in the sky, the geometry can be interpreted as weak and vice versa. Other factors that can increase the effective receiver-satellite geometry are obstructions such as buildings that caused the multipath effect. The geometric correlation between receiver and satellite are expressed as DOP and mathematically follows the positions of the usable satellites.

Table 5-12. Ambiguity resolution on various baselines (DOY 240, 2014)

Baseline	Distance (km)	AMBIGUITY FIX (%)							
		L1 (broadcast)	$\sigma$ (m)	L1 (IGS)	$\sigma$ (m)	L1+L2 (iono IGS)	$\sigma$ (m)	L1+L2 (IGS)	$\sigma$ (m)
ARIF – PBRT	<b>0.2</b>	99.90	0.01	92.10	0.02	100.00	0.01	100.00	0.01
TLMF – TLSE	<b>8.7</b>	95.00	0.05	99.40	0.02	99.40	0.02	94.90	0.02
MLVL-SMNE	<b>11.9</b>	100.00	0.02	100.00	0.03	99.30	0.02	99.50	0.02
AXPV - MARS	<b>23.7</b>	92.50	0.22	94.90	0.05	94.90	0.06	86.60	0.03
VILL – CEBR	<b>35.3</b>	85.90	0.19	78.60	0.15	93.50	0.06	82.80	0.03
MLVL – CREI	<b>47.2</b>	82.80	0.14	87.60	0.47	66.70	0.15	91.50	0.03
GANP - KRA1	<b>118.4</b>	8.4	1.83	22.4	1.65	26.90	0.44	94.40	0.03

Baseline	Distance (km)	AMBIGUITY FIX (%)							
		L1/L2 NarrowLane	$\sigma$ (m)	L1/L2 WideLane	$\sigma$ (m)	L1+L5 (broadcast)	$\sigma$ (m)	L1+L5 (iono IGS)	$\sigma$ (m)
ARIF – PBRT	<b>0.2</b>	99.90	0.01	92.50	0.02	-	-	-	-
TLMF – TLSE	<b>8.7</b>	85.20	0.12	98.50	0.02	91.50	0.03	76.30	0.04
MLVL-SMNE	<b>11.9</b>	98.40	0.03	99.60	0.03	-	-	-	-
AXPV - MARS	<b>23.7</b>	77.60	0.04	86.70	0.04	94.90	0.05	96.90	0.03
VILL – CEBR	<b>35.3</b>	33.10	0.08	95.90	0.02	93.40	0.06	82.90	0.03
MLVL – CREI	<b>47.2</b>	3.20	0.42	95.90	0.02	-	-	-	-
GANP - KRA1	<b>118.4</b>	1.90	0.53	94.80	0.04	1.90	2.97	17.20	0.43



Table 5-12 presents ambiguity fixing rates and position accuracies for various baseline lengths using L1 GPS, L1/L2 GPS and L1/L5 GPS data.

The resulting standard deviation in table 5-12 is almost equal for baseline lengths less than 40 km on both L1/L2 GPS and L1/L5 GPS combination. However, when the baseline length is over 40 km, the standard variation is varying. It would be appropriate to carry out a proper correction both on orbit and ionosphere corrections in order to further improve the coordinate position for baseline more than 40 km. In case of medium baselines, the L1/L5 GPS ambiguity success-rate values is varying up to 10% compared to L1/L2 GPS combination results. To improve the ambiguity success-rate, IGS corrections can provide a better solution both on standard deviation and the estimated coordinates.

### 5.2.2 The effect of observation time on ambiguity resolution

The observation time influences the achieved coordinate accuracy very much, but not the ambiguity success-rate. In order to obtain the best results, the duration of the observation has to be comprehensive enough at varying baselines. To ensure sufficient observation time and a successful ambiguity resolution at longer baselines is a prerequisite for a more refined position solution. The minimum observation time required is based on factors such as the baseline length, as well as equipment and parameters used. In this work baselines of up to 70 km were processed with observation periods varying from 5 to 60 minutes.

Table 5-13. Ambiguity resolution w.r.t observation time (VILL – CEBR baseline); DOY 300, 2014, 1 second sampling rate

VILL – CEBR (35 km)						
Observation Time (minutes)	AMBIGUITY FIX (%)					
	L1 (broadcast)	$\sigma$ (m)	L1/L2 (broadcast)	$\sigma$ (m)	L1/L2(NL)	$\sigma$ (m)
5	-	-	5.6	0.29	-	-
10	52.6	0.28	73.2	0.11	62.0	0.12
15	48.3	0.20	78.8	0.10	73.8	0.08
30	49.5	0.08	74.4	0.04	85.9	0.04
60	67.4	0.05	76.9	0.04	100	0.02

Table 5-13 shows L1/L2 GPS phase data processing using ionosphere-free linear combination only using broadcast data. The ambiguities have been fixed up to 100% after 60 minutes of observation time with 1 second sampling rate. The success rate becomes worse when less than 30 minutes data observations are available. Without IGS corrections it is difficult to get a successful ambiguity fixing. Orbit and ionospheric delay would affect the ambiguity success-rate and its standard deviation. As shown the results

obtained from data processing obviously are correlated with the observation time, as well as orbit and ionospheric correction.

To study with the impact of temporal variability (weather, satellite geometry, and coverage), the group was divided by 5 minutes, 10 minutes, and up to 60 minutes observation periods. Data observations were collected in the morning between 10:00 and 12:00 as well as in the afternoon from 13:00 to 15:00 MEZ (Middle European Zonal) time. To examine the observation period effect and baseline length on the coordinate position, a short baseline (TUWI-LEOP, 9.2 km) and a medium baseline (VILL-CEBR, 35.3 km) were established.

Table 5-14. Ambiguity resolution w.r.t. observation time (TUWI-LEOP baseline); DOY 343, 2014, 1 second sampling rate

TUWI-LEOP	DOY 343	Morning	9.2 km					
Observation Time	AMBIGUITY FIX (%)							
	L1(IGS)	$\sigma$ (m)	L1+L2 (IGS)	$\sigma$ (m)	L1+L2 NL	$\sigma$ (m)	L1+L5 (IGS)	$\sigma$ (m)
5	99.30	0.03	100.00	0.01	97.70	0.31	100.00	0.01
10	99.20	0.08	100.00	0.01	98.50	0.24	100.00	0.01
15	99.90	0.02	100.00	0.01	99.00	0.18	100.00	0.01
30	99.90	0.02	100.00	0.01	99.50	0.11	100.00	0.01
60	100.00	0.02	100.00	0.02	99.60	0.05	100.00	0.02
TUWI-LEOP	DOY 343	Afternoon	9.2 km					
Observation Time	AMBIGUITY FIX (%)							
	L1(IGS)	$\sigma$ (m)	L1+L2 (IGS)	$\sigma$ (m)	L1+L2 NL	$\sigma$ (m)	L1+L5 (IGS)	$\sigma$ (m)
5	99.00	0.07	99.70	0.06	99.70	0.06	99.70	0.06
10	96.30	0.05	99.80	0.05	99.80	0.05	99.80	0.04
15	96.90	0.04	99.90	0.04	99.90	0.04	99.90	0.04
30	99.60	0.04	99.90	0.03	88.40	0.23	99.90	0.03
60	99.80	0.03	100.00	0.03	94.20	0.68	100.00	0.03

In table 5.14, the L1/L5 GPS combination offers a similar performance as L1/L2 GPS and provides a high ambiguity success rate. In short baseline, dual frequency data can cover up the cycle slip problem with the double differencing mode even in short observation periods (5 minutes) both in the morning and the afternoon. On the other hand, at least 60 minutes observation data are needed to provide a good solution in case of the medium baseline (refer to table 5-13), while L1 GPS just offers a less ambiguity success-rate on short and medium baselines. On short baseline, the observation periods in the morning and the afternoon have only a slight effect on the ambiguity success-rate. As currently only 5 satellites with L5 GPS signal are available for a few hours at DOY 300, a selection of the observation time would affect the L1/L5 GPS ambiguity success-rate and its standard deviation.

To determine the influence of observation periods and the ionospheric delays, a medium baseline was tested out (VILL-CEBR baseline, 35 km). The data has 1 second sampling rate and were calculated always in the morning but for different seasons (summer and autumn).

Table 5-15. Ambiguity resolution w.r.t. observation time (1 second sampling rate GNSS data) at DOY 300 and DOY 240, 2014 (morning)

VILL - CEBR	DOY 300	morning	35 km					
Observation Time (min)	AMBIGUITY FIX (%)							
	L1 (brd)	$\sigma$ (m)	L1+L2(IGU)	$\sigma$ (m)	L1+L2 (brd)	$\sigma$ (m)	L1+L2 (NL)	$\sigma$ (m)
5	-	-	100.00	0.01	-	-	-	-
10	-	-	100.00	0.01	-	-	-	-
15	4.30	0.22	100.00	0.01	-	-	96.00	0.02
30	49.10	0.19	99.60	0.03	97.90	0.02	95.40	0.03
60	39.90	0.34	98.40	0.03	93.60	0.04	98.60	0.06

VILL - CEBR	DOY 240	morning	35 km					
Observation Time (min)	AMBIGUITY FIX (%)							
	L1 (brd)	$\sigma$ (m)	L1+L2(IGU)	$\sigma$ (m)	L1+L2 (brd)	$\sigma$ (m)	L1+L2 (NL)	$\sigma$ (m)
5	-	-	100.00	0.01	-	-	-	-
10	-	-	100.00	0.02	-	-	-	-
15	-	-	100.00	0.02	-	-	-	-
30	82.80	0.08	96.40	0.03	89.50	0.08	81.40	0.12
60	94.20	0.07	93.10	0.03	87.40	0.05	89.50	0.09

From table 5-15 and 5-16, it becomes obvious that introducing the IGS orbit corrections plays a major role for ambiguity resolution at medium baselines apart of ionospheric delay mitigation. The IGS orbit correction offers a high success-rate of ambiguity fixing in 5 minutes observation time. With broadcast orbit corrections, at least 30 minutes observation time span is required to get a similar success rate and standard deviation compared to the result using IGS corrections. For the medium baseline, L1/L2 GPS results in the morning offer a better performance within 5 minutes observation time by utilizing IGS corrections (more than 90% ambiguity success-rate and standard deviation up to 3 cm) compared to L1/L2 GPS observations in the afternoon.

Tables 5-15 and 5-16 confirm a significant difference in the coordinate standard deviation for a distance of more than 30 km. It takes at least 60 minutes for a high success-rate ambiguity resolution using 2 GPS carrier phase observation in the afternoon compared to 5 minutes observation time in the morning using 1 second sampling rate observations. These differences may arise due to the effect of the ionospheric delay variation over the day and in different seasons (summer and autumn) as mentioned by Wautelet and Warnant (2013).

Table 5-16. Ambiguity resolution w.r.t. observation time (1 second sampling rate GNSS data) at DOY 300 and DOY 240, 2014 (afternoon)

VILL - CEBR	DOY 300	afternoon	35 km		AMBIGUITY FIX (%)				
Observation Time (min)	L1 (brd)	$\sigma$ (m)	L1+L2(IGU)	$\sigma$ (m)	L1+L2 (brd)	$\sigma$ (m)	L1+L2 (NL)	$\sigma$ (m)	
5	-	-	-	-	-	-	-	-	
10	-	-	-	-	-	-	-	-	
15	-	-	-	-	-	-	70.00	0.02	
30	-	-	73.80	0.12	51.40	0.12	90.10	0.04	
60	-	-	100.00	0.12	69.50	0.09	67.60	0.05	

VILL - CEBR	DOY 240	afternoon	35 km		AMBIGUITY FIX (%)				
Observation Time (min)	L1 (brd)	$\sigma$ (m)	L1+L2(IGU)	$\sigma$ (m)	L1+L2 (brd)	$\sigma$ (m)	L1+L2 (NL)	$\sigma$ (m)	
5	-	-	100.00	0.01	-	-	-	-	
10	-	-	100.00	0.03	-	-	-	-	
15	-	-	77.90	0.03	77.90	0.02	94.80	0.02	
30	-	-	53.90	0.09	73.20	0.01	62.00	0.11	
60	44.20	0.07	17.10	0.17	78.80	0.01	85.90	0.04	

A test was conducted to simulate the effect of satellite geometry on the coordinate position, standard deviation, and DOP (a short baseline case). 4 areas (quadrant) are selected to represent the satellite to be used for data processing, e.g. a north quadrant means data processing only takes GPS signals received by the antenna from north azimuth part and neglecting the signals that received from other directions. The same procedure was applied for east, south, and west parts. To understand the results in table 5-17 and 5-18, please refer to figure 5-8 as the illustration.

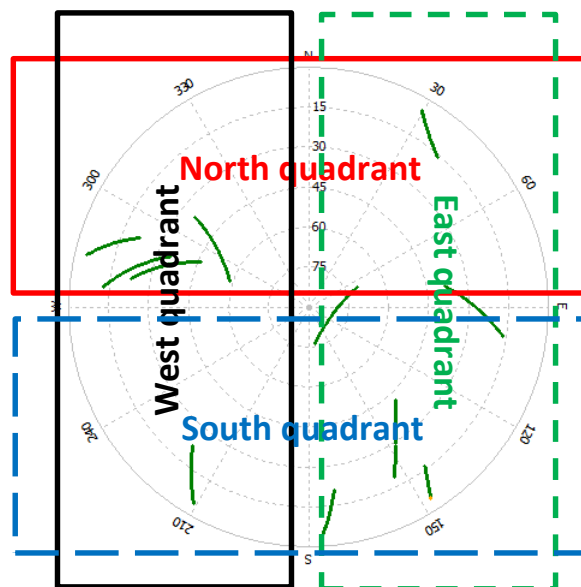


Figure 5-8. The satellites visibility at TUWI station in DOY 343, 2014

Table 5-17. The Effect of satellite geometry on position (L1/L2 GPS, 1 hour observation)

TUWI - LEOP	DOY 343	morning	9.2 km						
Observation time (min)	Ambiguity fix (%)								
	north quadrant	$\sigma$ (m)	East quadrant	$\sigma$ (m)	South quadrant	$\sigma$ (m)	West quadrant	$\sigma$ (m)	
5	100.0	0.01	-	-	99.7	0.05	100.0	0.07	
10	100.0	0.01	-	-	99.8	0.05	99.8	0.07	
15	100.0	0.02	99.7	0.02	99.9	0.05	99.9	0.07	
Observation time (min)	Satellite Elevation (%)								
	high (>15)	$\sigma$ (m)	low (<15)	$\sigma$ (m)	4 sats	$\sigma$ (m)	6 sats	$\sigma$ (m)	
5	100.0	0.01	-	-	42.2	0.07	100.0	0.01	
10	100.0	0.01	-	-	99.8	0.05	100.0	0.01	
15	100.0	0.02	-	-	99.9	0.03	100.0	0.01	

Table 5-17, confirms a significant effect on ambiguity resolution caused by satellite geometry and the number of satellites. It takes at least 10 minutes to fix the ambiguities using two frequencies in varying scenarios over short baselines to get an assurance for positioning with sufficient number of satellites (at least 4 satellites).

The satellite geometry (DOP) can be used to indicate a success rate of the ambiguity resolution. When the satellites spread evenly in all directions and provided a sufficient number of satellites, the DOP shows a low value and vice versa. The respective DOP-values are presented in table 5-18 based on the simulation (refer to figure 5-8).

Table 5-18. DOP Value at DOY 343, 2014 (TUWI-LEOP)

TUWI - LEOP	DOY 343	morning	9.2 km	Scenario					
DOP	north quadrant	East quadrant	south quadrant	west quadrant	High (>15°)	Low (<15°)	4 sats	6 sats	
GDOP	4.4	14.9	7.3	12.5	3.1	12.5	4.2	2.9	
PDOP	3.6	11.9	7.0	9.7	2.8	12.4	3.6	2.5	
HDOP	2.7	8.7	6.4	8.3	1.8	1.7	2.1	1.5	
VDOP	2.4	10.3	1.9	5.1	2.1	12.3	2.9	2.0	

### 5.2.3 Modernized GNSS signal linear combinations

This section provides the background information to evaluate which linear combinations shall be used in chapter 6 using real data and simulated data. There are several possibilities of linear combinations from the modernized GNSS that will be fully deployed in the near future. In the process, several errors are considered, i.e. orbital error, ionospheric error, tropospheric error, multipath, and receiver noise. For an in-depth look, several literature has to be taken into note.

The full deployment of modernized GPS and Galileo constellations are still quite a few years away. 5 scenarios were simulated to evaluate the performance of linear combinations, i.e. L1/L2 GPS, L1/L5 GPS, L1/L2/L5 GPS, E1/E5 Galileo, and E1/E5a/E5b Galileo. All the scenarios assume the observations are free of biases in particular in the short baseline case where the atmospheric errors cancel through differencing. Then on the medium baseline, all common errors sources are present.

To create the linear combinations, different GNSS signals are entered into the equations (please refer to Odijk, 2013) to simulate the required conditions. Since analyzing the results in the signal measurement domain, it is necessary to separate the errors from the carrier phase observables.

Time of observation and location has an essential effect on the results due to the satellite availability. A mask angle of 5 degrees was chosen. The receiver noise level was assumed as zero. Orbital errors were introduced with the use of the ultra-rapid orbits from IGS or the broadcast ephemeris (if IGS not available) hence the orbit error would be minimal. To correct tropospheric delays, the Saastamoinen model was used. And the studied GNSS signals are summarized in table 5-19.

Table 5-19. GNSS signals

carrier signal	notation	frequency (MHz)	$\lambda$ (cm)
<b>L1</b>	$\phi L1$	$154 \times 10.23 = 1575.42$	19.03
<b>L2</b>	$\phi L2$	$120 \times 10.23 = 1227.60$	24.42
<b>L5</b>	$\phi L5$	$115 \times 10.23 = 1176.45$	25.48
<b>E1</b>	$\phi E1$	$154 \times 10.23 = 1575.42$	19.03
<b>E5a</b>	$\phi E5a$	$115 \times 10.23 = 1176.45$	25.42
<b>E5b</b>	$\phi E5b$	$118 \times 10.23 = 1207.14$	24.83
<b>E5</b>	$\phi E5$	$116.5 \times 10.23 = 1191.79$	25.15

After the linear combinations are built, the carrier phase observations are parameterized by the wavelength of the respective carrier phase. Additionally, in most observation sessions satellites with extremely low elevation angles below 5 degrees are excluded.

According to Odijk (2003) several linear combinations could be introduced beside the standard L1/L2 GPS ionosphere-free linear combination. Moreover, it is even possible to design useful triple frequency linear combinations from all frequencies in GPS and Galileo.

As the ionospheric delay is dispersive, the phase observables delay of  $\Phi_i$  can be related to the delay of  $\Phi_j$  by the known ratio of wavelengths of the two observables:

$$i_j = (\lambda_j^2/\lambda_i^2)i_i \quad (5.26)$$

where the two observables are in order,  $\lambda_j > \lambda_i$ , and the ratio can be denoted as:

$$\frac{\lambda_j}{\lambda_i} = \frac{t}{n}, t > n \quad (5.27)$$

where both  $t$  and  $n$  are (positive) integers. Using the wavelength ratio, the ionosphere free linear combination  $\phi_{ij}$  of two observables is obtained as:

$$E\{\phi_{ij}\} = \frac{t^2}{t^2-n^2}E\{\phi_i\} - \frac{n^2}{t^2-n^2}E\{\phi_j\} \quad (5.28)$$

Introducing the integer ambiguities  $N_i$  and  $N_j$  (5.28) can be detailed as:

$$E\{\phi_{ij}\} = \rho + \frac{t^2}{t^2-n^2}\lambda_i N_i - \frac{n^2}{t^2-n^2}\lambda_j N_j - \left(\frac{t^2}{t^2-n^2} - \frac{n^2}{t^2-n^2}\frac{t^2}{n^2}\right)i_i + e_{ij} \quad (5.29)$$

The range of observable  $\rho$  appears in the same way as in the original phase observation equation. Moreover, the ionospheric delays are eliminated  $\left(\frac{t^2}{t^2-n^2} - \frac{n^2}{t^2-n^2}\frac{t^2}{n^2}\right)i_i \approx 0$ , and a combined ambiguity term remains, which does not seem to be integer valued. However, using equation (5.29) with  $t$  and  $n$  integer, it is possible to rewrite the ambiguity term to be:

$$E\{\phi_{ij}\} = \rho + \frac{t^2}{t^2-n^2}\lambda_i (tN_i - nN_j) + e_{ij} = \rho + \lambda_{ij} N_{ij} + e_{ij} \quad (5.30)$$

where  $\lambda_{ij}$  denotes the artificial wavelength and  $N_{ij}$  the integer ambiguity of the ionosphere free combination and  $e_{ij}$  denotes multipath and noise values.

A consequence of taking the ionosphere-free linear combination is that the noise of the ionosphere-free observable is increased compared to the noise of the original phase observations. When it is assumed that two original observables are uncorrelated and have same precision  $\sigma_{\Phi_i} = \sigma_{\Phi_j} = \sigma_{\Phi}$  in DD mode, the variance of LC follows:

$$D\{\phi_{ij}\} = \frac{t^4+n^4}{(t^2-n^2)^2} \sigma_{\Phi}^2 \quad (5.31)$$

where  $D\{\phi_{ij}\}$  denotes the mathematical dispersion.

Denoting the greatest common divisor as  $c$ , we may write for the numerator and the denominator of the wavelength ratio  $t = c \cdot t_c$  and  $n = c \cdot n_c$ , where  $c \geq 1$ .

In the triple linear combination case, it should be known that only the precision of the ambiguities is influenced by this longer wavelength. It is possible to draft from 3 carrier observations three different dual-frequency ionosphere-free combinations and it is also possible to form just one truly triple-frequency ionosphere-free combination.

These three dual-frequency combinations could be processed simultaneously in order to solve for the baseline coordinates and ambiguities. When ratios for three observables are denoted as:

$$\lambda_j/\lambda_i = t_j/n_i \text{ and } \lambda_k/\lambda_i = t_k/n_k \quad (5.32)$$

$\phi_{jk}$  can be written as linear combination of  $\phi_{ij}$  and  $\phi_{ik}$ ,

$$\phi_{jk} = \frac{t_k^2(t_j^2 - n_j^2)}{t_k^2(t_j^2 - n_j^2) - t_j^2(t_k^2 - n_k^2)} \phi_{ij} - \frac{t_j^2(t_k^2 - n_k^2)}{t_k^2(t_j^2 - n_j^2) - t_j^2(t_k^2 - n_k^2)} \phi_{ik} \quad (5.33)$$

Processing coordinates in one step from the three dual-frequency combination would make a too optimistic precision of unknown parameters. Since the processes are assumed to have more information of original phase data. Instead of using combinations of two frequencies, it is also possible to form ionosphere-free combinations that are linear of all three observable. A phase observable which preserves the integer ambiguity can be obtained as follows:

$$E\{\phi_{ijk}\} = \rho + \frac{1}{(t_j^2 - n_j^2) + (t_k^2 - n_k^2)} \lambda_i [(t_j^2 - n_j^2)N_i - t_j n_j N_j - t_k n_k N_k] + e_{ijk}$$

$$D\{\phi_{ijk}\} = \frac{(t_j^2 + t_k^2)^2 + n_j^2 + n_k^2}{(t_j^2 - n_j^2)^2 + (t_k^2 - n_k^2)^2} \sigma_\Phi^2 \quad (5.34)$$

the integer ambiguity  $N_{ijk}$  should be divided by the common divisor of three integers  $(t_j^2 - n_j^2)$ ,  $t_j n_j$ , and  $t_k n_k$ , where the wavelength  $\lambda_{ijk}$  should be multiplied with it.

The resulting sets for ionosphere-free dual- and triple –frequency linear combinations with integer ambiguities are summarized in table 5-20 based on the Odijk model.



Table 5-20. Results of GNSS Signals Linear Combinations

Signals	Linear combination	$\lambda$ (cm)	est. ambiguities	$\sigma$ factor
L1/L2	2.5457 $\phi$ L1 - 1.5457 $\phi$ L2	0.629	77a1 - 60a2	2.98
L1/L5	2.2606 $\phi$ L1 - 1.2606 $\phi$ L5	0.279	154a1 - 115a5	2.59
E1/E5	2.3379 $\phi$ E1 - 1.3379 $\phi$ E5	0.289	308e1 - 233e5	2.69
L1/L2/L5	2.3269 $\phi$ L1 - 0.3596 $\phi$ L2 - 0.9673 $\phi$ L5	11.019	154a1 - 120a2 - 115a3	2.55
E1/E5a/E5b	2.3149 $\phi$ E1 - 0.83646 $\phi$ E5a - 0.4857 $\phi$ E5b	11.062	154e1 - 115e5a - 118e5b	2.51

The triple frequency linear combinations are of a longer wavelength than the current L1/L2 GPS combination (about 11 cm compared to 0.63 cm). However, the precision of a triple frequency linear combination is worse compared to L1/L2 GPS as the noise is stacking up.

There is only a slight difference between L1/L5 GPS and E1/E5 Galileo in wavelength. Hence it expected the solution from these combinations of L1/L2 GPS and E1/E5 Galileo only shows small differences in the position and standard deviation.

To evaluate those combinations, an example calculation was carried out to analyze the performance of the ionosphere-free linear combinations. The data calculation complemented the theoretical models. Until the new GNSS are fully operational, there is no definite answer of the optimal linear combination for positioning applications. However, in the next chapter, an advanced look into which combinations should be considered and how they can be used to improve the accuracy of positioning is provided.

Table 5-21. The Influence of Linear of combinations on Position (VILL-CEBR, 35 km, DOY 300, 2014)

LC	CEBR Position				Diff			Amb. fix
	X(m)	Y(m)	Z(m)	$\sigma$ (cm)	$\Delta x$ (m)	$\Delta y$ (m)	$\Delta z$ (m)	
L1/L2	<b>4846624.448</b>	<b>-370192.623</b>	<b>4116894.418</b>	<b>1.2</b>	-	-	-	Ref.
L1/L2/L5	4846624.342	-370192.338	4116894.535	3.6	-0.11	0.29	0.12	fix
L1/L5	4846624.351	-370192.280	4116894.595	5.9	-0.10	0.34	0.18	float
E1/E5	4846624.320	-370192.338	4116894.441	1.2	-0.13	0.28	0.02	float
E1/E5a/E5b	4846624.782	-370192.490	4116894.452	3.4	0.33	0.13	0.03	float

In table 5-21, the precision is approximately equal for L1/L2 GPS and E1/E5 Galileo. However, the standard deviation for L1/L5 GPS is worse compared with the L1/L2 GPS as the reference (red color) because only a few of L5 GPS observations that are available for positioning. Furthermore, the difference in position in L1/L5 GPS shows the largest value. The coordinates deviate between each linear combination up to a few

centimeters. The significant deviations might be caused by a clear lack of observation data for L5 GPS, E1 and E5 Galileo signals.

To check how satellite elevation masking influences the standard deviation, the standard deviation of coordinate solutions from table 5-21 was extracted during similar observation periods. Then the standard deviation is grouped by satellite elevation mask. The sample group was divided by 5-15 degrees, 15-30 degrees, and 30-60 degrees. Figure 5-9 to 5-11 compare the GPS standard deviation and compared with the standard deviation of only a few epochs from Galileo linear combinations, as Galileo signals only available for a few hours.

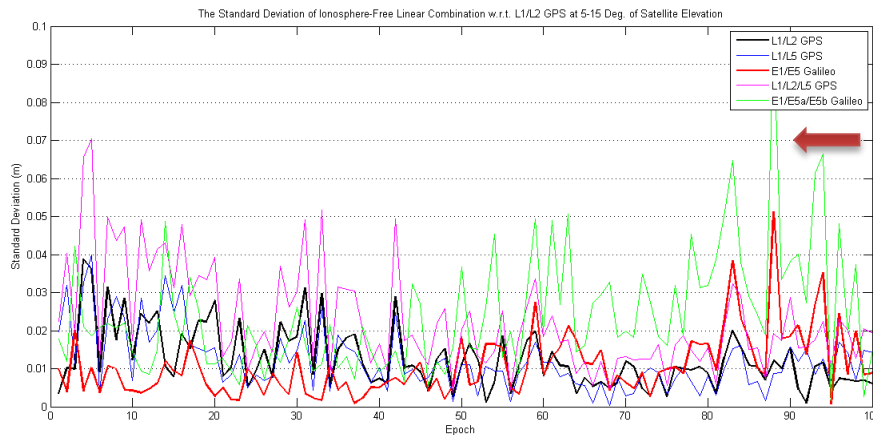


Figure 5-9. The standard deviation of coordinate solutions IF-LC w.r.t. L1/L2 IF-LC GPS at 5-15° satellite elevation mask on VILL-CEBR baseline (35 km)

In Figure 5-9, the standard deviation of the coordinate time series shows interesting features. The dual carrier phase combination, particularly from Galileo observable performs extremely well. It is mostly better (less than 2 cm) than the L1/L2 GPS standard deviation of ionosphere-free linear combination. On the other hand, the standard deviation of the L1/L5 GPS LC corresponds with the L1/L2 GPS pattern. A short time observation (at least 60 minutes) seems to be sufficient to resolve the ambiguity compared with the triple ionosphere-free linear combination such as L1/L2/L5 GPS in case of the VILL-CEBR baseline with a length approx. 35 km. With a modernized GNSS system, the E1/E5 Galileo linear combination seems to perform much better than the other dual/triple frequency combinations in low elevation of the angle of satellite. However, when insufficient Galileo observations are available (3 satellites) the standard deviation becomes worse than L1/L2 GPS (see red pointer in figure 5-9).

Figure 5-10 relates to a higher elevation mask. On Galileo LC solutions, it indicates the standard deviation are affected. Moreover, the noise level of the triple frequency is stacking up and provides a higher noise than double frequency ionosphere-free linear combination. Furthermore, the observables noise from triple frequency data processing

is contributing to the solution and its standard deviation. In figure 5-11, the standard deviation is plotted for several epochs. The elevation mask between 30-60° still offers sufficient observation data both on GPS linear combination (up to 10 satellites) and Galileo linear combination (up to 5 satellites). The Galileo LC shows a similar result as the L1/L2 GPS combinations.

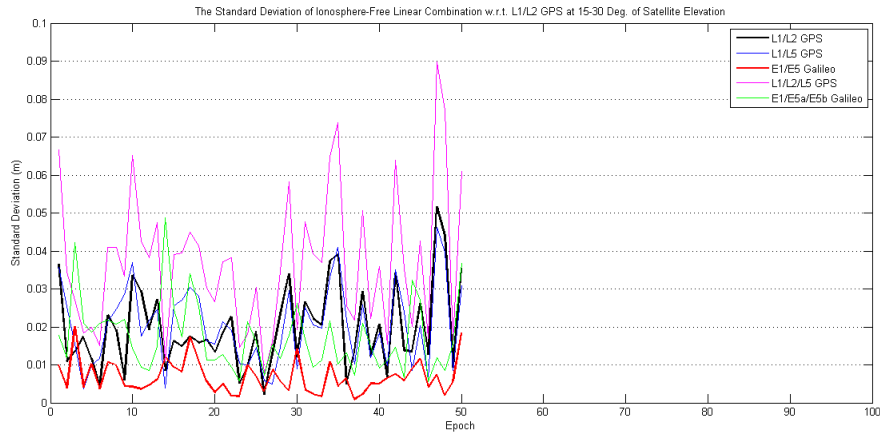


Figure 5-10. The standard deviation of coordinate solutions IF-LC w.r.t. L1/L2 IF-LC GPS at 15-30° satellite elevation mask on VILL-CEBR baseline (35 km)

The scenario of E1/E5 ionosphere-free linear combination provides a small standard deviation and performs better than the L1/L2 GPS standard deviation variances. And in relation to their noise values, the wavelength and the  $\sigma$  factor ratio could be a contribution factor that affects the variance level of each the linear combination.

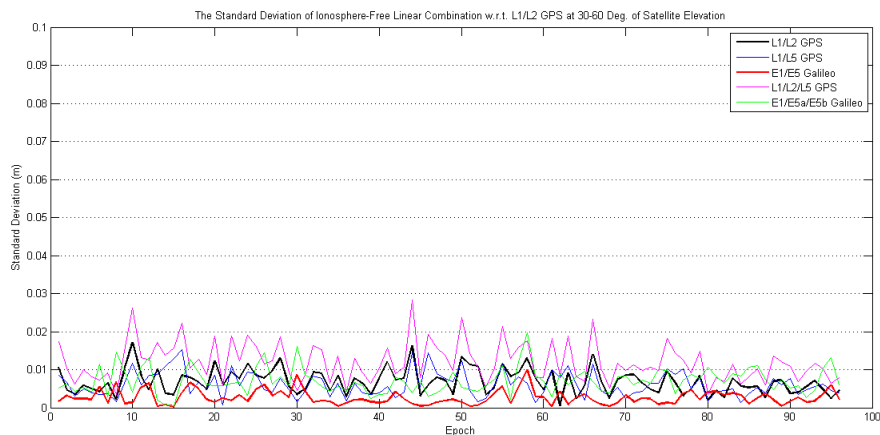


Figure 5-11. The standard deviation of coordinate solutions IF-LC w.r.t. L1/L2 IF-LC GPS at 30-60° satellite elevation on VILL-CEBR baseline (35 km)

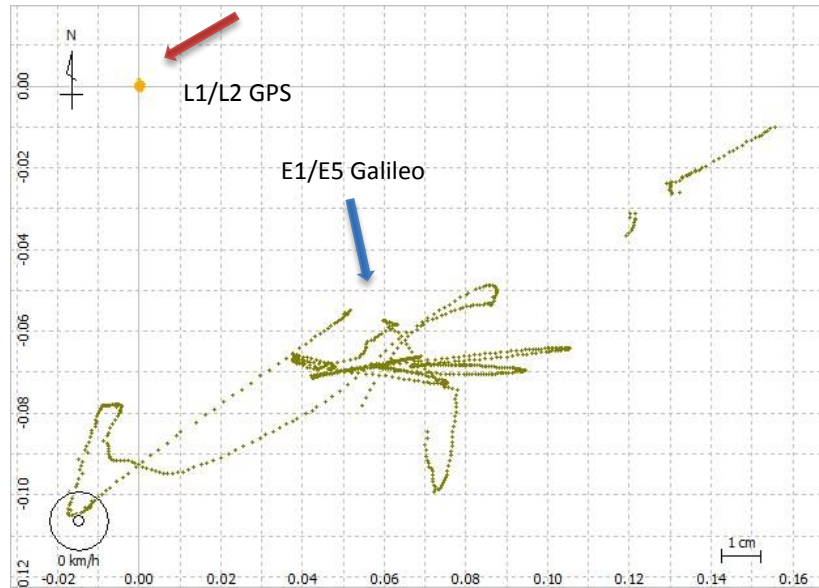


Figure 5-12. E1/E5 Galileo kinematic solutions w.r.t. L1/L2 GPS

Coordinates position biases of a kinematic solution are occurring because the observation period is too short (1 hour of observation) and the number of satellite signals is insufficient, i.e. L5 GPS and Galileo signals (E1, E5) with clock and orbit corrections for Galileo refer to the same reference system as for GPS. The kinematic positions obtained from the E1/E5 Galileo linear combination biases up to tens of centimeter (see figure 5-12) caused by insufficient Galileo observation data.

## 6. Real Data and Simulation Test

### 6.1 GNSS Reference Station Network

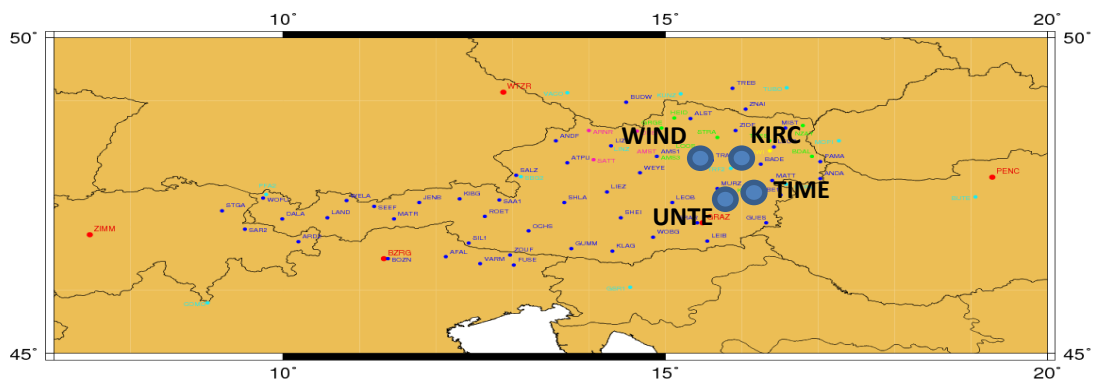


Figure 6-1. Austria Station Networks

To allow an assessment of GNSS positioning requirements, real as well as simulated data was processed. Several preliminary tests were performed to assess the methodology and equipment. Later on the performance analysis of the GNSS linear combinations was carried out.

The variation of selected test stations allows processing of a range of different baseline lengths utilizing both GPS and Galileo signals. The data collection time was chosen to maximize the number of visible modernized satellites of GPS and Galileo. Based from these requirements, several test stations from an Austrian Network were chosen.

Austrian companies manage a number of networks of Continuously Operating Reference Stations (CORS) that provide Global Navigation Satellite System (GNSS) data consisting of carrier phase and code range measurements in support of three dimensional positioning applications throughout the nation. These stations continuously collect and record GNSS data. Since GNSS receivers are made of different brands, most CORS systems support the receiver independent exchange (RINEX) for post-processing and the RTCM format for real-time data exchange. The mean distance of the reference sites is about 50 km.

In real-time positioning, the rover position shall be established with cm accuracy. The baseline calculation is degraded by biases which are satellite orbit, ionospheric, tropospheric, and multipath. A few of these Stations are used as IGS and EPN stations.

## 6.2 Test Stations

To test the performance of the new signals from GNSS systems, a linear combination model based on double differences was applied. Several baseline lengths ranging from about 20 km to 70 km are investigated. Two experiments were conducted for all data sets with 1 second sampling rate. The first experiment is a static positioning and the second experiment explores kinematic positioning.

For all baselines, the dual frequency L1/L2 GPS ionosphere-free linear combination solution over 1 hour data calculated from static positioning was considered as truth and will be used as reference. All GNSS data sets are then split into 5 minutes, 15 minutes, 30 minutes, and 60 minutes files. The results from each datasets and baselines were finally compared. The offset of the rover position and its standard deviation is presented in several tables for each scenario. Shown in table 6-1 are 4 distinct stations of the Austrian Network which were used and available for processing.

Table 6-1. List of selected stations of Austria Network

Station	X (m)	Y(m)	Z(m)	Baseline length to ref.	Receiver Type	Antenna + Radom	Note
TIME	4155544.893	1004486.586	4718007.303	Ref. station	Trimble NetR9	TRM55971	Base station
UNTE	4174381.364	998799.848	4702711.595	24.9 km	Trimble NetR9	TRM55971	Rover
KIRC	4154375.442	1044544.883	4710348.019	40.8 km	Trimble NetR9	TRM55971	Rover
WIND	4166953.269	1065727.054	4694854.304	66.0 km	Trimble NetR9	TRM55971	Rover

```

3.02 OBSERVATION DATA M (MIXED) RINEX VERSION / TYPE
TPP 3.1 20140712 165944 UTC PGM / RUN BY / DATE
COMMENT
COMMENT
COMMENT
KIRC MARKER NAME
Kirchdorf MARKER NUMBER
Trimble Navigation LTrimble Navigation Limited OBSERVER / AGENCY
5201K41225 TRIMBLE NETR9 Nav 4.85 / Boot 4.29REC # / TYPE / VERS
5000116877 TRM55971.00 TZGD ANT # / TYPE
4154375.4420 1044544.8830 4710348.0190 APPROX POSITION XYZ
0.0000 0.0000 0.0000 ANTENNA: DELTA H/E/N
G 12 C1C L1C S1C C2W C2X L2W L2X S2W S2X C5X L5X S5X SYS / # / OBS TYPES
R 9 C1C L1C S1C C2C C2P L2C L2P S2C S2P SYS / # / OBS TYPES
E 12 C5X L5X S5X C1X L1X S1X C8X L8X S8X C7X L7X S7X SYS / # / OBS TYPES
J 15 C1C C1X L1C L1X S1C S1X C2X L2X S2X C5X L5X S5X C6X SYS / # / OBS TYPES
L6X S6X SYS / # / OBS TYPES
C 9 C6X L6X S6X C2X L2X S2X C7X L7X S7X SYS / # / OBS TYPES
15.000 INTERVAL
0 RCV CLOCK OFFS APPL
16 LEAP SECONDS
66 # OF SATELLITES
2014 07 12 17 00 00.0000000 GPS TIME OF FIRST OBS
END OF HEADER

```

Figure 6-2. Excerpt of RINEX header for station Kirchdorf (EAG)

### 6.3 Simulated Data

To explore in addition a simulated data set, a software simulator NavX-NCS has been used to generate GPS and GALILEO data. The NavX - NCS is a multi-frequency signal generator providing in fully equipped mode GPS (L1/L2/L5), Galileo E1, E5 (E5a, E5b), Glonass, Beidou, QZSS, and SBAS observations. The Galileo constellation consists of 30 satellites according to the parameters described in Chapter 2 and for the GPS constellation 32 satellites in circular orbits are simulated, with the assumption that the time and coordinate reference frames of GPS and Galileo have been reconciled to the GPS system.

With user input of error scaling factors, the sampling rate, the masking angle and the coordinates of reference and user stations, the software is able to simulate pseudorange and carrier phase measurements on three carrier frequencies for both GPS and Galileo. Ionospheric errors, tropospheric errors, orbital errors, receiver noise, and multipath are included in the simulation as biases.

At the date of this simulation, the simulator only provided L1 GPS and E1, E5 Galileo data due license limitations. An excerpt of a RINEX header from simulated data for station TIME is displayed in figure 6-3.

```

3.02          OBSERVATION DATA      M          RINEX VERSION / TYPE
GSPF V1.7.0          20140926 105812 UTC PGM / RUN BY / DATE
TIME          MARKER NAME
NON_GEODETTIC    MARKER TYPE
                OBSERVER / AGENCY
                REC # / TYPE / VERS
                ANT # / TYPE
                APPROX POSITION XYZ
                ANTENNA: DELTA H/E/N
G  4 C1C L1C D1C S1C          SYS / # / OBS TYPES
S  4 C1C L1C D1C S1C          SYS / # / OBS TYPES
E  8 C1B L1B D1B S1B C8I L8I D8I S8I          SYS / # / OBS TYPES
2013      1      2      0      0      0.0000000      GPS          TIME OF FIRST OBS
G L1C 0.000000 0          SYS / PHASE SHIFT
S L1C 0.000000 0          SYS / PHASE SHIFT
C1C 0.000 C1P 0.000 C2C 0.000 C2P 0.000          GLONASS COD/PHS/BIS
                END OF HEADER

> 2013 01 02 00 00 0.0000000 0 17
G02 24938849.16807 131054493.38307          2932.60907          45.00007
G04 23649456.13807 124278694.75507          2068.78907          45.00007
G09 21040442.47207 110568251.54807          -2592.66507          45.00007
G12 20539463.57207 107935592.63707          1192.42707          45.00007
G14 22983414.54007 120778630.10707          2305.06507          45.00007
G15 24043122.03907 126347423.46907          -3639.26207          45.00007
G17 23338645.65407 122645380.10907          -2726.18607          45.00007
G24 20334750.83107 106859820.81907          -822.76707          45.00007
G25 22865897.55007 120161073.88007          2862.03407          45.00007
E01 24379040.78307 128112705.52407          -1693.98407          45.00007 24379042.09707 96916424.60307 -1281.48807          45.00007
E02 28027973.42507 147287952.61407          -2747.68507          45.00007 28027976.40007 111422367.90807 -2078.60607          45.00007
E08 26122438.91307 137274312.22307          2688.45807          45.00007 26122441.10307 103847117.10007 2033.80107          45.00007
E09 23181980.25107 121822112.22507          799.18207          45.00007 23181981.40507 92157632.25807 604.57607          45.00007
E15 26262525.49807 138010474.53307          2803.09907          45.00007 26262527.52207 104404019.76807 2120.52607          45.00007

```

Figure 6-3. Excerpt of RINEX header from NavX-Simulator (TIME station)

## 6.4 Investigated Characteristics

Different characteristics have to be investigated to evaluate the performance of GNSS linear combinations on short- and medium baselines. This involves accuracy, availability, continuity and integrity of the solution. Availability is a performance characteristic defined as the percentage of time at a certain accuracy. Integrity relates to the level of trust that can be placed in the information provided by the navigation system. It includes the ability of the navigation system to provide timely and valid warnings to users when the system must not be used for the intended operation (Feng, 2008).

Real-time positioning is aiming to achieve an accuracy at the centimeter level with as few as possible data epochs in real-time. This chapter presents a systematic review for real-time positioning performance characteristics and then evaluates the GNSS ambiguity resolution (AR) with various parameters. The wide-lane linear combination and position estimation with the specific GNSS signal combinations are utilized to check the performance according to its datasets of different baselines with respect to the original L1/L2 GPS signals.

For testing the ambiguity resolution, real and simulated data are used for the different baselines. Processing was carried out throughout several minutes to generate a statistical sample. Afterwards, the performance was evaluated in terms of the following characteristics.

First of all, the number of visible satellites influences the results. The number of visible satellites for both systems, above an elevation mask of  $5^\circ$  during the several minute calculations is taken into account. For the time to correctly fix ambiguities, a large number of trials are adopted and were calculated by averaging the time required to fix ambiguities in each attempt throughout a dataset under the specified conditions, such as specific baseline length and observation time. In the calculation of the mean time to fix, only the correctly fixed ambiguity sets are taken into account in the sample. Also the success-rate of Ambiguity Resolution is considered as the result of the number of fully correctly fixed ambiguity sets over the total number of fixed ambiguity sets.

As the distance limitation is mainly caused by the dependence of the ionospheric biases, the ionosphere-free linear combinations are used mainly for longer baselines. For the residual tropospheric errors, a standard Saastamoinen model correction is introduced. The effect of broadcast orbital errors is relatively small and may be ignored in case of short baseline and IGS orbit corrections can reduce significantly the orbit error for longer baselines in the data processing.

In an effort to evaluate the efficiency of the proposed ambiguity resolution algorithm, the L1 GPS and E1, E5 Galileo signals were processed with simulated data at one second sampling rate and over 25 km to 66 km baselines for a few hours. To be noted, the L2



GPS in the simulated data can be used as the simulator cannot provide L2 GPS signal when the simulated data is being processed. On the other hand, the L1, L2, and L5 GPS and E1, E5 Galileo signals in the real data were processed at one second sampling rate up to 66 km baselines. The resulting coordinates of the stations and their standard deviations are used for biases evaluation.

As a performance characteristic, the fixed rates of the integer estimation results can be defined. Ambiguity resolution (AR) may be impossible when the geometry is too weak or the available satellites are too few. AR success fixed-rate can be calculated when the ambiguity integers are correctly fixed, with respect to the total number of epochs of the processed session.

Real-time accuracy is defined as the difference of an estimated RTK position at a given time to a defined reference coordinate value (or 'true' value) which is obtained from an independent approach, preferably at higher level of accuracy. These parameters may be either all or selectively used to evaluate the performance of the positioning. The distance, time for ambiguity fix, AR reliability, availability, and accuracy are counted as the most important ones. Hence, the linear combination that gives the best performance can now be determined.

## **6.5 Results**

The general form of phase linear combinations was studied in chapter 5 for both GALILEO and the modernized GPS. Tests were conducted at distances below 30 km to medium baselines 70 km, at different observation periods with real and simulated data.

There are several signal linear combinations of the modernized GNSS that were already tested in chapter 5.2. From 5 scenarios that were simulated, only three linear combinations are chosen, i.e. L1/L2 GPS, L1/L5 GPS, and E1/E5 Galileo. It has been assumed that the observations are free of biases in particular on short baselines where the atmospheric errors cancel through differencing. Then on medium baselines, all common error sources are present. The linear combinations using dual frequency are predominantly used because only two ambiguities have to be resolved compared to triple frequency. When three carriers are employed, all three ambiguities need to be resolved. One has to consider the overall success-rate by taking into account measurement precision and observation scenario.

On a medium baseline, typically more than 30 km or longer, when corrective information is used from a network of active GNSS reference stations, a success rate at the level of 95% can be achieved using a dual combined GPS – Galileo systems (Tiberius, 2002). Ionosphere-free GNSS linear combinations based on two phase carriers are displayed in table 6-2.

First, the static processing tests were conducted with the narrow-lane linear combination as reference. Afterward the kinematic processing tests were conducted. In the process, several error sources are considered, i.e. orbital error, ionospheric error, tropospheric error, multipath, and receiver noise. To simulate realistic observations, it requires several files as input contains time of observation, test site location, multipath and noise level, troposphere correction, and last, ionospheric and orbit correction from IGS.

Table 6-2. Ionosphere-free Linear Combinations based on two signals

Obs	Linear combination	$\lambda$ (cm)	est. ambiguities	$\sigma$ factor
L1/L2	$2.5457\phi_{L1} - 1.5457\phi_{L2}$	0.629	$77a_1 - 60a_2$	2.98
L1/L5	$2.2606\phi_{L1} - 1.2606\phi_{L5}$	0.279	$154a_1 - 115a_5$	2.59
E1/E5	$2.3379\phi_{E1} - 1.3379\phi_{E5}$	0.289	$308e_1 - 233e_5$	2.69

The current GPS L1 and L2 frequencies are 154 times respectively 120 times the nominal frequency of 10.23 MHz (see also table 5-15 in chapter 5.2.3). For the ionosphere-free combination L1/L2 GPS, however, not the ratio 154 and 120 should be taken, but the ratio 77 and 60, since the greatest common divisor of 154 and 120 is 2,  $a$  or  $e$  are the integer double difference phase ambiguities respectively on the signal that is used.

For the test, the observations are assumed to be processed in double difference mode, hence the atmospheric errors and satellite clock error cancel. The data assumed to be collected correctly following the standard procedure. To improve ambiguity resolution, the LAMBDA method has been utilized.

When processing non ionosphere-free linear combinations, a stochastic ionosphere model (notably at long baseline more than 20 km) should be adopted. Over short baselines, others canceled in differencing, the observation noise dominates the error sources. However, with the increase of length of observation as well as ionospheric level, the residual error becomes the dominant error source. All error sources which are present in the observations were simulated with a certain condition in case of baselines about 20 – 70 km. During the test period, the levels of ionosphere and troposphere activity varied significantly. A mask angle of 5 degrees was chosen and the tropospheric correction according to the standard model was applied.

Finally, the results from the carrier phase processing are compared. For the analysis, it was necessary to choose data of visible satellites for the entire simulation. Additionally, since most satellites are in low elevation which effects positioning quality these certain cases are ignored to minimize the impact on the solution. In the real data approach, the results positioning are dominantly influenced by GPS as only few Galileo observations were available. An excerpt of the result file is displayed in figure 6-4.

```

% program : RTKPOST ver. 2.4.2
% inp file : C:\Users\dhota\Downloads\New folder (8)\wind0020.130
% inp file : C:\Users\dhota\Downloads\New folder (8)\time0020.130
% inp file : C:\Users\dhota\Downloads\New folder (8)\bdr0020.13p
% obs start : 2013/01/02 00:00:00.0 GPST (week1721 259200.05)
% obs end : 2013/01/02 00:05:00.0 GPST (week1721 259500.05)
% pos mode : kinematic
% freds : L1+L2+L5
% solution : combined
% elev mask : 5.0 deg
% dynamics : off
% tidecorr : off
% ionos opt : iono-free
% tropo opt : saastamoinen
% ephemeris : precise
% navi sys : gps galileo
% amb res : continuous
% val thres : 3.0
% antenna1 : ( 0.0000 0.0000 0.0000)
% antenna2 : ( 0.0000 0.0000 0.0000)
% ref pos : 48.010097360 13.588984867 510.4119
%
% (lat/lon/height=WGS84/ellipsoidal,Q=1:fix,2:float,3:sbas,4:dpps,5:single,6:ppp,ns=# of satellites)
% GPST lat(deg) lon(deg) height(m) Q ns sdn(m) sde(m) sdu(m) sdne(m) sdeu(m) sdun(m) age(s) ratio
2013/01/02 00:00:00.000 47.697997112 14.346262306 692.1022 1 13 0.0062 0.0048 0.0114 0.0019 -0.0032 0.0036 0.00 7.7
2013/01/02 00:00:01.000 47.697997112 14.346262306 692.1024 1 13 0.0062 0.0048 0.0114 0.0018 -0.0031 0.0037 0.00 8.5
2013/01/02 00:00:02.000 47.697997112 14.346262306 692.1022 1 13 0.0061 0.0047 0.0114 0.0017 -0.0031 0.0036 0.00 8.9
2013/01/02 00:00:03.000 47.697997112 14.346262306 692.1025 1 13 0.0063 0.0047 0.0114 0.0020 -0.0032 0.0036 0.00 9.2
2013/01/02 00:00:04.000 47.697997112 14.346262306 692.1024 1 13 0.0061 0.0048 0.0114 0.0019 -0.0032 0.0037 0.00 9.2
2013/01/02 00:00:05.000 47.697997112 14.346262306 692.1022 1 13 0.0061 0.0049 0.0114 0.0018 -0.0032 0.0037 0.00 9.3
2013/01/02 00:00:06.000 47.697997113 14.346262306 692.1024 1 13 0.0062 0.0050 0.0114 0.0016 -0.0030 0.0036 0.00 9.4
2013/01/02 00:00:07.000 47.697997112 14.346262306 692.1023 1 13 0.0062 0.0048 0.0114 0.0018 -0.0031 0.0037 0.00 9.4
2013/01/02 00:00:08.000 47.697997113 14.346262306 692.1024 1 13 0.0061 0.0046 0.0114 0.0016 -0.0032 0.0037 0.00 9.4
2013/01/02 00:00:09.000 47.697997113 14.346262306 692.1026 1 13 0.0062 0.0048 0.0114 0.0018 -0.0031 0.0036 0.00 9.5
2013/01/02 00:00:10.000 47.697997112 14.346262306 692.1025 1 13 0.0062 0.0049 0.0115 0.0020 -0.0032 0.0037 0.00 9.5
2013/01/02 00:00:11.000 47.697997112 14.346262307 692.1023 1 13 0.0061 0.0050 0.0114 0.0018 -0.0030 0.0035 0.00 9.5
2013/01/02 00:00:12.000 47.697997113 14.346262306 692.1025 1 13 0.0061 0.0047 0.0115 0.0019 -0.0032 0.0036 0.00 9.5
2013/01/02 00:00:13.000 47.697997111 14.346262305 692.1025 1 13 0.0062 0.0048 0.0114 0.0019 -0.0032 0.0037 0.00 9.5
2013/01/02 00:00:14.000 47.697997112 14.346262305 692.1025 1 13 0.0061 0.0048 0.0114 0.0018 -0.0031 0.0036 0.00 9.6

```

Figure 6-4. Excerpt of the solution file (TIME-WIND)

Figure 6-4 provides a description of the output from RTKLib. The output contains standard Rinex observation data and navigation message files from GPS and Galileo i.e. TIME and WIND stations. The file computes the relative positioning solution in kinematic carrier-based mode with 30 minutes observation time. The used carrier frequencies are L1+L2+L5, but in Galileo data processing, L2 frequency was not recognized, hence L1 represents E1 Galileo and L5 will be recognized as E5 Galileo.

5 degrees elevation mask was used to maximize satellite coverage. Kalman filtering was applied using the combined mode, which is a forward and backward iteration to get a smooth solution (10 times of iteration). To reduce ionospheric biases, an ionosphere free linear combination (and later a wide-lane linear combination) was used. The Saastamoinen model was used for tropospheric model correction.

Finally, the solution delivers in each epoch a latitude, longitude, and height coordinate. In addition, the standard deviation for n, e, u components is provided.

### 6.5.1 Real Data Results

Figure 6-5 shows the number of visible GPS and Galileo satellites from station KIRC for both systems above the elevation mask of 5° during the 3 hours observation period. As all 4 test sites are located within a few lengths of kilometers, the satellite visibility is similar for all stations. The numbers of visible GPS satellites is always about 12 to 15. As only 2 to 3 Galileo satellites were usually visible, it is impossible to obtain a position only from Galileo data.

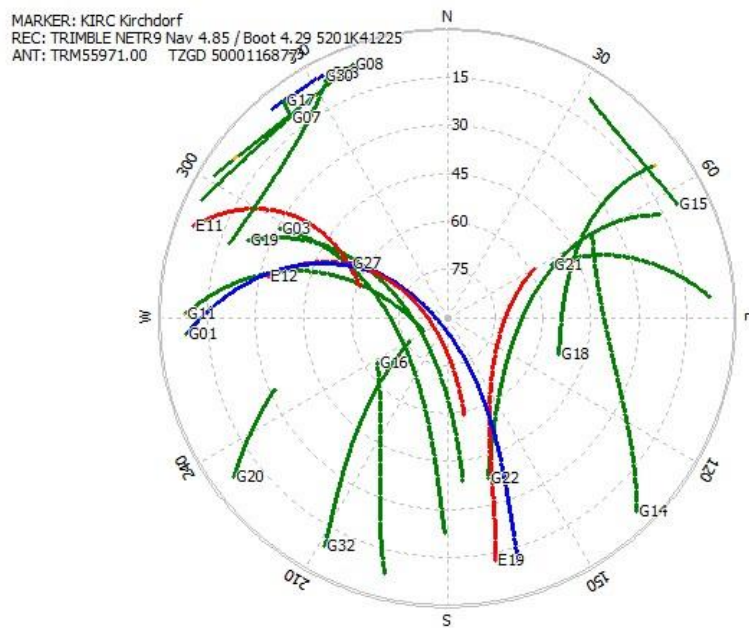


Figure 6-5. Satellite visibility at KIRC station, DOY 193, 2014 (green plot – L1/L2 GPS; blue plot - L1/L2/L5 GPS; red plot – E1/E5 Galileo)

In figure 6-6, the SNR and multipath errors for Galileo satellites are illustrated for all stations. The similar SNR can be explained by the same receiver and antenna for observation (the multipath can change depending on station conditions). At low elevations, the E1 and E5 Galileo signals show no difference in signal power. Meanwhile, when the satellite position gradually ascends to higher elevations, the E5 Galileo signal exhibits a better signal characteristic with a difference of up to 10 dBHz than E1 Galileo which remains with a similar characteristic like L1 GPS. On the other side, the multipath residuals of the E5 Galileo signal show variation ranging from 10 cm to 30 cm. The E5 Galileo provides a higher signal power and small-scale multipath residuals compared with the E1 Galileo signal which is affected by a 30 – 50 cm code noise.

Figure 6-7, 6-8, and 6-9 shows the different SNR values of the Galileo satellites E11, E12, and E19 at station KIRC. To further analyze, the SNR value obtained from same time on low elevation angles. The E5 Galileo signal exhibit an increased SNR of up to 10 dBHz compared to the E1, E5a, and E5b.

Figure 6-10 shows the SNR and code multipath/noise residuals for all available satellites. By taking a large number of all satellite observations, the SNR and the code multipath/noise residuals for E5 Galileo are smaller than L1, L2, L5 GPS and E1, E5a, E5b Galileo. On average, the E5 provides  $\pm 10$  cm error standard deviation. On the other hand, L5 GPS provides  $\pm 41$  cm error standard deviation in the code multipath/noise residuals result despite having the strongest SNR along with E5 Galileo (up to 55 dBHz).

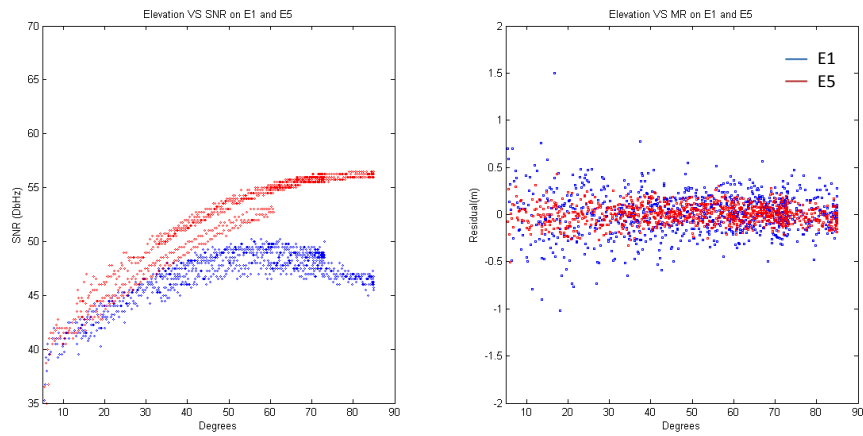


Figure 6-6. SNR and Code Multipath residual values of E1 and E5 Galileo at 4 stations (E11, E12, E19 Galileo)

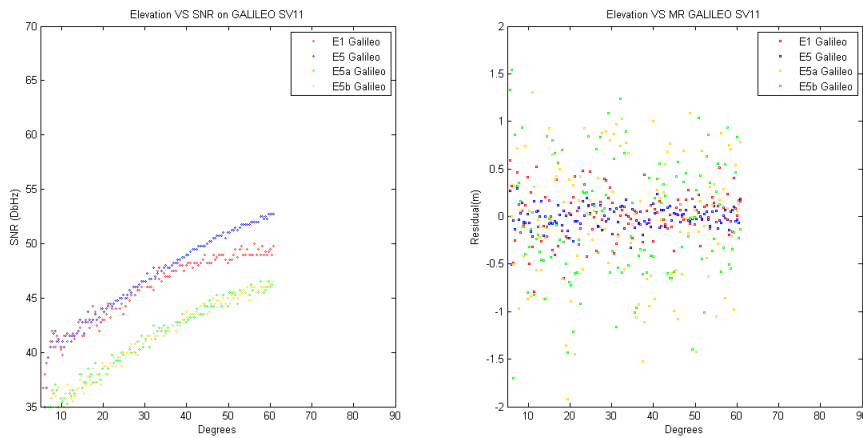


Figure 6-7. SNR and Code Multipath residuals for Galileo E11 at KIRC station, DOY 193, 2014

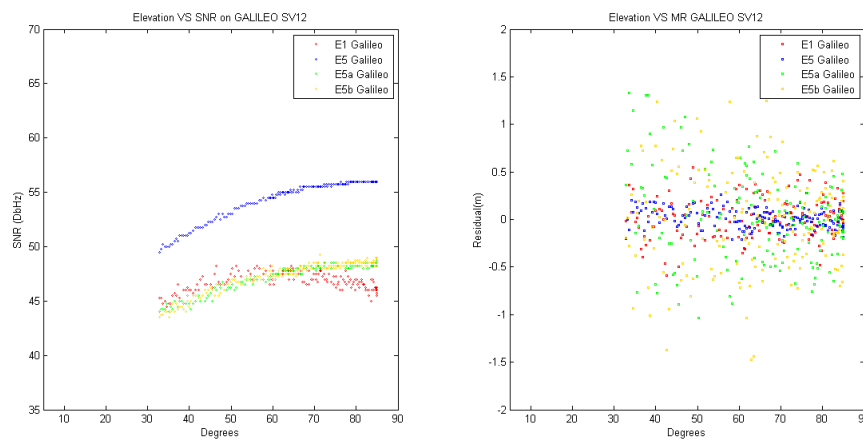


Figure 6-8. SNR and Code Multipath residuals for Galileo E12 at KIRC station, DOY 193, 2014

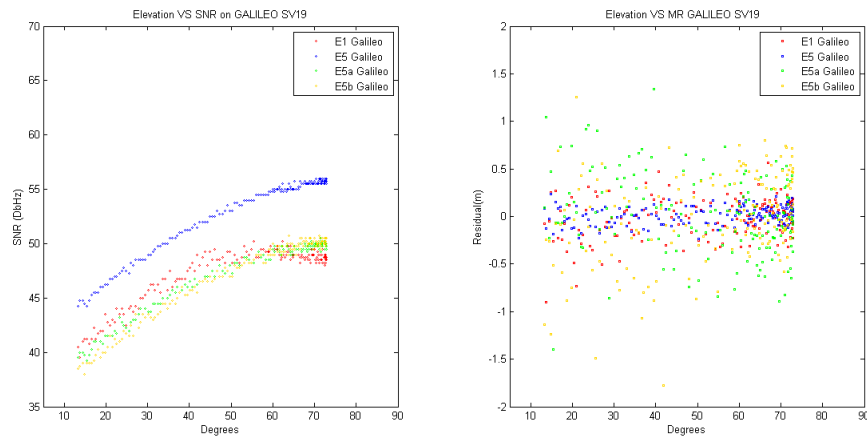


Figure 6-9. SNR and Code Multipath residuals for Galileo E19 at KIRC station, DOY 193, 2014

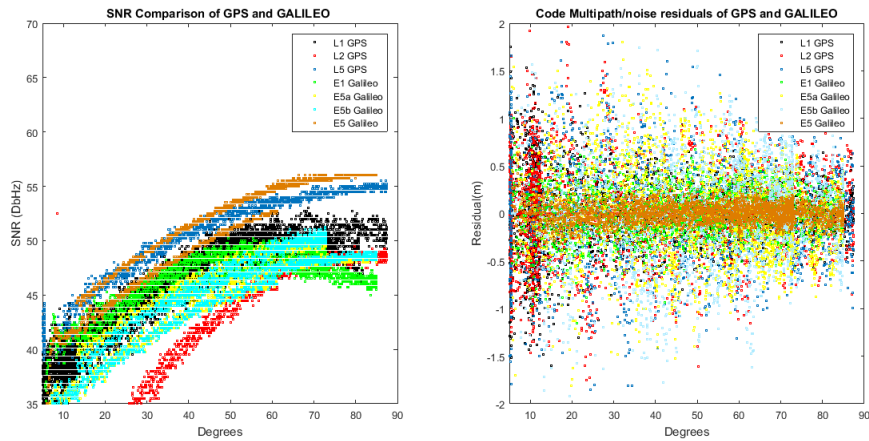


Figure 6-10. SNR and Code Multipath/noise residuals of GNSS (all satellites, GPS and Galileo) at KIRC station, DOY 193, 2014.

Moreover, L5 GPS and E5 Galileo allowed more accurate combined code-and-carrier observable to mitigate ionospheric errors because it has the strongest signal strength of the modernized GNSS signals tested. These characteristics can open the possibility of performing code-range measurements using modernized GNSS signals at the decimeter level and enable a better mitigation of multipath effects, particularly for E5 Galileo signal combination with small code residuals (see figure 6-10).

Figure 6-11 shows the code and carrier-phase residual for baseline WIND-KIRC (29.1 km) processed with GPS L1/L2 data. No fixed Galileo solution was possible due to only 3 available satellites. Hence, the utilization of GPS data as substitute signal in case of insufficient Galileo signal affects the result. Also the GPS L1/L5 solution lacks from missing IIF satellites (see table 6-3).

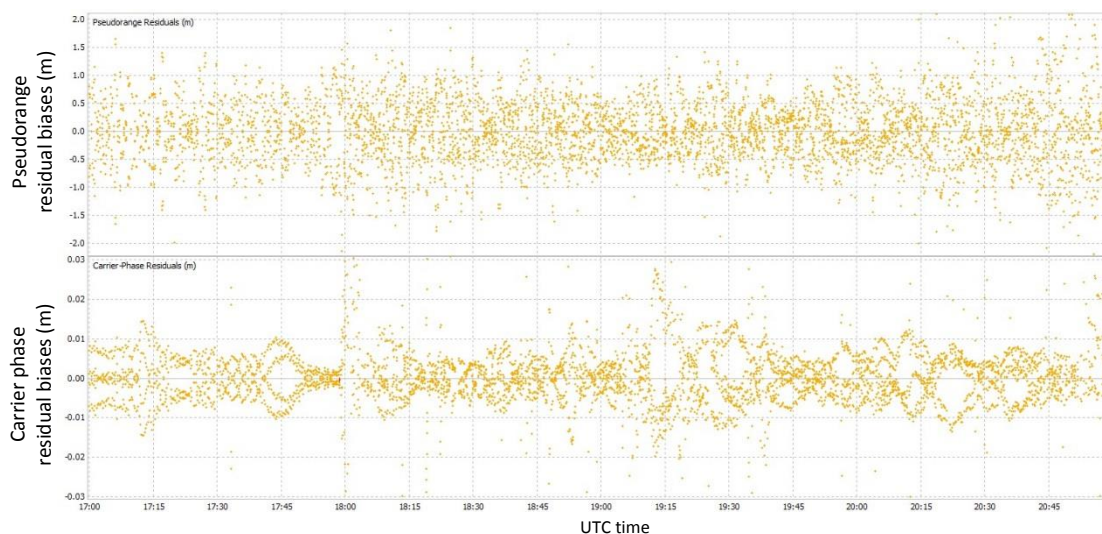


Figure 6-11. Pseudorange and Carrier Phase Residuals of E1/E5 Galileo w.r.t L1/L2 GPS (WIND – KIRC baseline, 29.1 km) at DOY 193, 2014

Figure 6-11 shows high-frequency noise affecting the estimated position with GPS data is forced to cover a lack of Galileo data. To further analyze, the pseudorange and the carrier phase residuals obtained from observation are compared. The figure shows that there is slightly higher-frequency carrier phase residuals up to 4 cm. However, when computing the standard deviation of the kinematic coordinates, the effect of errors interference dominates.

Table 6-3. Positioning results at KIRC (29.1 km), DOY 193, 2014.

LC	X(m)	Y(m)	Z(m)	$\Delta n$ (m)	$\Delta e$ (m)	$\Delta u$ (m)	$\sigma_n$ (m)	$\sigma_e$ (m)	$\sigma_u$ (m)	AR
L1/L2	4154375.442	1044544.883	4710348.019	0.000	0.000	0.000	0.02	0.01	0.03	Fix (static)
L1/L5	4154375.122	1044545.316	4710347.568	-0.320	0.433	-0.451	0.12	0.12	0.26	float
E1/E5	4154375.406	1044545.014	4710347.876	-0.036	0.131	-0.143	0.09	0.11	0.06	float

Table 6-3, presents the resulting positions calculated from individual linear combinations with E1/E5 Galileo data using 3 hours observations and 5 satellites. With sufficient data for data processing, the E1/E5 Galileo linear combination shows a better performance than L1/L5 GPS. The coordinate's difference to the traditional LC reference, i.e. L1/L2 GPS is still up to a few decimeters by the lack of data for the new LC. The time series are plotted in figure 6-12. The L1/L5 GPS and E1/E5 Galileo were processed epoch by epoch to get the time series position (see figure 6-11), then an averaging method was adapted to get mean values of the difference of position with respect to the L1/L2 GPS results ( $\Delta n$ ,  $\Delta e$ ,  $\Delta u$ , and  $\sigma_n$ ,  $\sigma_e$ ,  $\sigma_u$ ).

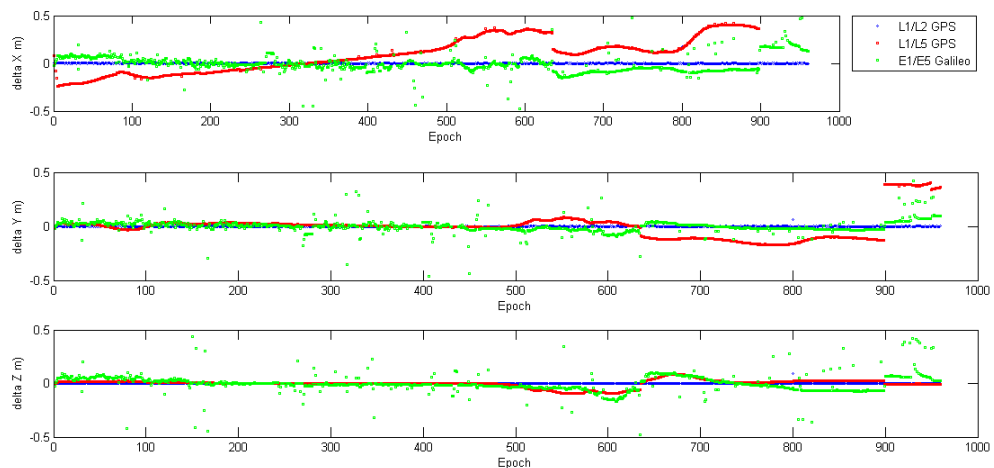


Figure 6-12. Time series position results w.r.t L1/L2 GPS LC at WIND-KIRC (29.1 km), DOY 193, 2014

According to figure 6-12, E1/E5 GPS+Galileo provides a poor result position (up to 45 cm) to L1/L2 GPS solution. However, the L1/L5 GPS gives a smooth pattern of result as L5 GPS has more satellites available than the Galileo system (5 versus 3) and the displays a systematic trend with respect to L1/L2 GPS. Once more, we have to take into account that the L1 GPS signal was used for processing when the L5 GPS and Galileo data is insufficient, so the effect from L1 GPS is expected on the results.

When using 1 hour or shorter observation periods, L1/L5 GPS and Galileo still cannot deliver a good performance because during data processing, sometimes only 2 satellites that provide L5 GPS signal were available. In Galileo data processing, the result is worse than GPS results. Hence, it is impossible to provide a position with resolving ambiguities.

To understand the performance with only (maximum) 3 Galileo satellites and 5 GPS satellites (L5 GPS signal) with 1 hour observation that were processed for positioning, table 6-4 and 6-5 represent the results with the utilization of L1 GPS signal to cover the lack of data. The results exhibits a low of ambiguity fixing success-rate with worse estimated position and standard deviation.

The residual level increases at the KIRC-UNTE baseline with 50.5 km (figure 6-13). Again, the ambiguities could not be fixed completely by utilized all satellites within 3 hours observation time span. However, there is a systematic residual pattern in the residuals which indicates systematic noise and that affected the position result (refer to figure 6-14 and table 6-5).



Table 6-4. The influence of length of observation time at KIRC (29.1 km) w.r.t. reference position at DOY 193, 2014

**WIND-KIRC 29.1 km GPS L1/L5**

Time	Static					Kinematic				
	$\Delta n(m)$	$\Delta e(m)$	$\Delta u(m)$	$\sigma(m)$	Fix(%)	$\Delta n(m)$	$\Delta e(m)$	$\Delta u(m)$	$\sigma(m)$	Fix(%)
5	0.18	0.13	0.24	1.04	0.80	-0.82	1.35	-0.36	1.30	1.70
15	-0.17	0.86	1.63	1.85	1.20	0.18	0.32	0.24	0.88	1.70
30	0.60	0.67	1.53	1.44	1.00	-0.43	-0.42	0.04	1.14	1.50
60	0.07	0.12	0.23	0.64	1.20	0.20	0.19	0.43	0.50	2.30

**WIND-KIRC 29.1 km L1+ Gal E1/E5**

Time	Static					Kinematic				
	$\Delta n(m)$	$\Delta e(m)$	$\Delta u(m)$	$\sigma(m)$	Fix(%)	$\Delta n(m)$	$\Delta e(m)$	$\Delta u(m)$	$\sigma(m)$	Fix(%)
5	4.16	0.58	0.04	8.42	0.00	0.95	-1.28	0.20	1.14	0.00
15	2.22	-1.19	-2.35	2.82	0.00	0.25	-0.72	-0.93	1.37	0.00
30	0.88	1.36	-1.13	1.61	0.00	0.24	-0.44	0.08	0.80	0.00
60	0.99	0.15	0.31	0.47	0.00	0.23	0.08	0.15	0.58	0.00

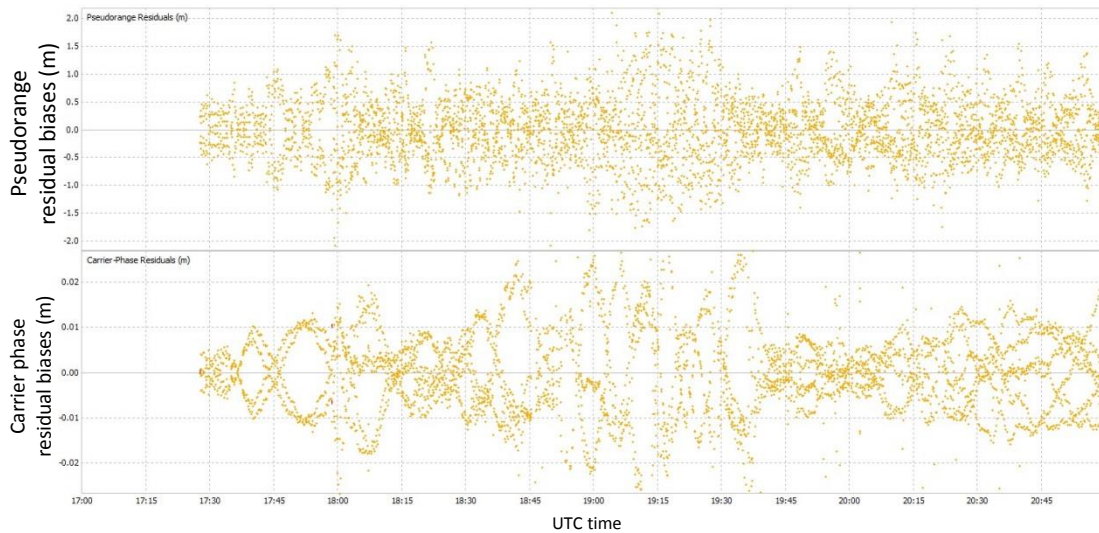


Figure 6-13. Pseudorange and Carrier Phase Residuals using Galileo satellites (KIRC – UNTE baseline, 50.5 km) at DOY 193, 2014

Figures 6-13 and 6-14 display that there is a significant difference in the residual level and also the median coordinate values differ up to tens of cm. This can be an effect from ionospheric biases in particular by using only E1/E5 Galileo signals. The graphic in figure 6-15 exhibit the position using Galileo (+GPS) with respect to GPS alone. The maximum shift in position between GPS and Galileo (+GPS) using real data observation is up to 19 cm. Even though using 3 hours observation data and utilizes all Galileo satellites (i.e. 5 satellites), it is impossible to provide resolved ambiguities using ionosphere-free linear combination (Narrow-Lane).

Table 6-5. The influence of length of observation time at KIRC (50.5 km) w.r.t. reference position at DOY 193, 2014

*KIRC-UNTE 50.5 km GPS L1/L5*

Time	Static					Kinematic				
	$\Delta n(m)$	$\Delta e(m)$	$\Delta u(m)$	$\sigma(m)$	Fix(%)	$\Delta n(m)$	$\Delta e(m)$	$\Delta u(m)$	$\sigma(m)$	Fix(%)
5	1.42	-0.91	1.28	3.38	float	0.98	-1.04	2.33	7.90	float
15	0.48	0.32	0.01	1.40	float	0.95	-1.03	1.24	7.15	float
30	0.64	-0.44	0.12	1.56	float	0.61	0.59	0.33	5.33	float
60	0.06	-0.02	0.12	0.17	float	0.18	0.05	0.52	0.42	float

*KIRC-UNTE 50.5 km Gal E1/E5*

Time	Static					Kinematic				
	$\Delta n(m)$	$\Delta e(m)$	$\Delta u(m)$	$\sigma(m)$	Fix(%)	$\Delta n(m)$	$\Delta e(m)$	$\Delta u(m)$	$\sigma(m)$	Fix(%)
5	0.18	2.08	4.70	4.17	float	0.12	-3.23	-5.98	6.54	float
15	0.88	1.41	1.02	5.09	float	0.60	-0.55	0.77	3.31	float
30	0.12	0.50	0.20	2.04	float	0.94	0.66	1.06	2.17	float
60	0.19	0.16	0.16	1.66	float	0.23	0.59	-0.98	0.54	float

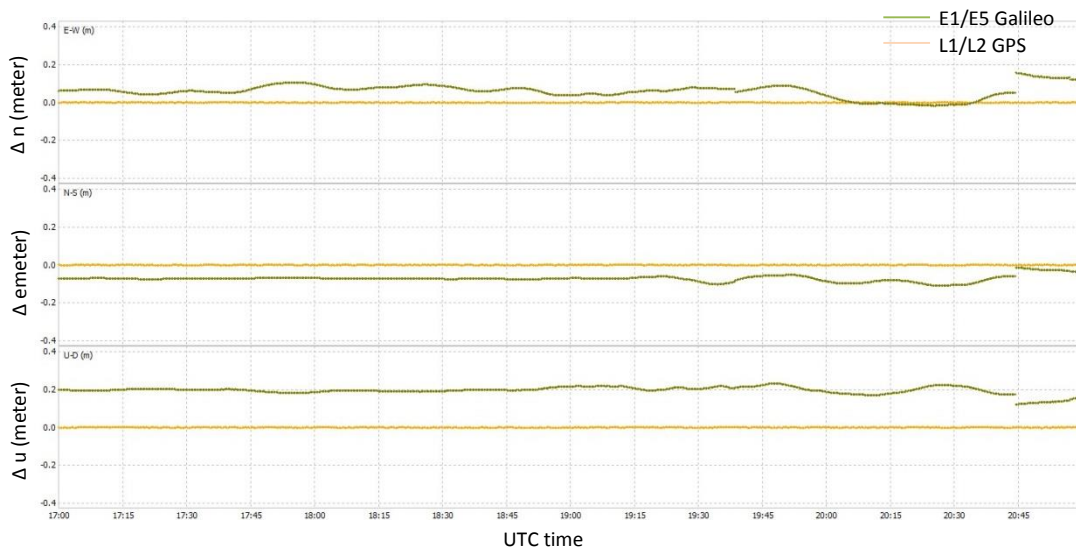


Figure 6-14. Time series position using E1/E5 Galileo wr.t. L1/L2 GPS (KIRC – UNTE baseline, 50.5 km) at DOY 193, 2014

As a matter of fact, the software forced the GPS to cover Galileo, hence the position is actually dominantly provided by GPS, not Galileo. However, in future, with additional external input such as more satellites and accurate orbital information, time correction, etc., the problem may diminish.

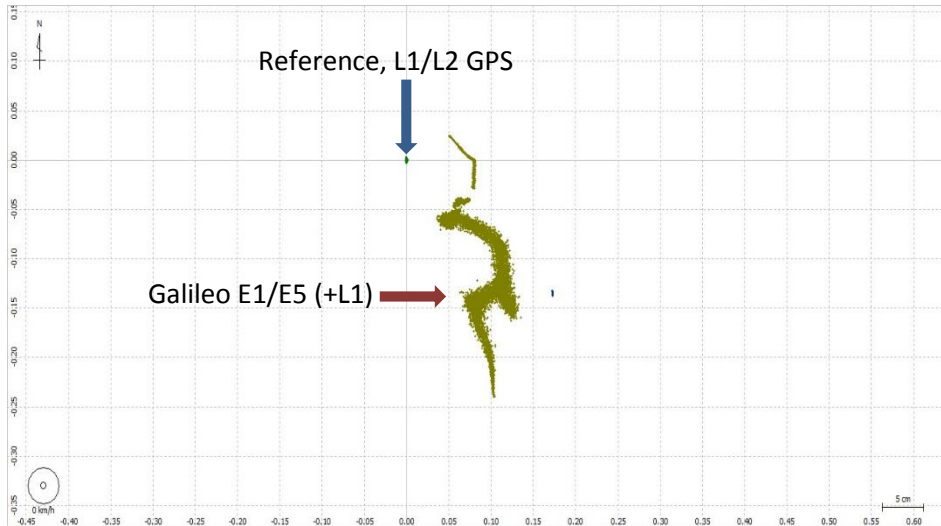


Figure 6-15. Galileo solution w.r.t. L1/L2 GPS at KIRC (29.1 km, DOY 193, 2014)

### 6.5.2 Simulated Data Results

Subsequently station observation for the 4 selected sites of the Austrian reference network TIME, UNTE, KIRC, and WIND was simulated in the NavX simulator.

Figure 6-16 shows that sufficient satellite data were generated to provide positions using GPS and Galileo, although there is a limitation that for GPS only the L1 signal could be generated.

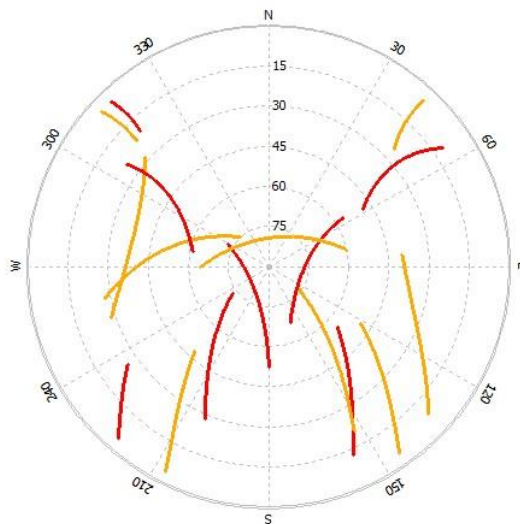


Figure 6-16. 3 hours satellite visibility at KIRC station. (Yellow plot – L1 GPS, red plot – E1/E5 Galileo), DOY 001, 2014

Tables 6-6, 6-7, and 6-8, exhibit the performance of simulated GPS and Galileo data on different baselines in terms of observation time. The numbers obviously show that Galileo always performs better at all baselines with 60 minutes observation with respect to the GPS solutions.

Increasing the observation time to more than 15 minutes does not result in a significant change of static positioning as of 100% success rate of ambiguity fix could always be obtained. For example, the standard deviation in the GPS+Galileo case is varying up to 2 cm at the 24.9 km of baseline to 10 cm in the 66 km baseline. On the other hand, in case of Galileo alone, the position varies about 4 cm to 13 cm w.r.t. reference station despite the success rate is similar 100%.

In other words, very fast ambiguity resolution is possible with two frequencies under the condition of a 15 minutes observation time on medium baselines (below 30 km, table 6-6). The success rate percentage for GPS/Galileo is affected and decreases drastically as the baseline length increases, especially in the 66 km baseline. The coordinate's accuracy decreases significantly from 25 km to 66 km baselines in case of an observation time less than 15 minutes. We have to keep in mind that the ambiguity fixing rate is for all baseline lengths slightly too optimistic as simulated data has been processed.

The estimated position was processed both on static and kinematic positioning and its standard deviation, then an averaging method was adapted to get mean values of the difference of position with respect to the coordinate reference to obtain  $\Delta n$ ,  $\Delta e$ ,  $\Delta u$ , and  $\sigma$  respectively.

For all estimated results, the solution over 1 hour data was calculated from both on static and kinematic positioning and the coordinate reference was considered as truth. The estimated results are then split into 5 minutes, 15 minutes, 30 minutes, and 60 minutes files. The results from each results were finally compared. The offset of the position and its standard deviation is presented in several tables and figures. Shown in table 6-6, 6-7, and 6-8 and figure 6-17, 6-18, and 6-19.

In figure 6-17, static and kinematic positions differ up to 5 cm from the reference coordinate with 15 minutes measurement time processed. The solution converges to the reference when the observation increases. When L1 GPS is used together with E1/E5 Galileo, the position improves, although after 30 minutes observation time and more, the position from GPS and Galileo have a similar position and accuracy both on static and kinematic position. To obtain a decent result using E1/E5 Galileo (without GPS), at least 30 minutes observation time are required.

Table 6-6. The influence of length of observation time at UNTE (24.9 km) w.r.t. reference position at DOY 001, 2014

TIME-UNTE		24.9 km		GPS L1 + Galileo E1+E5						
	Static					Kinematic				
Time	$\Delta n(m)$	$\Delta e(m)$	$\Delta u(m)$	$\sigma(m)$	Fix(%)	$\Delta n(m)$	$\Delta e(m)$	$\Delta u(m)$	$\sigma(m)$	Fix(%)
5	-0.08	0.03	-0.05	0.18	100.00	-0.04	0.04	-0.20	0.20	100.00
15	0.04	-0.03	0.10	0.10	100.00	-0.04	0.03	-0.20	0.10	100.00
30	0.02	0.03	-0.03	0.02	100.00	0.02	0.10	-0.09	0.02	100.00
60	0.01	0.01	0.01	0.01	100.00	0.01	0.01	0.01	0.01	100.00

TIME-UNTE		24.9 km		Galileo E1+E5						
	Static					Kinematic				
Time	$\Delta n(m)$	$\Delta e(m)$	$\Delta u(m)$	$\sigma(m)$	Fix(%)	$\Delta n(m)$	$\Delta e(m)$	$\Delta u(m)$	$\sigma(m)$	Fix(%)
5	-0.05	-0.04	0.21	0.12	100.00	0.05	0.04	0.21	0.13	100.00
15	-0.05	0.03	0.12	0.05	100.00	0.05	0.03	0.12	0.13	100.00
30	-0.05	-0.04	-0.02	0.05	100.00	0.05	0.04	0.13	0.05	100.00
60	0.01	0.01	0.01	0.01	100.00	0.01	0.01	0.01	0.01	100.00

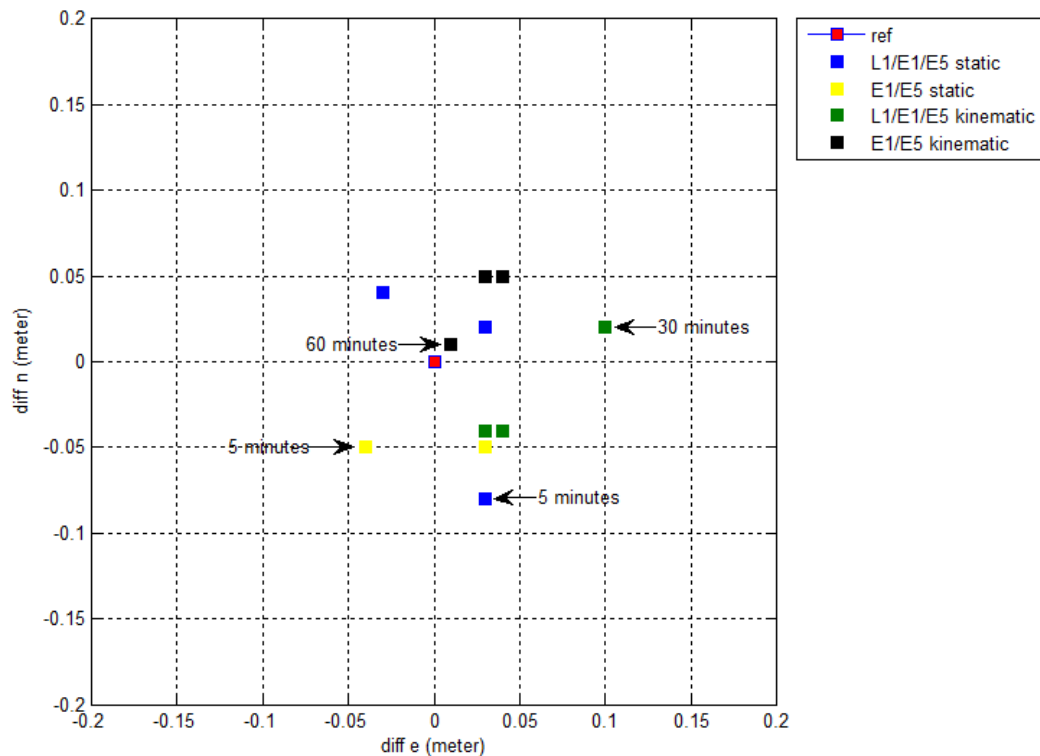


Figure 6-17. Static and kinematic position w.r.t. reference position at TIME – UNTE baseline (24.9 km), DOY 001, 2014

The Galileo ambiguity fixing success-rate increases most significantly compared to the GPS+Galileo results. For the Galileo results, it is expected a good performance when the baseline less than 30 km, as the errors i.e. orbit information, ionospheric errors were diminished and canceled by external corrections from IGS and its linear combination.

As more satellites are available (in simulated data, 8 GPS and 8 Galileo), hence the ambiguity resolution could fix biases in 15 minutes observation data. The solutions both for GPS+Galileo and Galileo alone are similar. Corrections, such as ionospheric correction, time-system offset correction, and orbit information may not provide better solutions in case the baseline is less than 30 km (refer to figure 6-17).

Table 6-7. The influence of length of observation time at KIRC (40.8 km) w.r.t. reference position at DOY 001, 2014

TIME-KIRC 40.8 km GPS L1 + Galileo E1+E5										
	Static					Kinematic				
time	$\Delta e(m)$	$\Delta n(m)$	$\Delta u(m)$	$\sigma(m)$	Fix(%)	$\Delta e(m)$	$\Delta n(m)$	$\Delta u(m)$	$\sigma(m)$	Fix(%)
5	0.09	0.04	-0.05	0.19	100.00	-0.08	0.04	-0.05	0.18	100.00
15	-0.04	0.04	-0.10	0.10	100.00	-0.04	0.03	-0.20	0.10	100.00
30	-0.03	0.09	-0.09	0.02	100.00	0.02	0.10	-0.09	0.03	100.00
60	0.01	0.01	0.01	0.01	100.00	0.01	0.01	0.01	0.01	100.00

TIME-KIRC 40.8 km Galileo E1+E5										
	Static					Kinematic				
time	$\Delta e(m)$	$\Delta n(m)$	$\Delta u(m)$	$\sigma(m)$	Fix(%)	$\Delta e(m)$	$\Delta n(m)$	$\Delta u(m)$	$\sigma(m)$	Fix(%)
5	0.05	0.03	0.20	0.20	100.00	-0.05	0.04	0.20	0.12	100.00
15	-0.05	-0.03	-0.21	0.12	100.00	-0.05	-0.04	-0.21	0.13	100.00
30	-0.05	0.04	-0.22	0.05	100.00	-0.05	0.04	0.23	0.05	100.00
60	0.01	0.01	0.01	0.01	100.00	0.04	0.05	0.02	0.01	100.00

Consistent to the TIME-UNTE baseline, obviously E1/E5 Galileo delivers a best performance in static and kinematic positioning also at the distance of 40.8 km within 30 minutes observation time with respect to reference coordinates. The Galileo result is shifted up to 5 cm after less than 30 minutes observation time. In case of Galileo with 30 minutes observation time and less, the resulting position and accuracy are better than GPS+Galileo results (see figure 6-18).

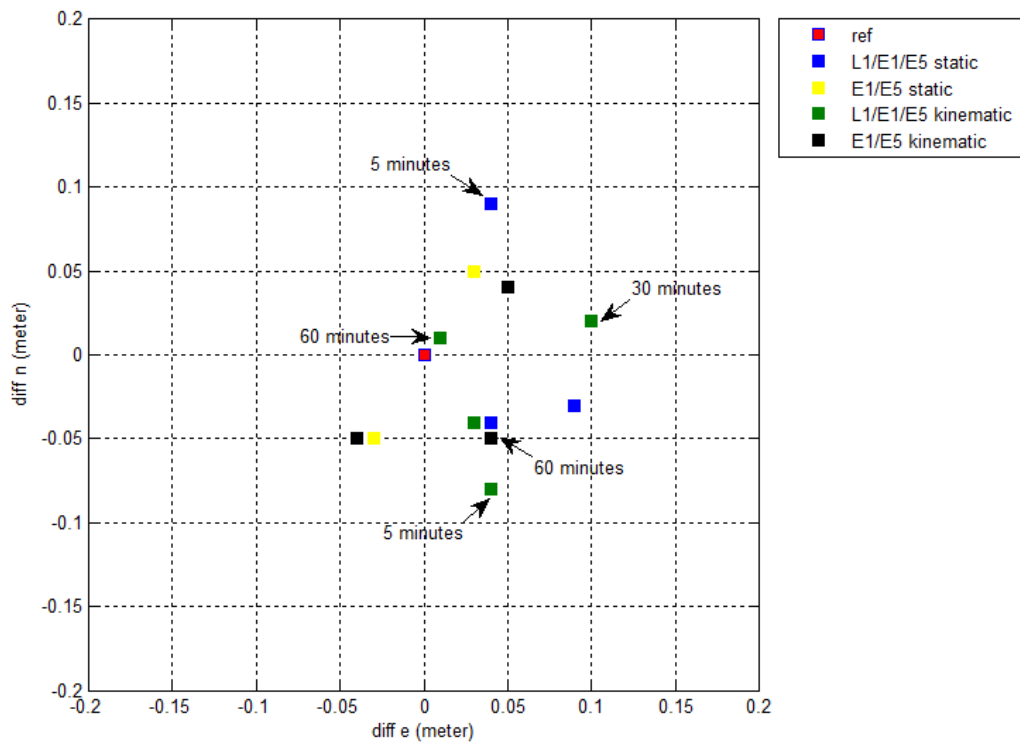


Figure 6-18. Static and kinematic position w.r.t. reference position at KIRC (40.8 km), DOY 001, 2014

Table 6-8. The influence of length of observation time at WIND (66.5 km) w.r.t. reference position at DOY 001, 2014

TIME-WIND 66.5 km GPS L1 + Galileo E1+E5

time	Static					Kinematic				
	$\Delta e(m)$	$\Delta n(m)$	$\Delta u(m)$	$\sigma(m)$	Fix(%)	$\Delta e(m)$	$\Delta n(m)$	$\Delta u(m)$	$\sigma(m)$	Fix(%)
5	0.08	-0.03	0.05	0.18	100.00	-0.10	0.04	-0.06	0.18	77.10
15	0.04	-0.04	0.20	0.10	100.00	0.04	-0.04	-0.20	0.10	73.10
30	0.03	0.10	0.10	0.10	100.00	0.09	0.09	0.09	0.09	87.70
60	0.06	0.07	0.03	0.02	94.10	0.07	0.07	0.10	0.04	94.60

TIME-WIND 66.5 km Galileo E1+E5

time	Static					Kinematic				
	$\Delta e(m)$	$\Delta n(m)$	$\Delta u(m)$	$\sigma(m)$	Fix(%)	$\Delta e(m)$	$\Delta n(m)$	$\Delta u(m)$	$\sigma(m)$	Fix(%)
5	-0.04	-0.03	-0.21	0.12	100.00	-0.05	-0.03	0.20	0.13	100.00
15	0.05	0.04	0.21	0.13	100.00	-0.05	-0.04	0.21	0.13	100.00
30	-0.05	-0.04	0.13	0.05	100.00	-0.05	-0.04	-0.22	0.05	96.20
60	-0.02	-0.03	0.08	0.01	99.60	0.03	-0.01	0.06	0.03	93.30

In table 6-8, both on GPS+Galileo static and kinematic solutions delivers poor performance at TIME-WIND baseline. The E1/E5 Galileo linear combination provide a good performance for estimated position as the results delivers a consistent solution less than 5 cm from the reference position with 15 minutes observation (figure 6-19). However, on 30 minutes observation time or more, the results both from GPS+Galileo and Galileo alone has a similar solution close to the reference coordinate in the range less than 5 cm in all baselines with 60 minutes data observation (figure 6-17, 6-18, 6-19). In case of 66.5 km baseline (TIME - WIND) with 30 minutes observation time and more, the ambiguity fix success-rate is less than 100% as the effect of the ionospheric errors that may be not entirely diminished by linear combinations.

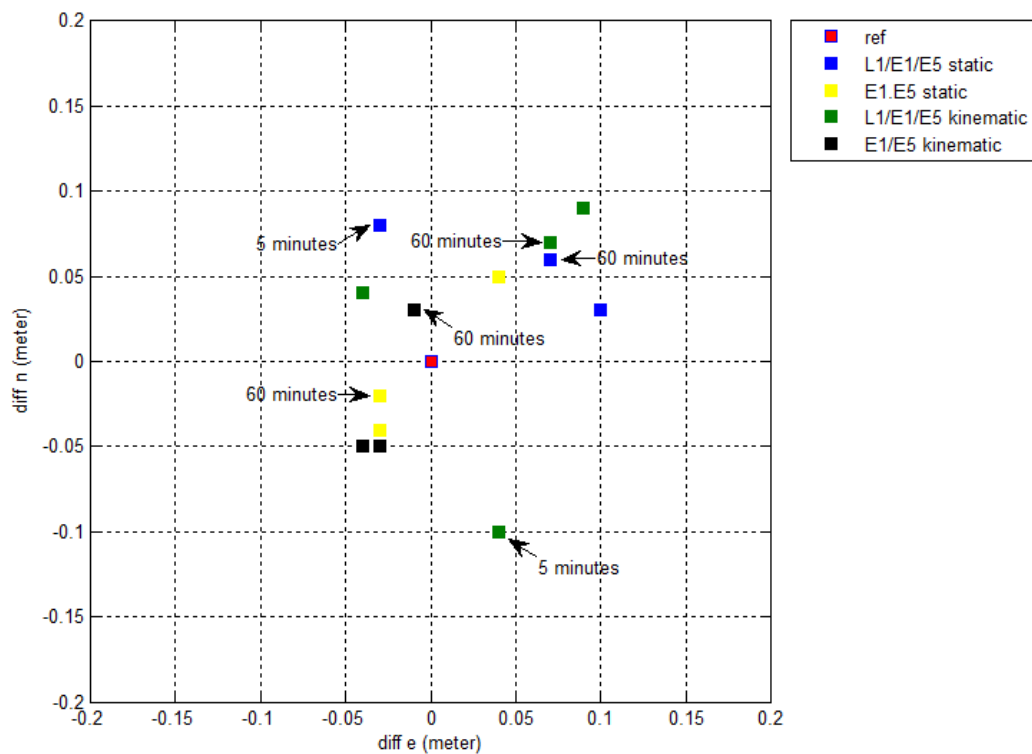


Figure 6-19. Static and kinematic position w.r.t. reference position at WIND (66.5 km), DOY 001, 2014

In baselines less than 30 km baseline, errors can be efficiently eliminated through double differencing and the observation noise less affects the solutions. However, at longer baselines, the measurement error turns to be the main problems, both on GPS+Galileo and Galileo alone. Over all the baselines, the Galileo performs better than GPS+Galileo when utilizing Wide-Lane/WL linear combination to diminish the ionospheric errors which exhibits the advantage of the Galileo signal linear combination.



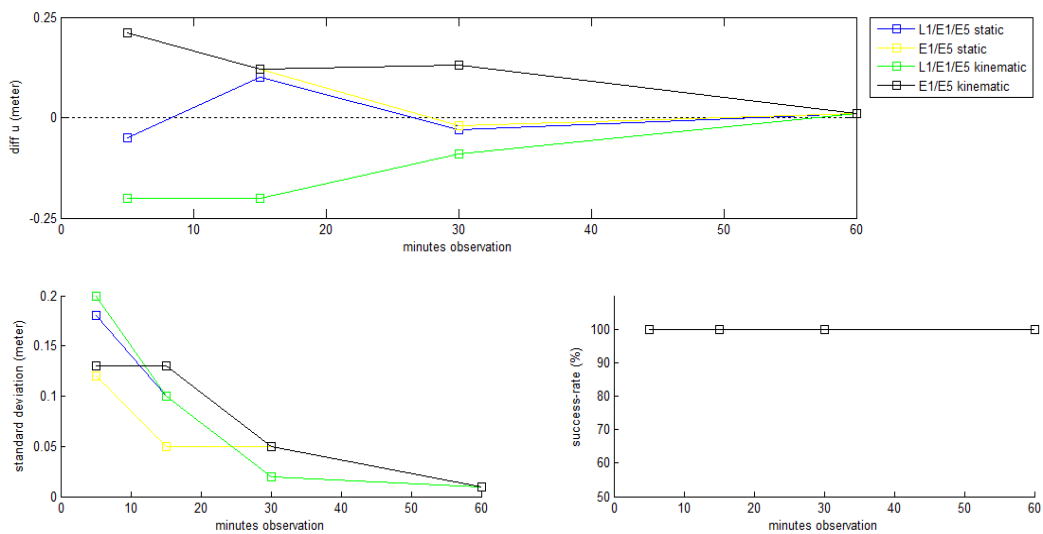


Figure 6-20. Height difference, standard deviation, and ambiguity success-rate at TIME-UNTE baseline (24.9 km), DOY 001, 2014

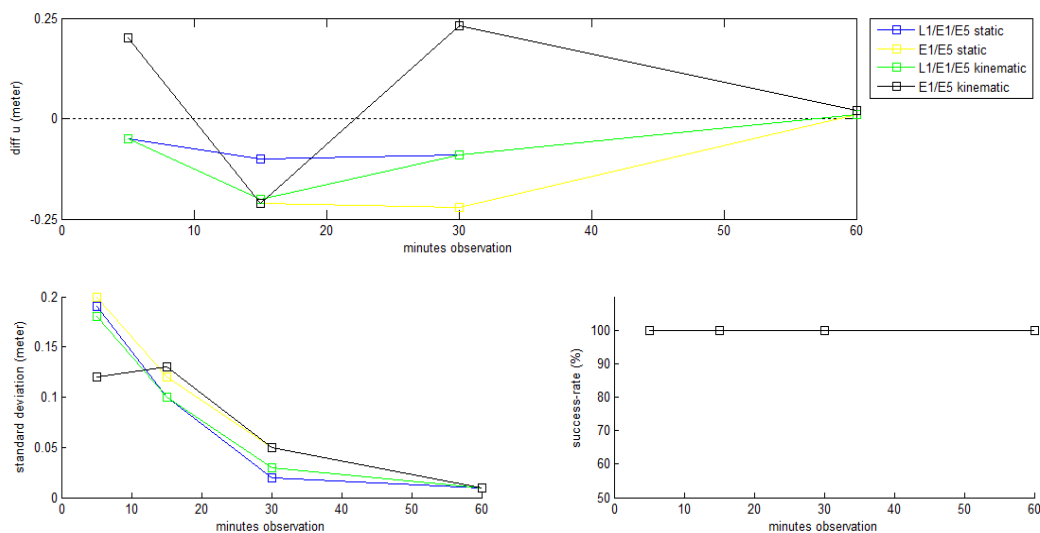


Figure 6-21. Height difference, standard deviation, and ambiguity success-rate at TIME-KIRC baseline (40.8 km) DOY 001, 2014

The height bias and standard deviations corresponded to the observation time periods shown in figures 6-20, 6-21, and 6-22. The height varies up to 20 cm both on static and kinematic position at TIME-UNTE baseline (24.9 km) using GPS+Galileo and Galileo alone. The coordinate standard deviation significantly decreases to less than  $\pm 5$  cm for all linear combinations after 30 minutes observation times. However, the ambiguity fixing success rate remains 100%. All the solutions deliver a similar performance and closing up to the height reference with 60 minutes observation. Comparing the 24.9 km baseline with results at longer baselines, the Galileo alone provides a good solution and have performs better than GPS+Galileo at the observation time span more than 15 minutes.

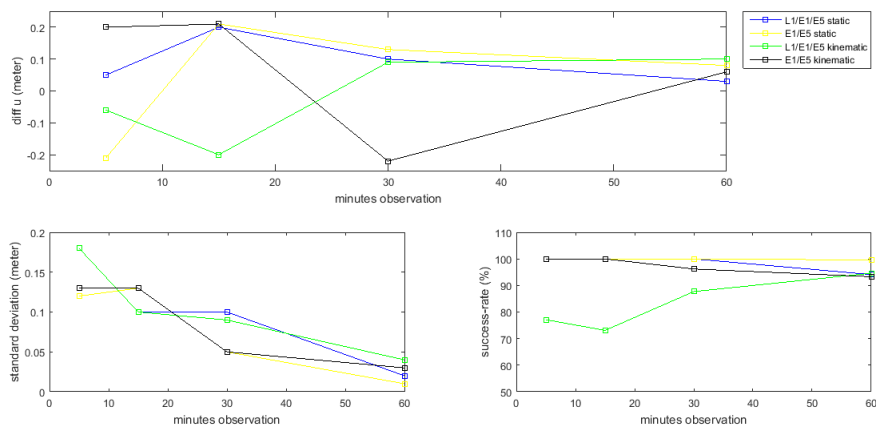


Figure 6-22. Height difference, standard deviation, and ambiguity success-rate at TIME-WIND baseline (66.5 km), DOY 001, 2014

According to the results from the simulated data observation, the Galileo performs the best, in particular at medium baselines (more than 30 km), albeit in case of short baseline, L1 GPS dominantly affects the solutions. The GPS+Galileo success rate is decreasing approximately 13% on over 66 km baseline when the kinematic method was applied. Moreover, the Galileo always have consistent result in short and medium baselines and the Galileo signal itself possesses the best insusceptibility in the presence of errors.

An ambiguity resolution can be obtained with short observation time span for Galileo on short and medium baselines. For ambiguity resolution on medium baselines, the reduction of measurement noise is necessary, and in addition, corrections are also necessary to get successful ambiguity resolution i.e. precise orbit information. And last, looking on simulated data, the E1/E5 Galileo combinations has potencies to provide the best performances in static and kinematic positioning under certain conditions and assuming there are no errors that diminished the performance.

## 7. Conclusions and Recommendations

This research has been conducted to study the performance of the GNSS real time positioning technology introducing modernized signals on short, medium, and long baselines by means of a free software application. Most of the investigated signal linear combinations are capable to deliver accurate, precise and consistent position solutions, although they perform differently in terms of noise, ionospheric content and ambiguity resolution ability. The thesis does not touch so-called RTK-network solutions, but focuses on single baselines observed over short to medium periods.

This chapter summarizes the identified main outcomes of this thesis. Conclusions are drawn from both, a thorough literature review and from GNSS data processing. Several aspects of the positioning models are described. Finally, some suggestions for future work are argued in order to develop and further enhance accurate GNSS positioning.

### 7.1 Summary

To modernize GPS a new signal at L5 and an improved signal structure at L2 were introduced. These efforts aim to improve the system performance and make it more reliable, particularly in terms of compatibility and interoperability with other GNSS systems, i.e. Galileo. GPS and Galileo transmit similar signal structures at the same center frequencies L1/E1 and L5/E5a, hence it will be easy to track both systems in parallel with the same equipment.

This thesis includes a theoretical analysis concerning an improved positioning performance when using these additional signals. The results are complemented by figures and tables in chapters 4, 5, and 6. The processed observation data was obtained from several sources e.g. BKG, IGS with sampling intervals between 1 to 30 seconds. Baseline lengths up to 70 km were studied with observation periods ranging from a few minutes up to 24 hours.

To evaluate the performance of the investigated linear combinations static and kinematic positioning solutions were calculated. The positioning quality is of course limited by ionospheric errors, tropospheric errors, satellite orbital errors and multipath noise as well as determined by the performance parameters signal/noise ratio, observation time, geometry and ambiguity resolution success rate. For GPS data processing of medium and long baselines legacy IGS products were used. Concerning Galileo the data pool and precise orbits of the IGS MGEX campaign were utilized.

Because multipath errors are site-specific the rover environment has to be chosen carefully. In case of evident multipath the E5 Galileo delivers an advantage compared to other signals due to its more multipath resistant codes which also goes in parallel with a higher received signal strength. The E5 Galileo signal is therefore more resilient against outside interference. Other unencrypted signals (L1 GPS and E1, E5a, E5b Galileo) provide similar SNR-values with a difference of approximately 1-5 dBHz and range noise in zenith direction of up to 0.25 m. On the other hand, the GPS L2 signal in this research shows the lowest SNR value with differences up to 10 dBHz and zenith range noise up to 0.4 m.

Currently L5 GPS and all Galileo signals cannot be fully used for positioning. The small number of satellites available and therefore small amount of available observation data in general prohibits building the necessary number of observation differences and therefore also limits the ambiguity resolution. In this research, the wide-lane/narrow-lane linear combinations for short observation periods as well as the ionosphere free linear combination for longer observation periods were built and processed.

Focusing on short-term observations of baselines less than 30 km dual-frequency positioning (L1/L2 GPS) yields a horizontal accuracy of about +/- 1-2 cm. Here, the triple-frequency (L1/L2/L5 GPS) solutions give comparable coordinate estimates but with a standard deviation 3 times worse than the dual-frequency solutions. On the other hand triple-frequency linear combinations deliver the same ambiguity fixing success-rates as dual-frequency solutions.

Using GPS L5 data for processing baselines less than 30km with dual frequency data does not significantly affect the positioning results. The standard deviation of the position differences using dual frequency L1/L5 GPS data of several minutes (up to 60 minutes) is very close to the L1/L2 GPS solution. L5 GPS signals can be used as advanced substitute and simultaneously in case of insufficient or improper L2 GPS observations.

In a further step real observation data as well as simulated data (Simulator) of a GNSS network were used to analyze the performance parameters 'baseline length' and 'observation time' of the linear combinations in the measurement domain. The simulation data set was established under the assumption of a complete Galileo orbit segment.

When processing real data, the Galileo linear combinations can currently not compete with GPS solutions as there is a lack of available Galileo satellites. The small number of satellites during the investigated period clearly harms ambiguity resolution on all baseline lengths. So also a combined Galileo+GPS solution is to date also dominated by the GPS data. The results are of course affected by the number of available satellites, satellite geometry, and observation time spans.

As proved by the simulated data results, in particular the Galileo E5 signal deliver a potency to provide best performance in static and kinematic positioning. Compared to GPS L1/L2 a clear advantage to use E1/E5 Galileo linear combination becomes apparent in order to reduce signal noise and multipath significantly. With respect to L1/L2 GPS results, the positioning with E1/E5 Galileo linear combinations reveals biases up to a few centimeters. These offsets might be caused by un-modeled intersystem biases between GPS and Galileo signals.

Processing simulated data on small and medium baselines a high ambiguity resolution success-rate can be obtained within 15 minutes of observation time both for static and kinematic positioning as a sufficient number of satellites is available (usually 8 GPS and 8 Galileo per epoch). For baseline lengths up to 70 km (medium and long baselines) a sufficient observation period and IGS corrections are required to provide an optimum performance with high ambiguity fixing success-rates and low position standard deviation level for both GPS and Galileo linear combinations.

In the absence of any errors using simulated data GPS+Galileo linear combinations reveal a good performance, which exhibits the advantage of the modernized GNSS signals and their number of satellites for positioning.

Until the new GNSS signals are fully operational, a definite answer about the optimal linear combinations for positioning cannot be obtained. However, by analyzing the simulated data we can get even today an advanced look into which linear combinations should be considered and how they can be used to improve the accuracy of positioning.

## **7.2 Conclusions and Recommendations**

Today a complete set of GPS L5 and Galileo measurements can only be obtained from simulation. From this analysis and from real-data signal noise and multipath investigations in particular the E5 Galileo signal emerges as the best alternative. A similar analysis could be performed with combinations using a combination with the E5 Galileo signal. Also these combinations deliver a carrier phase with a low noise level and position solutions with low coordinate standard deviation.

Several IGS processing centers are now producing precise ephemeris for all GNSS. Therefore this study should be extended to include also Glonass or Beidou observations to explore their contribution in positioning. Especially the Glonass FDMA signals may impose further difficulties when fixing ambiguities. In any case, an additional receiver clock bias and a system reference frame bias to cover all constellations have to be introduced.

Since the best performance was only tested using a limited simulated data, these tests should be carried out again when a complete Galileo segment is available providing sufficient real data for further testing. In this context the various options to build promising wide-lane or ionospheric-free linear combinations shall be studied in depth.

Further studies are also required on how the modernized GNSS signals perform in RTK network modeling and on relevant inter-system and intra-system biases.

## References

- Amiri-Sikoochi, A., Tiberius, C., C., J., M. (2007).** *Assessing Receiver Noise Using GPS Short Baseline Time Series.* GPS Solution, Vol. 11. Pp21-35 DOI 10.1007/s10291-006-0026-8.
- de Bakker, P., F., van der Marel, H., Tiberius, C., C., J., M. (2009).** *Geometry-free Undifferenced, Single and Double Differenced Analysis of Single Frequency of EGNOS, and GIOVE –A/B measurements.* GPS Solution, Vol 13. Pp305-314. DOI 10.1007/s01291-009-0123-6.
- de Bakker, P., F., Tiberius C., C., J., M., van der Marel, H., van Bree, R., J., P. (2011).** *Short and zero baseline analysis of GPS L1 C/A, L5Q, GIOVE E1B, and E5aQ signals.* GPS Solution. DOI 10.1007/s10291-011-0202-3
- Brunner, F., and Welsch, w. (1993).** *Effect of the Troposphere on GPS Measurements.* GPS World. Volume 12. pp 42-51.
- Butsch, F. (2002).** *A Growing Concern: Radiofrequency Interference and GPS.* GPS World, Vol. 13 Issue 10, 40p. October.
- Chang, X.W., Yang, X., and Zhou, T. (2005).** *MLAMBDA: A modified LAMBDA Method for Integer Least-squares Estimation.* Journal Geodesy. Vol.79.
- Chen, D. and G. Lachapelle (1995).** *A comparison of the FASF and least-squares search algorithms for on-the-fly ambiguity resolution.* Navigation: Journal of The Institute of Navigation, Vol. 42, No. 2, pp. 371-390.
- Chen, X.U., Vollath, H., Landau, K., Sauer (2004).** *Will Galileo/Modernized GPS Obsolete Network RTK?,* European GNSS 2004 Conference, 16-19 May, Rotterdam, The Netherlands.
- Cocard, M., Bourgon, S., Kamali, O., Collins, P. (2008).** *A systematic investigation of optimal carrier-phase combinations for modernized triple-frequency GPS.* Journal of Geodesy, Vol. 82, pp. 555–564. DOI 10.1007/s00190-007-0201-x.
- Dai, L., Han, S., Wang, J., and Rizos, C. (2004).** *Comparison of Interpolation Algorithms in Network-Based GPS Techniques.* Navigation: Journal of The Institute of Navigation, Vol. 50, No. 4, Winter 2003-2004, pp. 277-293.

- Davaine, M. (2011).** *Code Bias and Multipath Estimation with Cascaded Kalman Filter*. Thesis. Institute for Communication and Navigation, Technische Universität München. Munich, November.
- Dawidowicz, K. (2010).** *Antenna Phase center Variations Corrections in Processing of GPS Observations with the use of commercial Software*. Technical Science. No 13, DOI 10.2478/v10022-010-0012-9.
- Elmas, Z.G., Aquino, M., Marquez, H.A., Monico, J.F.G. (2011).** *Higher order ionospheric effects in GNSS positioning in the European region*. Annals of Geophysics. Vol. 29. pp. 1383-1399.
- Euler, H.J. and H. Landau (1992).** *Fast GPS ambiguity resolution on-the-fly for real-time application*. Proceedings of Sixth International Geodetic Symposium on Satellite Positioning, Columbus, Ohio, 17-20 March, pp. 650-659.
- European GNSS (Galileo) Open Service. (2010).** *Signal in Space Interface Control Document*. OS SIS ICD, Issue 1.1, September.
- Eva and Torben, S. (2007).** *Active GNSS networks and the benefits of combined GPS+Galileo Combination*. insideGNSS. November.
- Feng, Y., Wang, J. (2008).** *GPS RTK Performance Characteristics and Analysis*. Journal of Global Positioning Systems, Vol. 7, No. 1, pp. 1-8.
- Fernandez-Plazaola, U., Martin-Guerrero, T.M., Entrambasaguas-Munoz, J.T., Martin-Neira, M. (2004).** *The Null Method Applied to GNSS Three-carrier Phase Ambiguity Resolution*. Journal of Geodesy, Vol. 78, pp. 96-102. DOI 10.1007/s00190-004-0376-3.
- Fernandez-Plazaola, U., Martin-Guerrero, T.M., Entrambasaguas-Munoz, J. T. (2008).** *A New Method for Three-carrier GNSS Ambiguity Resolution*. Journal of Geodesy, Vol. 82, pp. 269-278. DOI 10.1007/s00190-007-0177-6.
- Fontana, R.D., Cheung, W., Stansell, T. (2001).** *The Modernized L2 Civil Signal*. GPS World, pp. 28-34. September.
- Frei, E. and Beutler, G. (1990).** *Rapid Static Positioning Based on the Fast Ambiguity Resolution Approach FARA: Theory and First Results*. Manuscripta Geodaetica, Vol. 15, pp. 325-356.



- Grejner-Brzezinska D.A., Kashani I., Wielgosz, P. (2005).** *On Accuracy and reliability of instantaneous network RTK as a function of network geometry, station separation, and data processing strategy.* GPS Solution, Vol. 9, pp. 212-225.
- Gurtner, W. (2009).** RINEX The Receiver Independent Exchange Format Version 3.01. [igsb.jpl.nasa.gov/igsb/data/format/rinex301.pdf](http://igsb.jpl.nasa.gov/igsb/data/format/rinex301.pdf). Accessed on September 2014.
- Hatch, R. (1990).** *Instantaneous ambiguity resolution.* Proceedings of KIS'90, Banff, Canada, 10-13 September, pp. 299-308.
- Harris, R., A. (1997).** *Direct Resolution of Carrier-Phase Ambiguity by 'Bridging the Wavelength Gap'.* ESA Publication "TST/60107/RAH/Word", February.
- Hannah, B.M. (2001).** *Modeling and Simulation of Multipath Propagation.* Ph.D Thesis. The Cooperative Research Centre for Satellite Systems. Queensland University of Technology. Australia. 375p. March.
- Henkel, P., and Günther, C. (2007).** *Three frequency linear combinations for Galileo.* Proceedings of the 4th Workshop on Positioning, Navigation and Communication. Hannover, Germany, pp. 239-245.
- Hofmann-Wellenhof, B., Lichtenegger, H., and Collins, J. (2001).** *Global Positioning System: Theory and Practice.* 5<sup>th</sup> Ed., Springer, Berlin.
- Hofmann-Wellenhof, B., Lichtenegger, E. Wasle. (2008).** *GNSS-Global Navigation Satellite Systems.* Springer, Wien.
- Hoque, M.M. & Jakowski, N. (2007).** *Higher order ionospheric effects in Precise GNSS Positioning.* Journal of Geodesy, Vol. 81, Pp. 259-268. DOI 10.1007/s00190-006-0106-0.
- Hoque, M.M., and Jakowski, N. (2012).** *Ionospheric Propagation Effects on GNSS Signals and New Correction Approaches, Global Navigation Satellite Systems: Signal, Theory and Applications,* Prof.Shuanggen Jin (Ed.). InTech, pp. 381-404. ISBN: 978-953-307-843-4.
- International GNSS Service (IGS), RINEX Working Group and Radio Technical Commission for Maritime Services Special Committee 104 (RTCM-SC104). (2013).** RINEX-The Receiver Independent Exchange Format. Accessed on October 2014, <ftp://igs.org/pub/data/format/rinex302.pdf>.

- International GNSS Service (IGS)**, *International GPS Service Annual Report 2000*, IGS Central Bureau, Jet Propulsion Laboratory. Pasadena, California, 2001.
- Jensen, B.O. (2002)**. *Numerical Weather Predictions for Network RTK*. National Survey and Cadastre – Denmark, Publication Series 4, Vol.10.
- Joosten, P., T. Pany, and J. Winkel. (2002)**. *The Impact of unmodelled multipath on ambiguity resolution*. Proceedings of ION GPS-02, Portland, OR, pp. 953 - 959. 24-27 September
- Julien, O. A., Lves, P., Cannon, M., & Lachapelle, G. (2004)**. *Improved triple-frequency GPS/Galileo carrier phase ambiguity resolution using a stochastic ionosphere modeling*. Proceedings of ION, NTM, 01–26.
- Jung, J., P. Enge, B. Pervan (2000)**. *Optimization of cascade integer resolution with three civil frequencies*. Proceedings of ION GPS 2000, The 13th International Technical Meeting of the Satellite Division of the Institute of Navigation, Salt Lake City, Utah, USA, 19-22 September, pp. 2191-2200.
- Joseph, A. and Petovello, M. (2010)**. *Measuring GNSS Signal Strength*. Inside GNSS. November, pp. 20-25.
- Kim, D. and R.B. Langley (1999)**. *An optimized least-squares technique for improving ambiguity resolution performance and computational efficiency*. Proceedings of ION GPS'99, Nashville, Tennessee, 14-17 September, pp. 1579-1588.
- Lachapelle, G., Alves, P., Fortes, L.P., Cannon, M.E. (2000)**. *DGPS RTK Positioning Using a Reference Network*. ION GPS-00 (Session C3). Salt Lake City. September.
- Lachapelle, G., Alves, P., Fortes, L.P., Cannon, M.E., and Townsend, B. (2000)**. *DGPS RTK positioning using a reference network*. Proceeding of the 13th International Technical Meeting Satellite Division US Institute of Navigation (ION), Salt Lake City, UT, 19–22 September, pp. 1165–1171.
- Landau, H., Vollath, U., Chen, X. (2004)**. Benefits of modernized GPS/Galileo to RTK positioning. In GNSS 2004, Sydney, Australia.
- Langley, R. B. (1996)**. *GPS Receivers and the Measurements*. Lecture Notes in Earth Sciences (60): GPS for Geodesy, Springer-Verlag, pp141-173.
- Langley, R.B. (1997)**. *GPS receiver system noise*. GPS world. pp. 40-45.

- Leick, A. (1995).** *Satellite GPS Surveying*. 2<sup>nd</sup> edition. Wiley-InterScience, 560p.
- Liu, D. and Langley R.B. (2000).** *A search space optimization technique for improving ambiguity resolution and computational efficiency*. *Earth Planets Space*, 52, pp 807–812.
- Luo, X., Mayer, M., Heck, B. (2009).** *Improving the Stochastic Model of GNSS Observations by Means of SNR-based Weighting*. *Observing our Changing Earth*, IAG Symposia 133, 725. Springer-Verlag, Berlin.
- Mendes, V.B. (1999).** *Modelling the Neutral-Atmospheric Propagation Delay in Radiometric Space Techniques*. Ph.D dissertation, Department of Geodesy and Geomatics Engineering. Technical Report No.199, University of New Brunswick, New Brunswick, Canada, 378p. April.
- Moudrak, A., Konovaltsev, A., Furthner, J., Hammesfahr, J., Bauch, A., de Fraigne, P., Bedrich, S. (2004).** *Timing aspects of GPS-Galileo interoperability: challenges and solutions*. In *Proceedings of the 2004 Precise Time and Time Interval Meeting (PTTI)*, 279–292.
- Odijk, D. (2003).** *Ionosphere-Free Phase Combinations for Modernized GPS*. *Journal of Surveying Engineering* Vol. 129. November.
- Odijk, D., Teunissen, P.J.G., and Tiberius C.C.J.M. (2002).** *Triple-Frequency Ionosphere-Free Phase Combinations for Ambiguity resolution*. *Proceeding of ENC GNSS*. Copenhagen, Denmark.
- Parkinson, B.W., and Spilker Jr., J.J. (1996).** *Global Positioning System: Theory and Applications Volume 1*. Vol. 163, American Institute of Aeronautics and Astronautics, Washington DC.
- Paziewski, J. and Wielgosz P. (2014).** *Assessment of GPS + Galileo and multi-frequency Galileo single-epoch precise positioning with network corrections*. *GPS Solution* Vol.18, pp. 571–579. DOI 10.1007/s10291-013-0355-3.
- Petovello, M. and Takac, F. (2009).** *GNSS Solution: GLONASS inter-frequency biases and ambiguity resolution*. *Inside GNSS*.
- Ray, J.K. (2000).** *Mitigation of GPS Code and Carrier Phase Multipath Effects Using a Multi-Antenna System*. Department of Geomatics Engineering. UCGE Reports 20136. University of Calgary. Alberta, Canada.285p. March.
- RTKLIB ver. 2.4.2 Manual, Release Notes April (2013).**

- Richert, T., and N. El-Sheimy (2007).** *Optimal linear combinations of triple frequency carrier phase data from future global navigation satellite systems.* GPS Solutions, Vol. 11, No. 1, pp. 11-19. DOI 10.1007/s10291-006-0024-x.
- Rost, C. and Wanninger, L. (2009).** *Carrier Phase multipath mitigation based on GNSS signal quality measurements.* Journal of Applied Geodesy 3, de Gruyter, pp. 1-8. DOI 10.1515/JAG.2009.009.
- Sahmoudi, M., Kouki A., Landry L. Jr. (2010).** *A New Approach for Mitigating Carrier Phase Multipath Errors in Multi-GNSS Real-Time Kinematic (RTK) Receivers.* IEEE. DOI: 978-1-4244-4296-6/10.
- Schloderer, G., Bingham M., Awange J.L., Fleming K.M. (2010).** *Application of GNSS-RTK Derived Topographical Maps for Rapid Environmental Monitoring: A Case Study of Jack Finnelly Lake (Perth, Australia).* Journal of Environmental Monitoring and Assessment. December. DOI: 10.1007/s10661-010-1778-8.
- Serrano, L. (2013).** *Carrier-Phase Multipath Mitigation In RTK-Based GNSS Dual-Antenna Systems.* Ph.D. dissertation, Department of Geodesy and Geomatics Engineering, Technical Report No. 287, University of New Brunswick, Fredericton, New Brunswick, Canada, 227p.
- Smyrnaiois. M., Schoen, S., and Nicolas, M.L. (2013).** *Multipath Propagation, Characterization, and Modeling in GNSS.* <http://dx.doi.org.10.5772/54567>
- Shrestha, S.M. (2003).** *Investigations into the Estimation of Tropospheric Delay and Wet Refractivity Using GPS Measurements.* Department of Geomatics Engineering. UCGE Reports 20180. University of Calgary. Alberta, Canada. 156p. July.
- Takasu, T. and Yasuda, A. (2008).** *Evaluation of RTK-GPS Performance with Low-cost Single-frequency GPS Receivers.* International Symposium on GPS/GNSS 2008. Tokyo International Exchange Center, Japan. 11-14 November.
- Toho, H.D., Bock H., Schuler T., Junker S., Kiroe A. (2012).** *Exploiting the Galileo E5 Wideband Signal for Improved Single Frequency Precise Positioning.* Inside GNSS. October.
- Teunissen, P.J.G. (1993).** *Least squares estimation of the integer GPS ambiguities.* Invited lecture, Section IV: Theory and methodology, IAG General Meeting, Beijing, China, August.

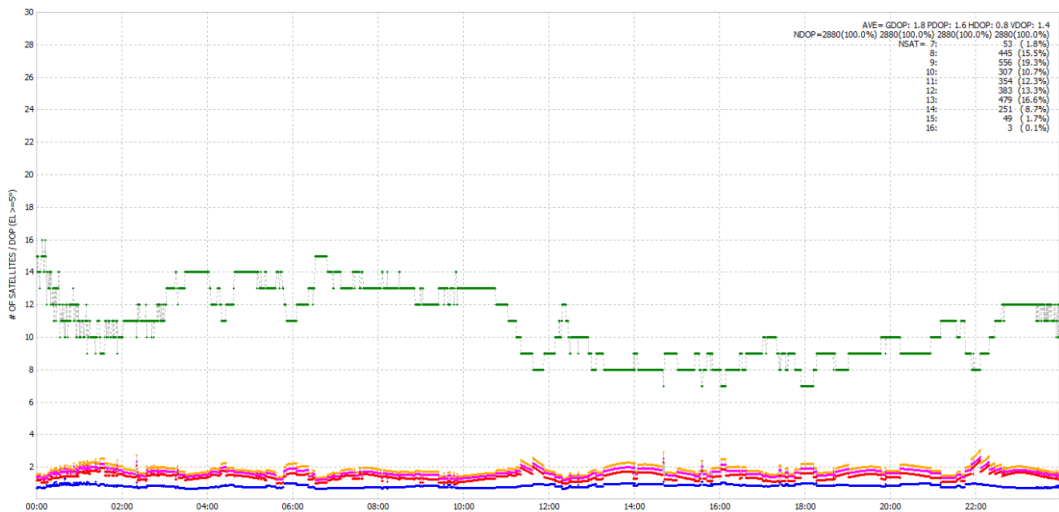
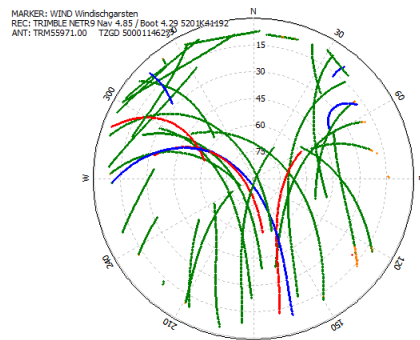
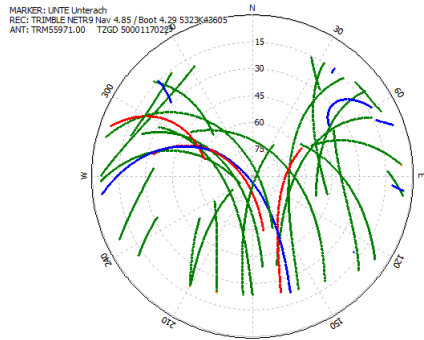
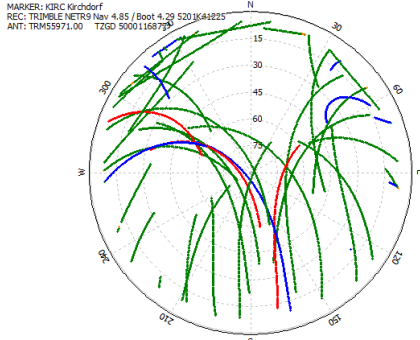
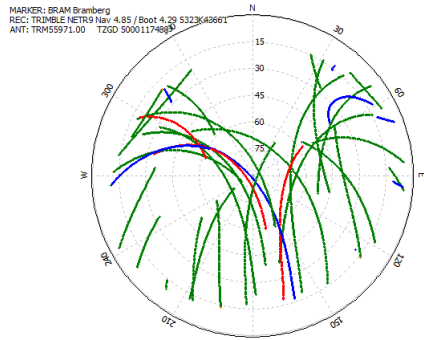
- Teunissen, P. J. G., (1995).** *The Least-square Ambiguity Decorrelation Adjustment: A Method for Fast GPS Ambiguity Estimation.* Journal Geodesy, vol.70.
- Tiberius, C., Pany, T., Eissfeller, B., Joosten, P., Verhagen, S., (2002).** *0.99999999 confidence ambiguity resolution with GPS and Galileo.* GPS Solutions Vol 6: pp 96–99. DOI 10.1007/s10291-002-0022-6.
- Ueno, M. (2001).** *Assessment of Atmospheric Delay Correction Models for the Japanese MSAS.* ION GPS 2001, Salt Lake City, UT 11-14 September.
- Urquhart, L., (2009).** *An Analysis of Multi-Frequency Carrier Phase Linear Combinations for GNSS.* Senior technical report, Department of Geodesy and Geomatics Engineering Technical Report No. 263, University of New Brunswick, Fredericton, New Brunswick, Canada, pp71. February.
- Victoria, A.H. (2005).** *Data Assimilation for 4-D Wet Refractivity Modelling in a Regional GPS Network.* Department of Geomatics Engineering. UCGE Reports 20210. University of Calgary. Alberta, Canada. 190p. January.
- Vollath, U., Roy. E. (2001).** *Ambiguity Resolution using Three Carriers, Performance Analysis using "Real" Data.* Proceedings of the GNSS-2001 conference, 9-11 May, Sevilla, Spain.
- Vollath, U., Patra, R., Chen, X., Landau H. (2004).** *GALILEO/Modernized GPS: A New Challenge to Network RTK.* Trimble Terrasat GmbH, Germany.
- Wu, J.T., S.C. Wu, G.A. Hajj, W.I. Bertiger, and S.M. Lichten. (1993).** *Effects of antenna orientation on GPS carrier phase.* Manuscripta Geodaetica. Vol. 18. pp. 91-98.
- Wallner, S.H., Ein, G.P., Any, T.A., Vila-Rodriguez, J., & Osfay, A. (2005).** *Interference computations between GPS and Galileo.* ION GNSS 2005, 13–16
- Walter, T., Enge, P., Blanch, J., Pervan, B. (2008).** *Worldwide Vertical Guidance of Aircraft Based on Modernized GPS and New Integrity Augmentations.* Proceedings of the IEEE Vol. 96, Issue: 12, pp. 1918 – 1935. December. DOI 10.1109/JPROC.2008.2006099
- Wanninger, L. (2008).** *Introduction to Network RTK.*  
IAG Working Group 4.5.1: Network RTK (2003-2007). Accessed on September 2014. <http://www.wasoft.de/e/iagwg451/intro/introduction.html>.

**Warnant**, R., Foelsche, U., Aquino, M., Bidaine, B., Gherm, V., Hoque, M.M., Kutiev, I., Lejeune, S., Luntama, J.P., Spits, J., Strangeways, H.J., Wautelet, G., Zernov, N., Jakowski, N. **(2009)**. *Mitigation of Ionospheric Effects on GNSS*. Annals of Geophysics Vol. 52. pp. 373-390. August.

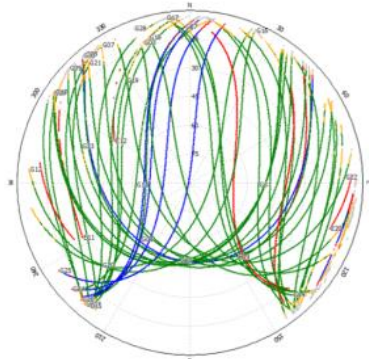
**Wautelet**, G. and Warnant, R. **(2013)**. *Modeling and Forecasting the Occurance of Ionospheric Irregularities in Mid-Latitude regionals*. Beacon Satellite Symposium. Bath, UK. July.

**Xu**, G. **(2007)**. *GPS: Theory, Algorithms and Applications*. 2<sup>nd</sup>ed. Springer. September.

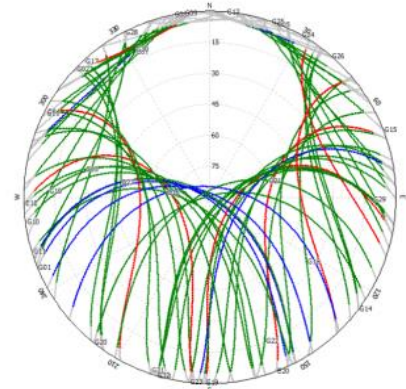
# Appendix A



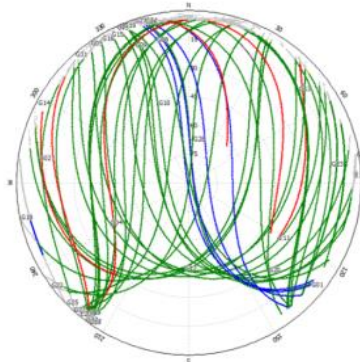
HANDED: 0410 13000004  
REC: TRIMBLE NETS A 70 85790  
ANT: TRIMBLE\_01 HORN 14051



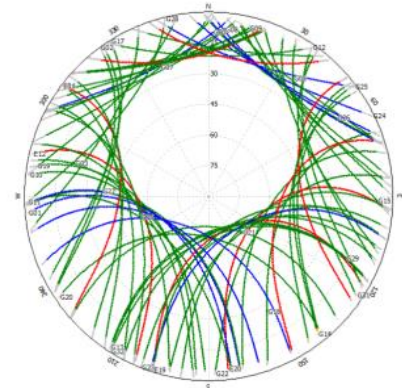
HANDED: DEFT-22 13000009  
REC: TRIMBLE NETS A 81 00000704  
ANT: LEIAR25\_R3 LEFT 0000006



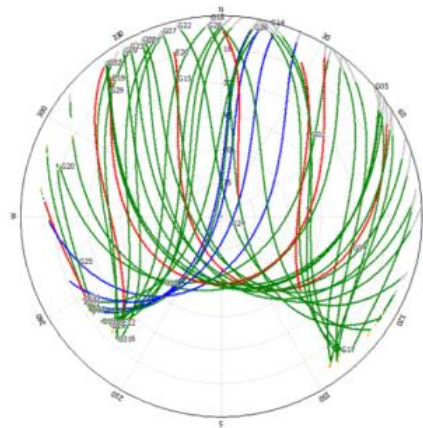
HANDED: 0411 13200402  
REC: DEPT POLARIS 2.3.2 0002047  
ANT: USAC03\_R4 HORN 170219



HANDED: 0418 14420402  
REC: TRIMBLE NETS A 82 000007040  
ANT: LEIAR25\_R3 LEFT 00000016



HANDED: N40R 0018 09001  
REC: DEPT POLARIS 4-0.5.3 patch 1 0001026  
ANT: SEPCHOKE\_MC HORN 1122





# Appendix B

Comparison of L1 (green) w.r.t. L1/L2 (blue).

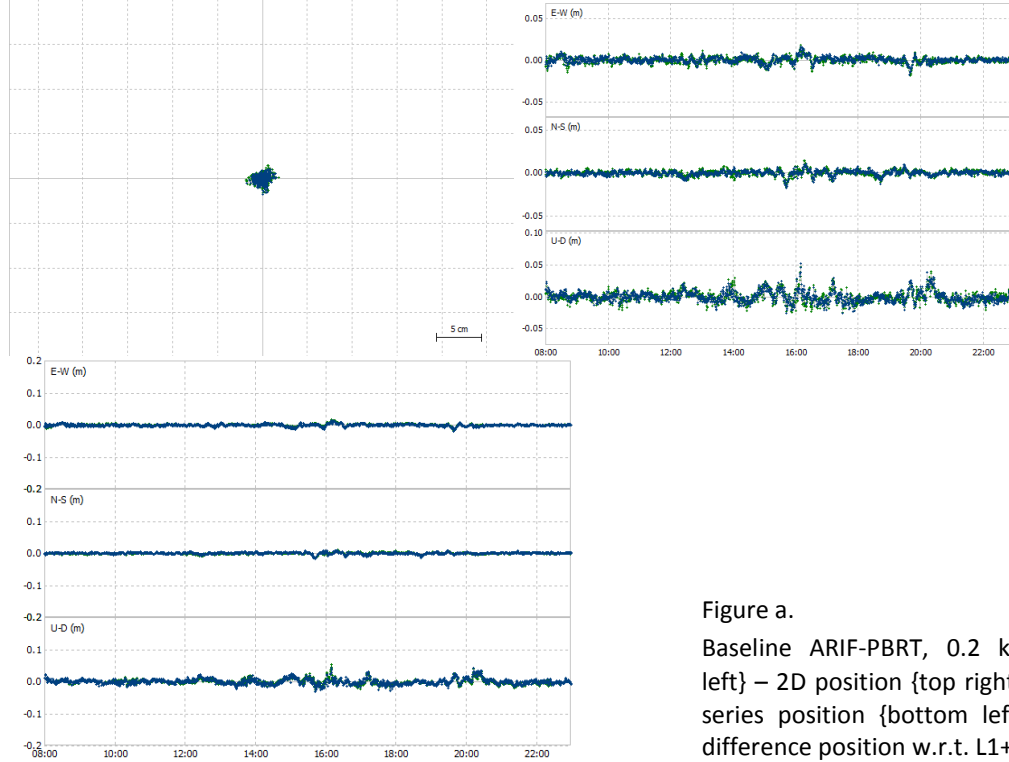


Figure a.  
Baseline ARIF-PBRT, 0.2 km, {top left} – 2D position {top right} – time series position {bottom left} – the difference position w.r.t. L1+L2

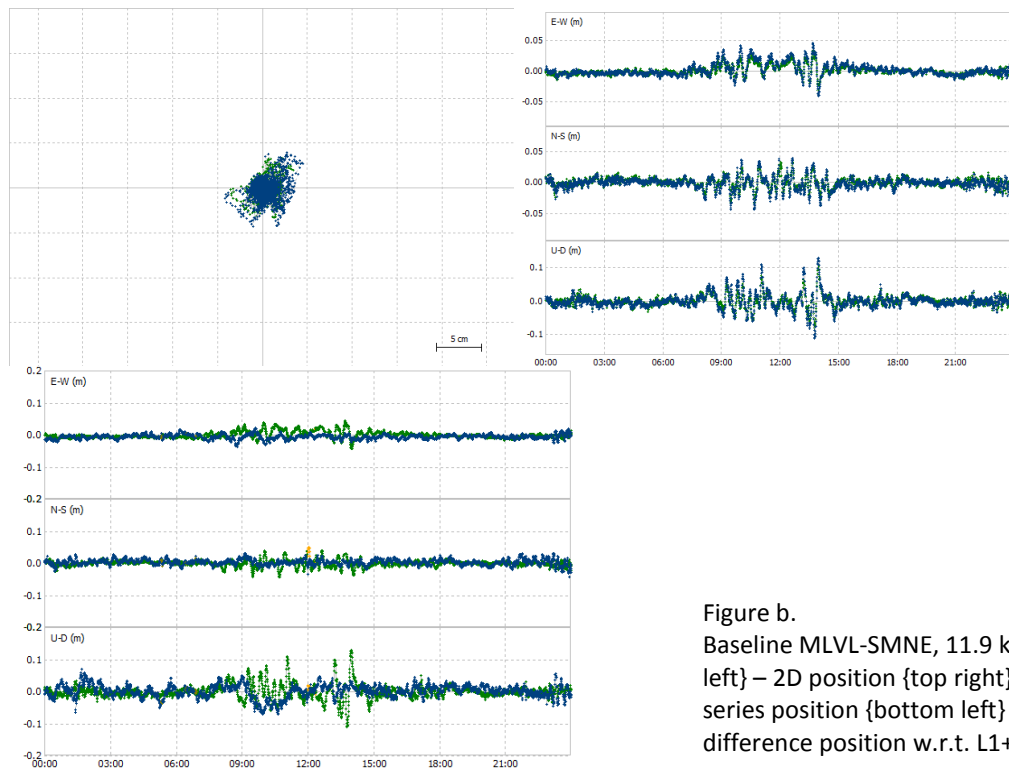


Figure b.  
Baseline MLVL-SMNE, 11.9 km, {top left} – 2D position {top right} – time series position {bottom left} – the difference position w.r.t. L1+L2

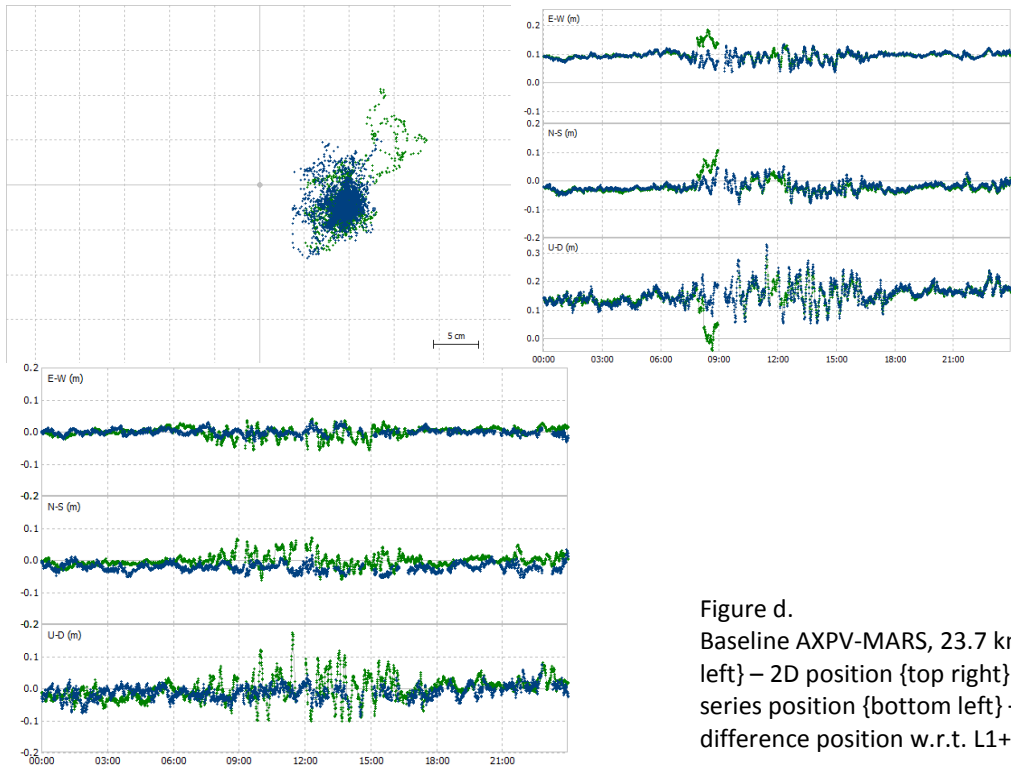


Figure d.  
 Baseline AXPV-MARS, 23.7 km {top left} – 2D position {top right} – time series position {bottom left} – the difference position w.r.t. L1+L2

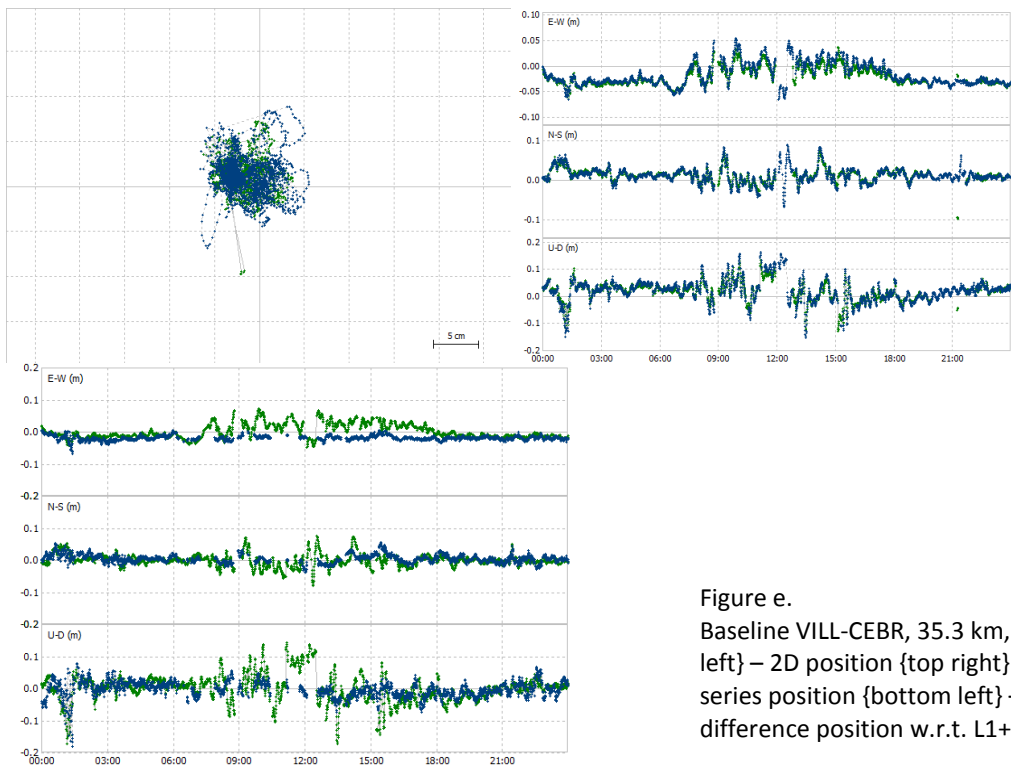


Figure e.  
 Baseline VILL-CEBR, 35.3 km, {top left} – 2D position {top right} – time series position {bottom left} – the difference position w.r.t. L1+L2

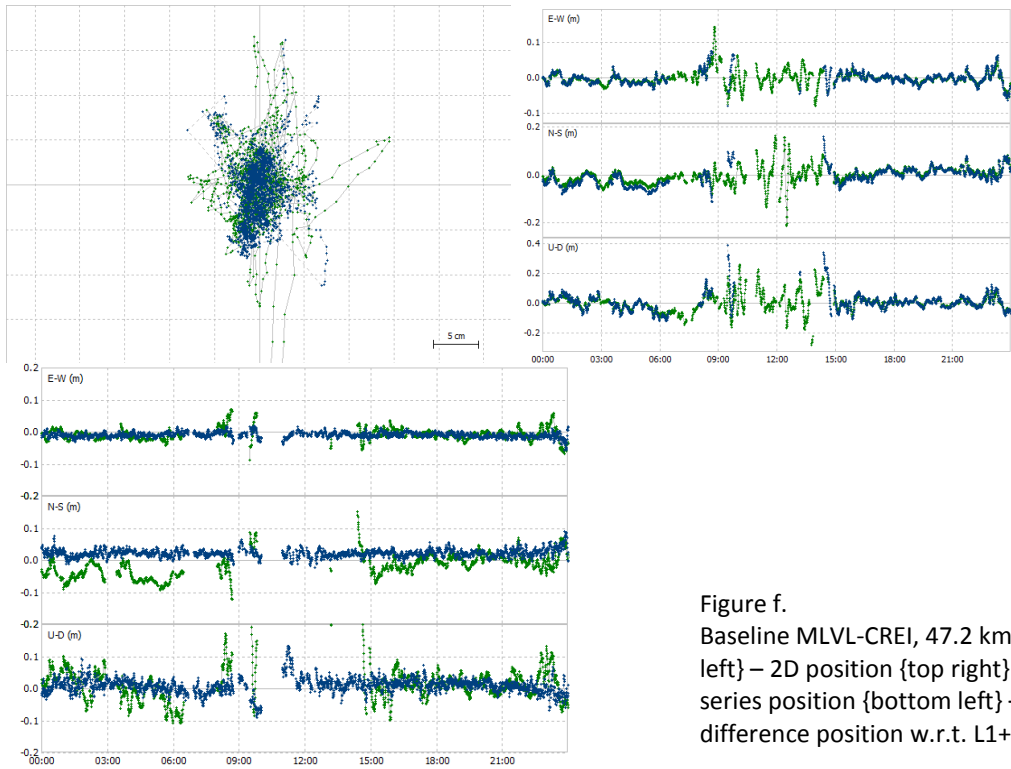


Figure f.  
 Baseline MLVL-CREI, 47.2 km, {top left} – 2D position {top right} – time series position {bottom left} – the difference position w.r.t. L1+L2

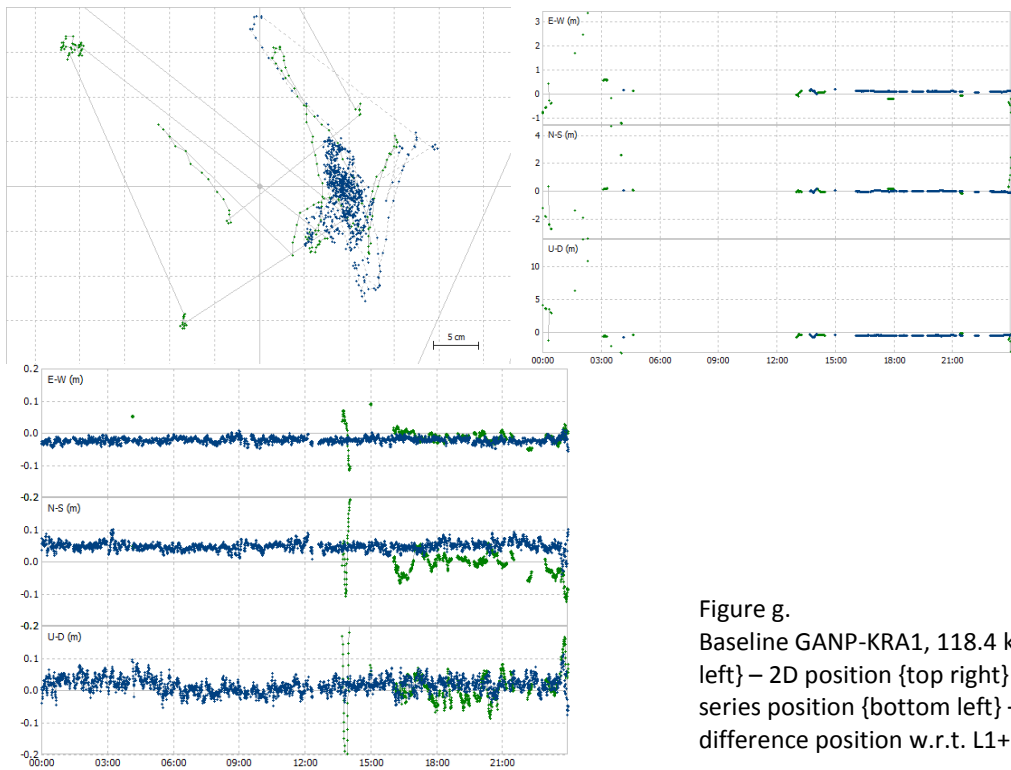
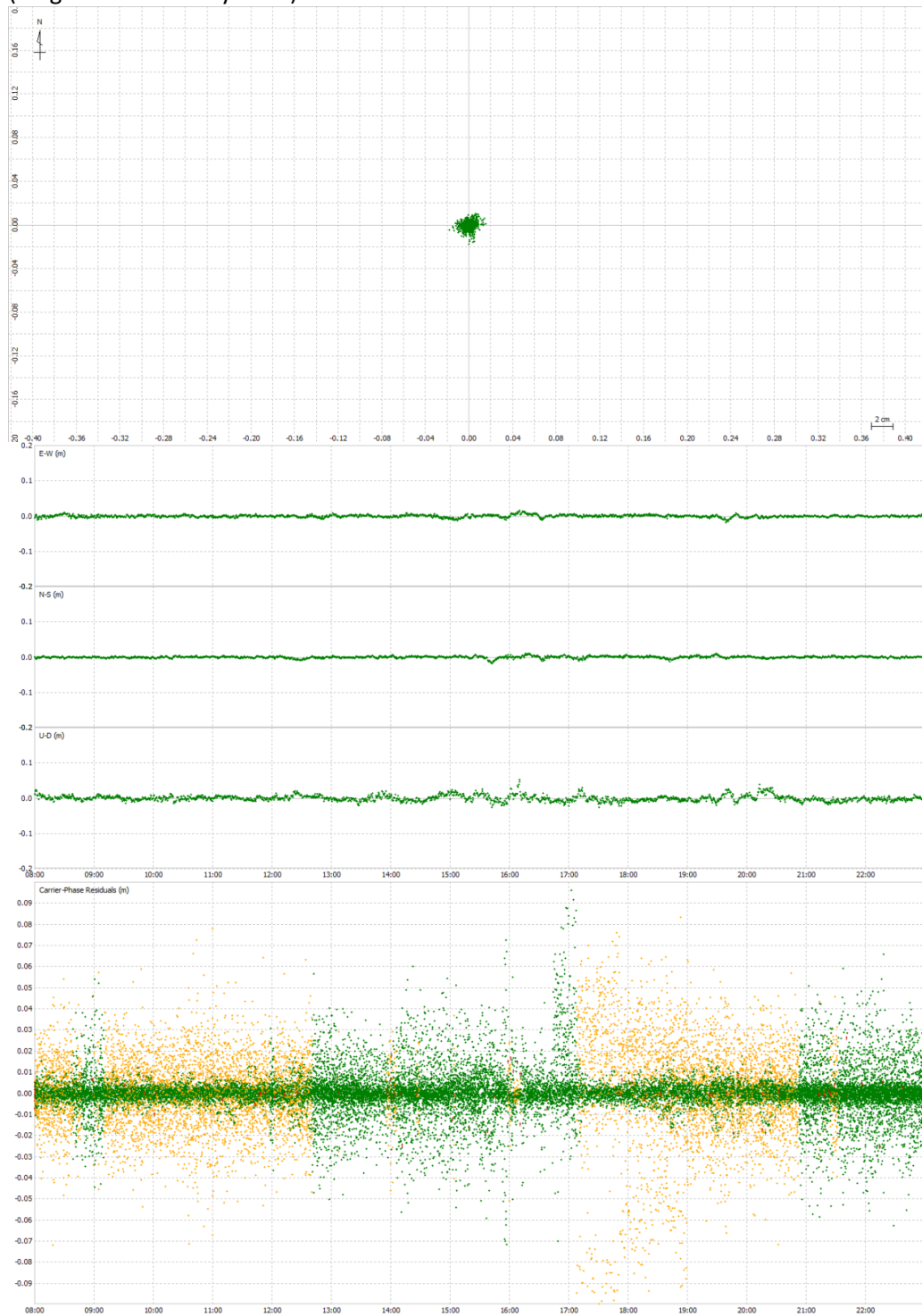


Figure g.  
 Baseline GANP-KRA1, 118.4 km, {top left} – 2D position {top right} – time series position {bottom left} – the difference position w.r.t. L1+L2

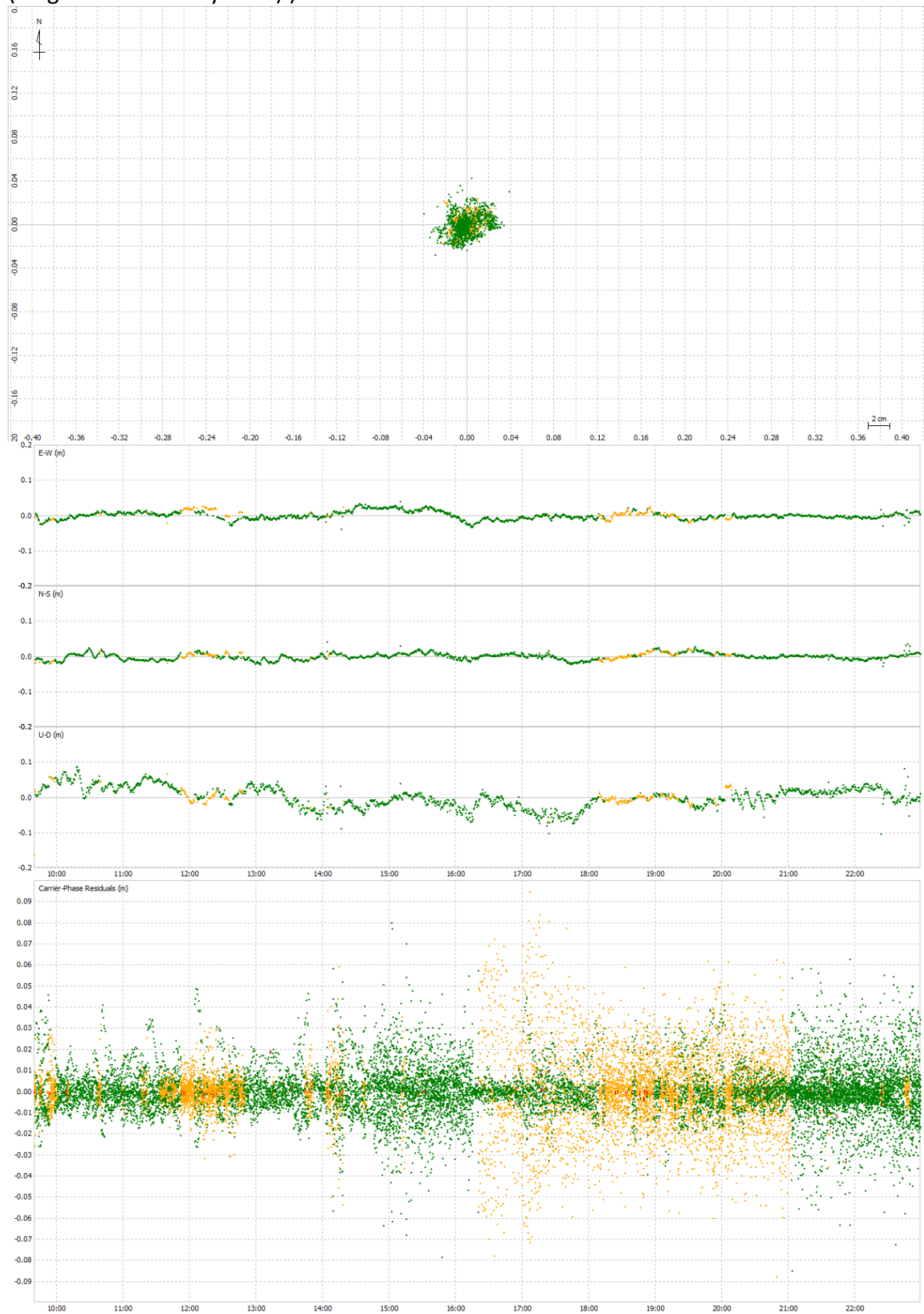
0.2 km baseline, L1/L2 LC, time series of position results and carrier phase residuals (fix-green and float-yellow).



7.2 km baseline, L1/L2 LC, time series of position results and carrier phase residuals (fix-green and float-yellow).



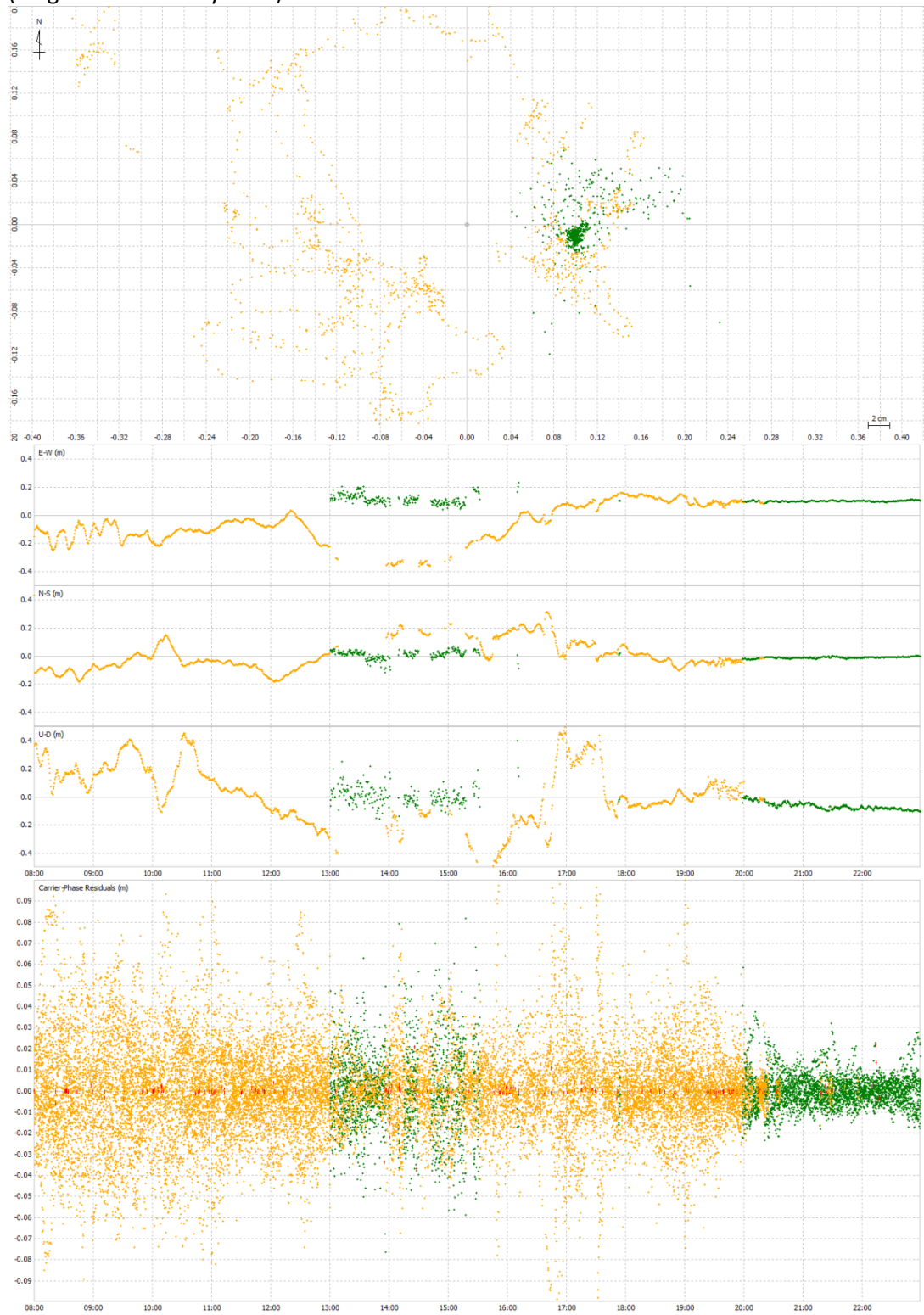
17.7 km baseline, L1/L2 LC, time series of position results and carrier phase residuals (fix-green and float-yellow.)



25.9 km baseline, L1/L2 LC, time series of position results and carrier phase residuals (fix-green and float-yellow).



35.1 km baseline, L1/L2 LC, time series of position results and carrier phase residuals (fix-green and float-yellow).





42 km baseline, L1/L2 LC, time series of position results and carrier phase residuals (fix-green and float-yellow).

